Integrated Heat Pump Options for Heat Upgrading in Cu-Cl Cycle for Hydrogen Production

By

MOHAMED ALMAHDI

A Thesis Submitted in Partial Fulfilment

of the Requirements for the degree of

Master of Applied Science

in

Mechanical Engineering

Faculty of Engineering and Applied Science

University of Ontario Institute of Technology

Oshawa, Ontario, Canada

Abstract

The Copper Chlorine (Cu-Cl) hydrogen production cycle is a promising green method to meet the future demand for hydrogen. The Cu-Cl cycle has a number of endothermic reactions that take place at high temperature level. One of the highest temperature demanding components in the Cu-Cl cycle is the copper oxychloride decomposition reactor. This thesis proposes two potential methods to address this demand by using a cuprous chloride (CuCl) vapor compression heat pump cascaded with a mercury heat pump as a first option, and cascaded with a biphenyl heat pump as a second option. These cascaded heat pumps are meant to upgrade heat from nuclear power plants with a heat input of approximately 300°C or industrial waste heat to meet the copper oxychloride decomposition reactor demand. A comprehensive energetic, exergetic, and exergoeconomic assessment is made to understand the heat pump performance and costs.

The CuCl-mercury heat pump had an overall energetic coefficient of performance of 1.93 and an exergetic performance of 1.25. Its total estimated cost is US$1,446,554 which is 62% higher than that estimated for its CuCl-biphenyl counterpart. Nevertheless, the CuCl-mercury heat pump has the lowest exergy destruction cost flow rate of 2,045 $/hour.

The CuCl-biphenyl heat pump, on the other hand, also shows high coefficient of performance for certain operating conditions of compressors isentropic efficiencies, and excess CuCl feed temperature. Its base energetic and exergetic coefficient of performances are 1.76 and 1.15, respectively. Its estimated cost of $892,440 is lower than its CuCl-mercury counterpart. However, its overall exergy destruction cost flow rate was two times higher, 4,903 $/hour.

Keywords: Cascaded heat pumps, hydrogen production, mercury, biphenyl, CuCl, energy, exergy, coefficient of performance.

Acknowledgement

Firstly, I would like to express my sincere gratitude to my advisors Prof. Ibrahim Dincer and Prof. Marc A. Rosen for the continuous support of my study and related research, for their patience, motivation, kind spirit, and immense knowledge. Their guidance was a very fruitful experience. I also want to thanks Dr. Calin Zamfirescu, his support, availability and immense knowledge are greatly appreciated. A special thanks to Mr. Joel Stewart for his help, kind heart, and support.

I would like to thank all of my colleagues in CERL lab and ACE3030B. I have learnt too much from them, academic-related and beyond. Very special thanks goes to Mohamed Al-Ali for being a great colleague and a friend during my stay in Canada. Also a very warm thanks to Farrukh Khalid for his help in many academic things, motivation, support, useful chatting, and smiley face. I also want to thanks Reza Soltani, talking about chemistry with him has finally borne its fruit. Thanks to the optimist Vishvadeep, working with him for long hours and talking about life interest was joyful, fruitful. Big thank you goes to these great guys who were a big support to me during my stay in Canada: Sadiq Albader, Mohammed Al-Mohamed-Ali, Mahdi Alhaddad, Saeed Alalawiyat, Mohamed Aljaroudi, Hasan Abu-sarer, Mohamed Aldabous and Mahmood Alabed.

Special thanks to Rita Booth, The land lady that has hosted me in this country since my arrival. Knowing her is a pleasure and has given me a great insights about life. I will really miss her when I return back home.

All thanks, deepest and sincere gratitude goes to my parents Ahmed Almahdi and Noora Alameer. As I age in this world I become more certain that they managed to give me all they have to see me, my brother and my sister in the best status. I apologize for any short coming from my side, whatever I do, I will not be able to return the favor.

Last but not least, I want to thank my brother and friend Ebrahim Almahdi for motivating me and supporting me and teaching many things about life. Very big thank you to my sister Fatima Almahdi for standing with me spiritually, and taking care of my parents during my absence, I am glad to have her, her great husband Ahmed, and her son Ali in my life. Warm thank you to my beloved wife and friend Zainab Jadeed, without her love winter wouldn't have been spring, and white snow wouldn't have been so colorful.

Table of Contents

List of Tables

List of Figures

Nomenclature

a_i	Coefficient
c	Cost per unit of exergy flow rate ($/kW)
$\dot{C}$	Cost flow rate ($/s)
COP	Coefficient of performance
C_p	Constant pressure specific molar heat (kJ/kmolK)
CRF	Capital recovery factor
ex	Molar exergy (kJ/mol)
$\dot{E}x$	Exergy flow rate (kW)
f	Exergoeconomic factor
g	Specific molar Gibbs free energy (kJ/mol)
h	Specific molar enthalpy (kJ/mol)
m	Mass (kg)
$\dot{m}$	Mass flow rate (kg/s)
n	Equipment life time (years)
$\dot{n}$	Mole flow rate (mol/s)
N	Equipment annual operation period
P	Pressure (bar)
Q	Heat (kJ)
$\dot{Q}$	Heat flow rate (kW)
R	Gas constant (kJ/kmolK)
RCD	Relative cost difference
s	Specific molar entropy (kJ/mol.K)
t	Time (s)
T	Temperature (K, °C)
v	Specific molar volume (m^3/mol)
$\dot{W}$	Mechanical power (kW)
X	Heat recovery ratio
Z	Purchase cost ($)
$\dot{Z}$	Purchase cost flow rate ($/s)

Greek Letters

η	Efficiency
φ	Maintenance factor
ω	Acentric factor

Subscripts

bottom	Bottom heat pump
c	Critical
ch	Chemical
cv	Control volume
c_i	Compressor
d	Destruction
en	Energetic
evap	Evaporation
ex	Exergetic
F	Fuel
gen	Generation
i	State point
in	Inlet
k	Component
n	Species
o	Reference
P	Product
q	Heat
w	Mechanical power input
o	Reference state
1, 2,...	State numbers

Acronyms

BZT	Bethe-Zel'dovich-Thompson
C	Compressor
CEPCI	Chemical engineering plant cost index
Cu-Cl	Copper-Chlorine

CuCl	Cuprous chloride
$(C_6H_5)_2$	Biphenyl
EES	Engineering Equation Solver
Fe-Cl	Iron-Chlorine
Hg	Mercury
HX	Heat exchanger
Mg-I	Magnesium-Iodine
RCD	Relative cost difference

Superscripts

o	Reference
*	Relative to base case
Q	Heat
n	Species

Chapter 1: Introduction

1.1 Sustainable Development

Global warming is a motivation behind many research efforts in academia and industry, aimed at mitigating or eliminating its causes. This is especially important from an environmental point of view, which is directly or indirectly related to other pillars of sustainability: economic sustainability and social sustainability (Dincer and Rosen, 2007, Rosen, 2008). As all components of sustainability are linked to energy, it has become important to shift toward energy sustainability, as a step in achieving sustainable development. Sustainability concepts are causing many conventional notions in economy, politics, and technology to be reconsidered (Dincer, 2012).

Many requirements are to be considered in striving to achieve energy sustainability and, eventually, sustainable development. A particular requirement of interest is the enhancement of sustainable energy resources utilization to produce sustainable energy carriers that have high quality and quantity. These sustainable energy carriers can replace conventional ones (e.g. gasoline, kerosene, coal, natural gas) that are not environmentally sustainable as they contribute to global warming (Dincer and Rosen, 2007). Moreover, usage of the conventional fuels indirectly hinders achieving socioeconomic sustainability due to the negative effects of its emissions (e.g. CO_2, sulfur compounds, and NO_x compounds) on agriculture (e.g. acid rains) and health (e.g. respiratory diseases) (Dincer and Rosen, 2007). Sustainable energy carriers are used in sustainable thermal systems (i.e. energy systems). Sustainability is characterized by meeting the needs of the present generation without compromising the ability of future generations to meet their needs. Anything characterized as sustainable should be cost-effective, has no or low negative impact on the environment, and is non-harmful if not useful to society.

Hydrogen is an important energy carrier to facilitate the need of many major chemical processes as a feedstock. Hydrogen also can potentially be utilized as a transportation fuel in vehicles, and can be efficiently converted to electric power by employing fuel cells. This is consistent with a future hydrogen economy in which hydrogen is a major material energy carrier for meeting many of the global energy needs (Dincer, 2012). Moreover, as hydrogen is an essential feedstock for many petrochemical processes by which fertilizers are made, its abundance is

necessary to meet the nutritional needs of future population increase (Dincer and Rosen 2007; Sigfusson, 2007; Dincer, 2012).

The approximate global annual production of hydrogen is 50 million metric tons per annum compared to approximately 4000 million metric tons per annum of oil produced globally. Nowadays, 90-95% of hydrogen supplied is to meet the demand of the petrochemical industries, while the rest is used to meet the demand of merchants/consumers. The demand for hydrogen expected to increase annually by 5%-7% until 2018 (Bakennea et al., 2016). Figure 1.1 shows the average hydrogen production (according to methods) and applications based on 2004-2013 data.

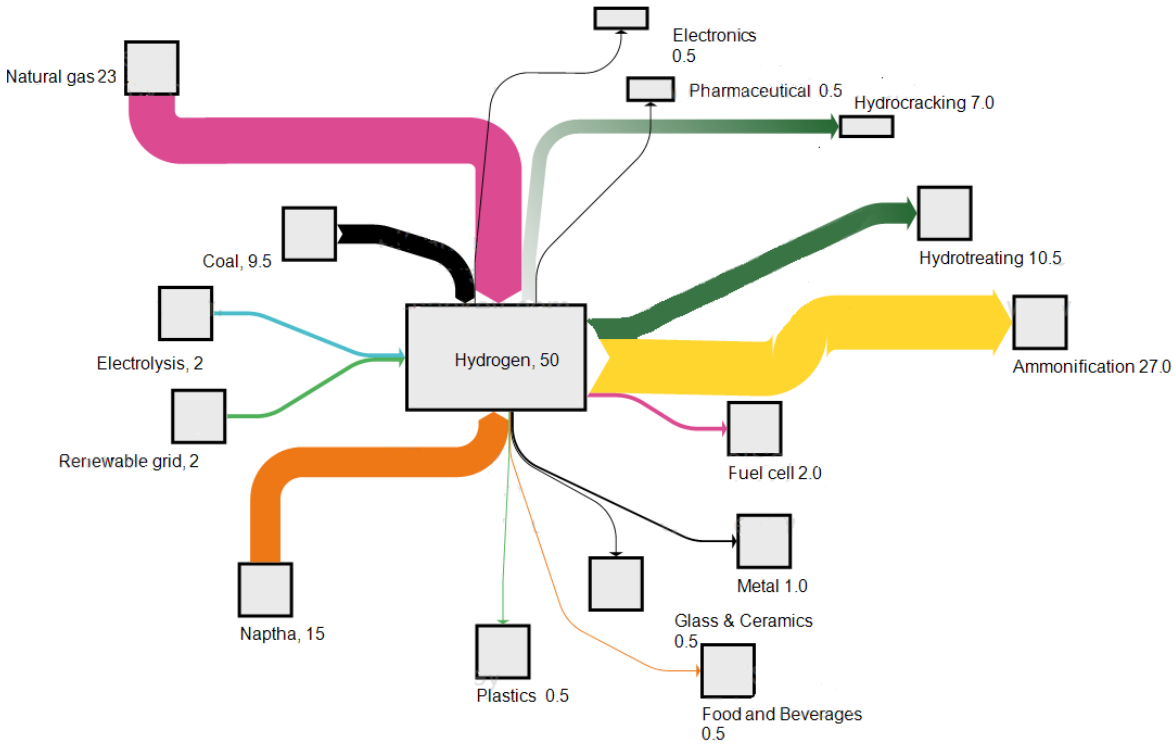

Figure 1.1. Average global hydrogen production and applications (modified from Bakennea et al. (2016)). Values are in million metric ton

1.2 Hydrogen Production Methods

There are many means of hydrogen production. But methods that are consistent with environmental sustainability can only be achieved utilizing green energy resources. Conventional methods of hydrogen production, for example steam methane reforming of fossil fuels are still

dominant and accounts for 90% of hydrogen produced while green methods of hydrogen production are still utilized to meet only 10% of the global demand (Dincer, 2012, Ozbilen et al., 2011). Steam methane reforming, for example, is produced in three steps. Methane is initially mixed with steam and converted into hydrogen and carbon monoxide (syngas). The second step is the potential route of producing hydrogen by converting carbon monoxide and water to hydrogen and carbon dioxide, the water-gas shift. To date, steam methane reforming is one of the least expensive hydrogen production methods (Bakennea et al., 2016).

Environmentally sustainable hydrogen production can also be achieved by using sustainable renewable energy resources to run sustainable hydrogen production systems. Solar energy can be used in different routes in terms of solar based hydrogen production method. Solar energy can be harvested by photovoltaic cells to produce electricity to run hydrogen production water electrolyzers. Another indirect solar based route to run electrolyzers is by using electric power produced solar thermal energy. Running electrolyzers by solar thermal electric power production is found to be more efficient and more environmentally friendly than running electrolyzers using electricity produced by photovoltaic cells (Joshi et al., 2011). Furthermore, other solar based hydrogen production methods include solar thermochemical, photoelectrochemical, photo biological, and photocatalytic (Dincer, 2012).

Electrolysis hydrogen production can also be coupled with other energy resources. For instance, geothermal, wind, hydro, and ocean thermal can all be used to produce electric power to meet electricity demand and simultaneously run electrolysis hydrogen production (Dincer, 2012).

Nuclear energy, and thermal energy recovered from industries, are also environmentally friendly energy sources that can be utilized by means of thermal energy or electric energy to produce hydrogen. The review by Bakennea et al. (2016) suggests that hydrogen production through water electrolysis processes, coupled with nuclear energy power plants, can be the least expensive (e.g. reported values collected from literature are 2.4 \$/kg-H_2) compared to electrolysis processes coupled with renewable energy harvesting systems (e.g. minimum reported value for onshore wind range 2.4-3.3 \$/kg-H_2) (Bakennea et al., 2016). In addition, nuclear energy and industrial heat recovery can be good sources for thermochemical hydrogen production methods, whether by high temperature sources that can be used directly, or lower sources that can have their heat upgraded.

One of the promising future options to be considered for hydrogen production, in terms of environmental and energy sustainability, is thermochemical water splitting. This process is based on the idea that a particular chemical reaction route can be taken with the inclusion of water, which in turn leads to having hydrogen as a product in the end. Based on safety, environmental, technical, and financial factors, thermochemical hydrogen production cycles such as the sulfur-iodine (S-I), the copper-chlorine (Cu-Cl), the iron-chlorine (Fe-Cl), the magnesium-iodine (Mg-I), and other cycles are expected to be commercially viable hydrogen production methods (Lattin and Utgikar, 2009; Naterer et al., 2009; Adewale et al., 2015).

1.3 Copper-Chlorine (Cu-Cl) Thermochemical Hydrogen Production

The Copper-chlorine (Cu-Cl) thermochemical water splitting cycle is a promising technology compared to its counterparts, particularly due to its lower temperature requirement (below 550°C) as other thermochemical cycles require a minimum temperature of 800°C. Other advantages include the availability of chemical agents, low electrochemical cell voltage, and financial advantages. The latter are due to less expensive materials and maintenance expenditures (Naterer et al., 2009, Naterer et al., 2013). There is also the possibility to have the Cu-Cl cycle thermal needs met by waste heats and heat recovery from lower temperature heat sources (Naterer et al., 2009, Naterer et al., 2013).

Many experimental, theoretical, and economic studies have been reported on the enhancement of the Cu-Cl cycle, including initiatives to overcome its challenges, integrate it with other systems, and identify and locate its major exergy destruction (Lewis et al., 2009; Ferrandon et al., 2010; Ozbilen et al., 2011, 2012; Ratlamwala and Dincer, 2012; Aghahosseini et al., 2013; Naterer et al., 2013; Ratlamwala and Dincer, 2013, 2014; Pope et al., 2015).

The Cu-Cl hydrogen production cycle can be achieved in different configurations. Cu-Cl cycle hydrogen production systems that are proposed differ from each other in the number of steps. The cycle can exist in two-steps, three-steps, four-steps, or five-steps according to the chemical reaction steps existing in the system. Besides, each of these cycles, differing in number of reaction steps, may be proposed in different options (Orhan et al., 2012). The options for each process with a particular number of step differ from other configurations in their sequence, elimination, or inclusion of a particular reaction step that should not necessary exist in others. The reactions steps

of the four-step Cu-Cl cycle is shown in Table 1.1. It can be noticed from the table that the reaction step with the maximum temperature (500°C) is the oxygen production step, which involves the decomposition of copper oxychloride into cuprous chloride and oxygen. A schematic diagram of a particular four-step Cu-Cl cycle option is shown in Figure 1.2.

Table 1.1. Reactions in the four-step Cu-Cl cycle.

Step	Reaction	Temperature °C
Hydrogen production	$2CuCl\,(aq) + 2HCL\,(aq) \rightarrow 2CuCl_2 + H_2(g)$	<100 (electrolysis)
Drying	$CuCl_2(aq) \rightarrow CuCl_2(s)$	<100
Hydrolysis	$2CuCl_2(s) + H_2O(g) \rightarrow Cu_2OCl_2(s) + 2HCL(g)$	400
Oxygen production	$Cu_2OCl_2(s) \rightarrow 2CuCl\,(l) + O_2(g)$	500

(Source: Naterer et al., 2009)

The Cu-Cl hydrogen production cycle has a thermal efficiency in a range of 43-55% (Lewis et al., 2009; Orhan et al., 2012; Ratlamwala and Dincer, 2012) and can be increased further with heat integration and internal heat recovery. The cost of hydrogen produced in the Cu-Cl cycle is relatively low compared to other green hydrogen production methods and can reach up to 1.7 $/kg-$H_2$ (Bakennea et al., 2016). Moreover, Figure 1.3 shows that the CO_2 emission caused by the Cu-Cl cycle during its life cycle can be very low compared to the conventional and green hydrgoen production methods.

An important factor in the Cu-Cl hydrogen production cycle is the thermal energy requirement. A thermal energy supply to the Cu-Cl cycle is needed at suitable temperatures to satisfy the needs of its endothermic reactions and processes. The temperature range required for different processes of the Cu-Cl cycle range from 100°C to 530°C. In all Cu-Cl cycles proposed, the oxygen production step in the copper oxychloride (Cu_2OCl_2) decomposition reactor demands the highest thermal energy supply temperature (500°C to 530°C). The thermal need of the Cu-Cl cycle can directly be met by existing nuclear reactor temperatures (i.e. super-water cooled reactor). Lower temperature heat sources like industrial wastes/processes or CANDU reactor (Naterer et al., 2009; Naterer et al., 2013) can also be utilized to meet the thermal energy needed by the Cu-Cl cycle.

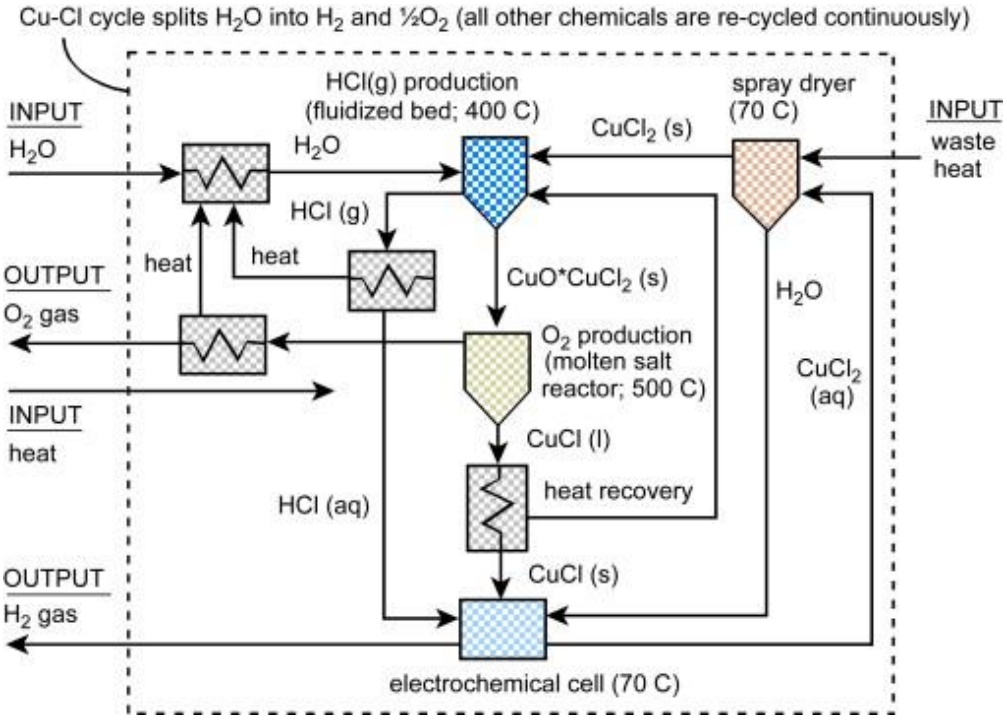

Figure 1.2. Schematic diagram of a four-step copper chlorine (Cu-Cl) hydrogen production process (Naterer et al., 2009).

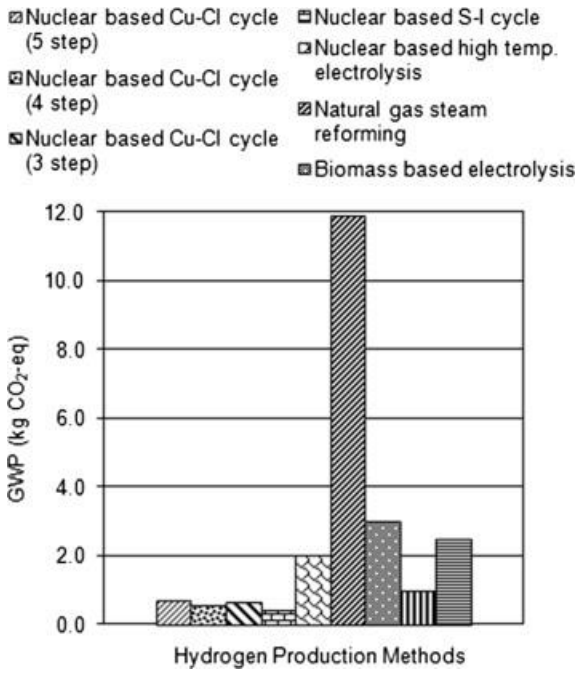

Figure 1.3. Life cycle analysis results of different hydrogen production methods with global warming potential (Naterer et al., 2011)

1.4 Literature Review

Although the Cu-Cl cycle does not demand as high temperatures of thermal energy supply as the other thermochemical water decomposition cycles listed previously, the high temperature requirement for its endothermic reactions is still demanding. Nevertheless, the lower operating temperature range compared to other cycles allow the Cu-Cl to be coupled with many other processes (e.g. industrial, power plants). A number of studies have examined proposals to upgrade heat from nuclear power plants or industrial waste to the temperature level needed to satisfy the thermal energy requirement of the Cu-Cl cycle. We now review these heat upgrading approaches, noting that most heat upgrading efforts reported in literature are limited to domestic applications (e.g. moderate or low temperature output).

1.4.1 Mechanical (vapor compression) heat pumps

A number of works propose vapor compression heat pumps as a method to upgrade heat for high temperature applications and processes including the Cu-Cl cycle.

Zamfirescu and Dincer (2009) presented four configurations of high temperature heat pumps that work with Bethe-Zel'dovich-Thompson BZT fluids. A number of 17 BZT retrograde heat pump working fluids were studied. It was shown that a heat pump operating with the BZT fluid that have a T-s diagram that is skewed compared to that for regular fluids (See Figure 1.4) has the greatest COP compared to other heat pump configurations. The conditions for high coefficient of performance, like high compressor isentropic efficiencies, are pointed out.

In other works, Zamfirescu et al. (2009) investigated the performance of the vapor compression heat pump with four working fluids, two organic fluids: biphenyl $(C_6H_5)_2$, naphthalene $C_{10}H_8$, and two titanium based fluids: titanium tetrabromide $TiBr_4$, and titanium tetraiodide TiI_4. All of the showed a promise means of upgrading heat as they all exhibit good energetic and exergetic COPs. The lowest COPs occur for a system using (COP_{en}: 1.9–4.6; COP_{ex}: 1.1–2.2) and the highest for a system using titanium tetraiodide (COP_{en}: 2.8–7.3; COP_{ex}: 1.6–4.3). In the study, some conditions were set as constraints. Biphenyl and naphthalene are both retrograde fluids and their usage in heat upgrading requires superheating prior to compression from the evaporator pressure. Such superheating can be achieved by internal heat recovery from the high temperature fluids prior to expansion of the saturated vapor leaving the evaporator, see Figure 1.5. A significant constraint for the titanium based fluids is that they require a two-phase compression

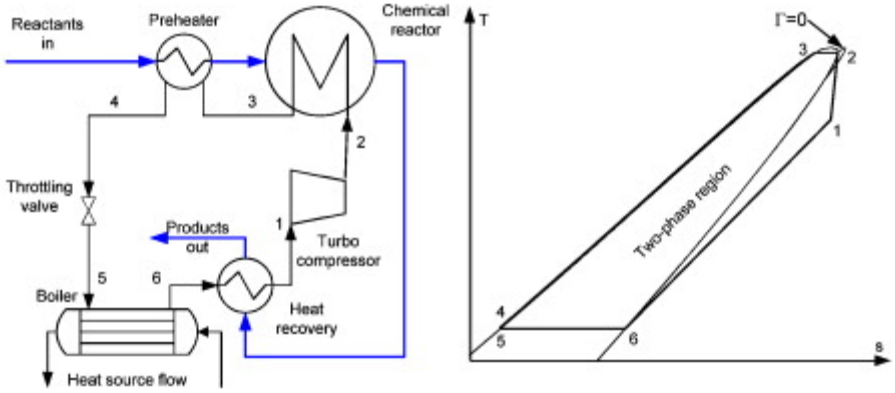

Figure 1.4. A schematic diagram and T-s diagram of the BZT heat pump configuration and suitable retrograded T-s diagram shape that achieves highest COPs (modified from Zamfirescu and Dincer (2009))

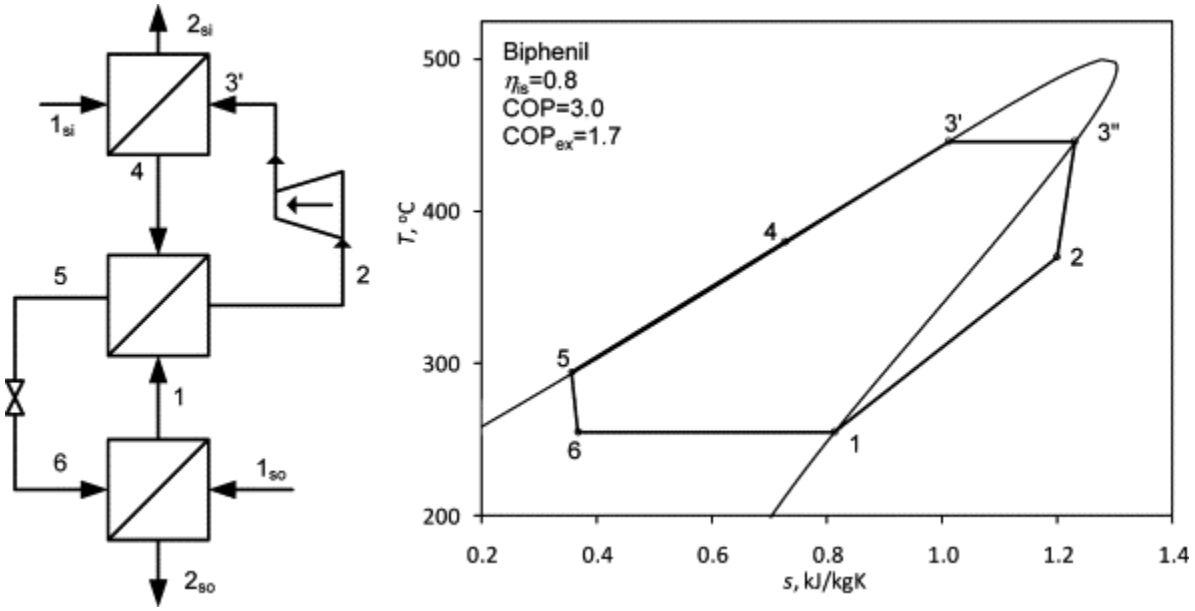

Figure 1.5. A schematic diagram and T-s diagram shows the biphenyl heat pump that requires superheating prior compression due to the retrograded characteristic of the fluid (modified from Zamfirescu et al. (2009))

An additional effort related to vapor compression options is the cuprous chloride (CuCl) heat pump coupled with the copper oxychloride (Cu_2OCl_2) decomposition reactor studied by Zamfirescu et al. (2011), see Figure 1.6. This CuCl heat pump is based on the fact the CuCl is a

molecular compound not a salt formed by ionic bond (Powles, 1975). The CuCl was used as a working fluid that is heated by multi-stage compression with intercooling so that it can be fed to the copper oxychloride decomposition reactor as excess CuCl and as a thermal energy source for the endothermic reaction. Zamfirescu et al. (2011) obtained a high COP, in the range of 4.5 to 11 energetically and 2.5 to 6.0 exergetically.

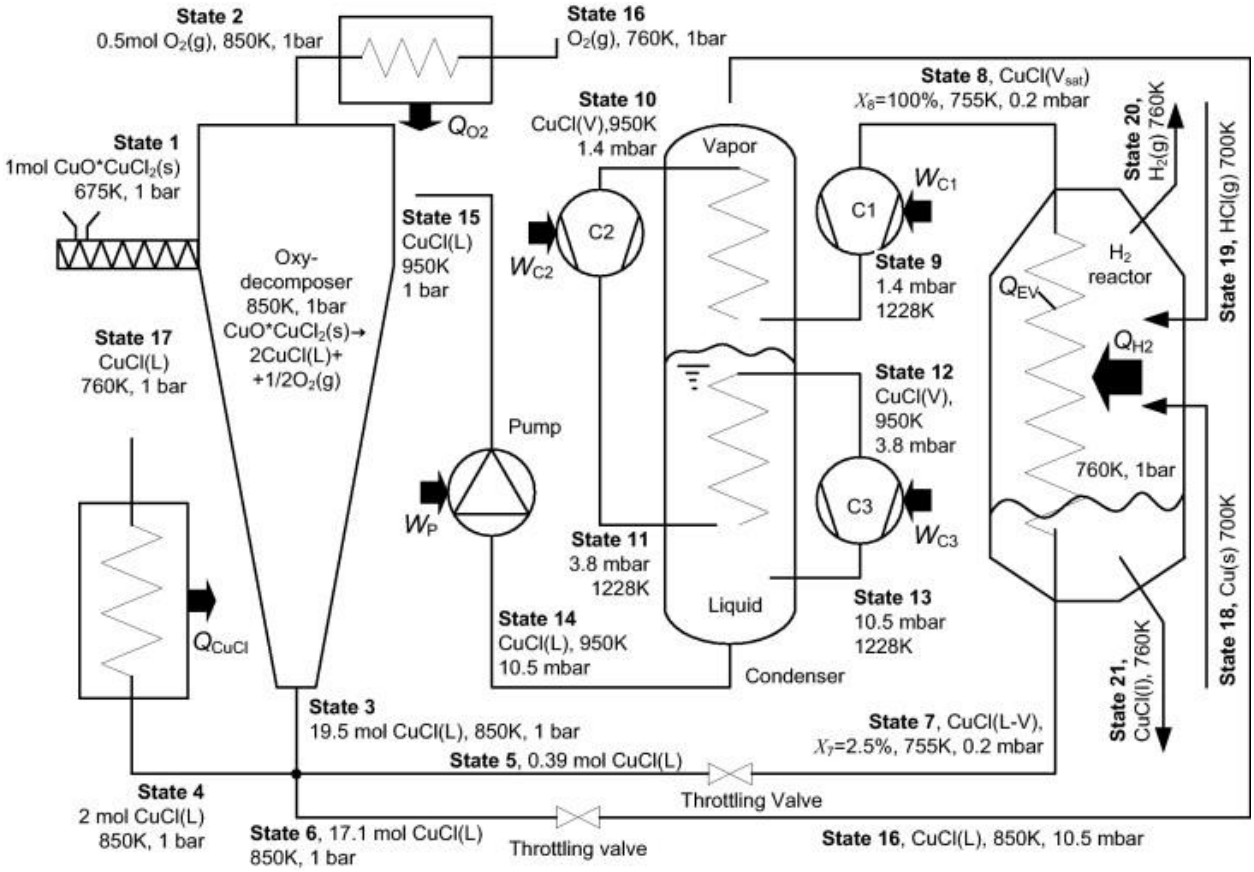

Figure 1.6. A schematic diagram shows the CuCl vapor compression heat pump coupled with the Cu-Cl cycle copper oxychloride decomposition reactor that produces CuCl and O_2 as products. CuCl produced is then utilized in the completion of the Cu-Cl cycle for hydrogen production (modified from Zamfirescu et al. (2011)).

1.4.2 Endothermic/exothermic chemical heat pumps

A number of chemical heat pumps based on endothermic and exothermic reactions were also proposed in other heat upgrading studies (i.e. temperature amplification mode) (Naterer et al., 2008). In Odukoya and Naterer (2014), the utilization of hydration and dehydration nature of CaO and $Ca(OH)_2$ in a chemical heat pump to supply heat to the copper oxychloride decomposition reactor was studied thermodynamically. The chemical heat pump was meant to recover heat from

a cement plant and had a COP of 4.6 at moderate operating conditions. The chemical heat pump was assumed to be operating as a continuous process (i.e. steady state), its transient state was again studied by Odukoya and Naterer (2015) to investigate the maximum temperature achievable. Another chemical heat pump study was done on the $CaO/Ca(OH)_2$ hydration/dehydration and $CaO/CaCO_3$ carbonation/decarbonation by Arjmand et al. (2013). They reported the results as an energetic efficiency of 0.83 and an exergetic efficiency that ranges from 0.84 to 0.88 for $CaO/CaCO_3$, and an energetic efficiency of 0.71 and exergetic efficiency that ranges from 0.60 to 0.65 for $CaO/Ca(OH)_2$.

Another endothermic/exothermic chemical heat pumps were studied with different source/sink temperature differences, only $CaO/Ca(OH)_2$ (450-550°C), $CaO/CaCO_3$ (850-950°C), and $BaO/Ba(OH)_2$ (700-800°C) covers the temperature of interest (>500°C) (Kerskes et al., 2011).

As most of these technologies are batch processes, Spoelstra et al. (2002) and Ogura et al. (2007) studied and proposed chemical heat pumps with continuous heating setting.

1.5 Motivation

A temperature greater than 500°C is needed for the copper oxychloride decomposition reactor, which is necessary in all Cu-Cl cycles options and regardless of the number of steps. In addition, Cu_2OCl_2 decomposition is considered to be the most thermal energy demanding process among other endothermic steps in the Cu-Cl cycle. Thus finding a means of upgrading heat from environmentally sustainable resources of an input temperature of 300°C (e.g. CANDU nuclear reactor (Khalid et al., 2016)) to a temperature range suitable for the reactor process (500-530°C) could contribute to making the Cu-Cl cycle viable from a sustainability point of view. The route relating sustainable development with the Cu-Cl copper oxychloride decomposition thermal need is shown in Figure 1.7.

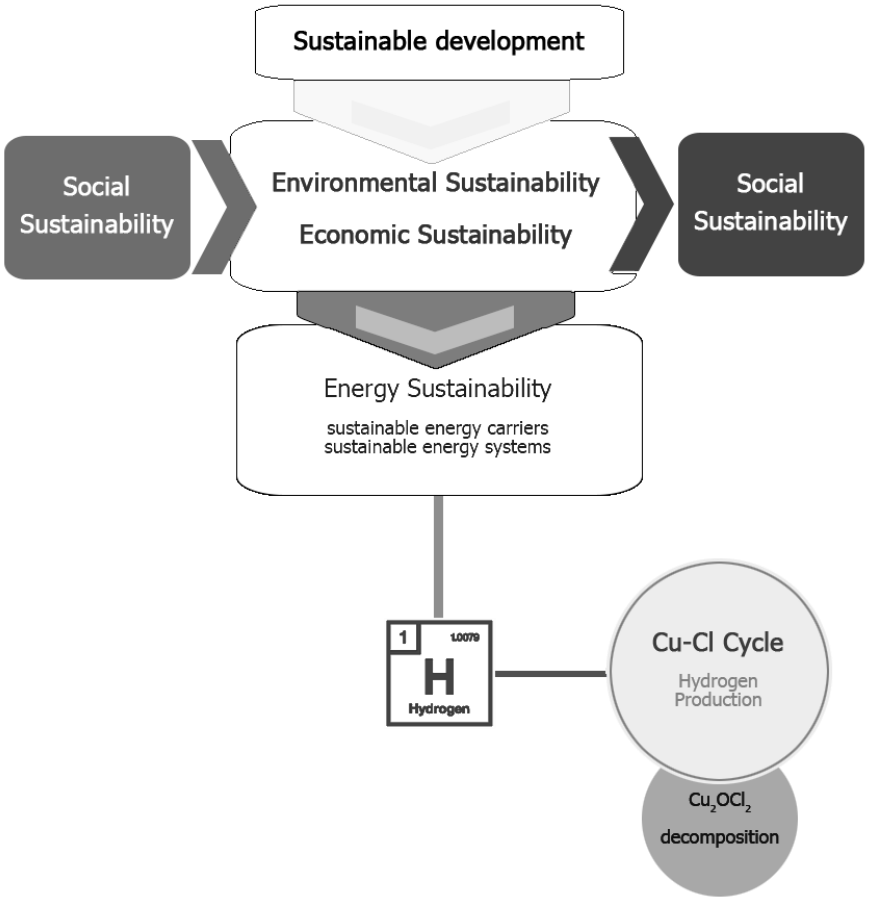

Figure 1.7. The relationship between copper oxychloride decomposition and sustainable development.

1.6 Objectives

Upgrading heat from a CANDU nuclear power plant, which produces heat at a temperature around (300°C), or industrial waste heat temperatures close to that value, are seen to be a future option to achieve the needed heat for the endothermic reactions. The CuCl vapor compression heat pump proposed by Zamfirescu et al. (2011) is an option to meet the highest temperature requirement in Cu-Cl cycle, the Cu_2OCl_2 decomposition reactor (500-530°C). However, the CuCl heat pump requires a bottom heat pump be cascaded with it, as its evaporator operates at significantly sub-

atmospheric pressure (0.2 mbar) to accommodate source temperatures greater than 755 K (482°C) and to achieve an evaporator temperature of 300°C. To accommodate nuclear reactor heat, therefore, the evaporator pressure needs to be very low, below 0.00038 mbar.

The specific objectives of this thesis study are listed as follows:

- To develop and improve understanding of a cascaded heat pump consisting of a CuCl vapor compression heat pump and a bottom heat pump to upgrade heat from about a 573 K (300°C) source temperature to the required temperature of the copper oxychloride decomposition reactor or 773-803 K (500-530°C).
- To study the properties of three potential working fluids to be utilized in high temperature heat pumps for heat upgrading applications and determine suitable thermodynamic methods and equations of states for high accuracy thermophysical properties calculation. These working fluids are cuprous chloride (CuCl), mercury (Hg), and biphenyl ($C_6H_5)_2$. In addition, the most suitable heat pumps configurations (i.e. number of compression and intercooling stages required) are to be considered based on the working fluids nature.
- To develop a comprehensive thermodynamic model and exergoeconomic model for analysis of the systems thermodynamically and exergoconomically using balance equations derived from thermodynamic and economic principles.
- To create a flowsheet for the systems and calculate the state points, use them to calculate the exergy destruction rate in each system component, and to quantify the energetic and exergetic coefficient of performances for sole heat pumps and cascaded heat pumps.
- To perform a comprehensive parametric study on the base case of the systems to evaluate the influence of important parameters in each of the top and bottom heat pumps on the performance parameters (e.g. COP, recovery ratios) and exergoeconomic evaluation parameters (e.g. total cost flow rate and exergy destruction cost flow rate). Assess the performance of overall cascaded heat pumps and individual heat pumps and compare their performance and costs to see the advantage of each one over the other.

Chapter 2: System Description

We present here the proposed heat pumps to supply heat to copper oxychloride decomposition reactor in the copper chlorine Cu-Cl hydrogen production cycle. Unlike the work of Zamfirescu et al. (2011), two systems are proposed, each consisting of two cascaded heat pumps. For cascading we have to include a number of heat exchangers and remodel the CuCl heat exchanger used for intercooling to be two heat exchangers, HX3 and HX4. The cuprous chloride (CuCl) vapor compression cycle is selected to be the top cycle in both options. In system 1 the bottom heat pump cycle uses mercury (Hg) in a multi-stage vapor compression using three compressors, while in system 2 the heat pump uses the organic material hydrocarbon biphenyl in a single compression unit with an internal heat recovery heat exchanger.

2.1 System One: Cuprous Chloride – Mercury Cascaded Heat Pump (CuCl-Hg)

The heat pump shown in Figure 2.1 uses mercury (Hg) as the bottom cycle and cuprous chloride in the top cycle. We begin explaining the system from the heat recovery point where the heat source is from either a nuclear power plant or industrial waste heat. The lowest heat temperature at the source is taken to be at about 573 K (300°C) as a base (i.e. reference case). The two phase fluid mercury at state 28 flows into the heat recovery heat exchanger and is converted to a saturated vapor at state 21 as it leaves. The saturated vapor at state 21 is compressed by the first multi-stage compressor in mercury heat pump C4 and exits at state 22 as a compressed superheated vapor with a higher pressure and higher temperature. The superheated vapor leaving compressor C4 at state 22 is intercooled in HX5 before entering the second compression stage of compressor C5 at state 23. As the vapor is compressed from state 23 to state 24, it is intercooled in another heat exchanger HX6.

Intercooling is significant process in multistage compression. As the superheated vapor temperature increases due to compression, so does its specific volume. The increase in specific volume contributes to the increase in mechanical power consumption needed to meet the compression requirement. Thus intercooling is placed between each two compression stages to lower the temperature of the superheated vapor and reduce the power consumption. Another factor

to be considered is the fact that direct compression with a single compressor may lead to a very high temperature superheated fluid leaving the compressor that the less expensive conduit materials cannot withstand. Moreover, the chemical stability may also be a concern, as the temperature of the compressed vapor could reach sufficiently high temperature that would lead to material degradation.

The intercooling stages in the mercury heat pump, taking place in HX5 and HX6, simultaneously contribute to the evaporation stage of the two-phase CuCl of the top heat pump evaporator. HX7 is the last heat exchanger in the mercury heat pump where the vapor compressed in the last compression stage C6, and leaving as state 26, contributes to fully convert the two-phase CuCl in the top heat pump evaporator to a saturated vapor to be compressed. The fluid at state 27 leaves the heat exchanger HX7 as a saturated liquid or a two phase fluid having a low vapor quality. The hot stream temperature approach to the cold stream is taken to be constant at 5 K for HX5 and HX6. The pressure increase across each compressor are equivalent (i.e. $\Delta P_{c4} = \Delta P_{c5} = \Delta P_{c6}$) in the base case.

As any typical vapor compression heat pump, the evaporator of the CuCl heat pump has the lowest pressure in the cycle and in which the CuCl is converted from a mixture of vapor and liquid to a saturated vapor by gaining heat from the bottom mercury heat pump. So the expanded two-phase mixture of state 7 first enters heat exchanger HX1, where sensible heat is recovered from the CuCl (enters as state 4, exits as state 4-1), produced from the decomposition reaction, before it is exported for hydrogen production applications. After leaving HX1 at state 7-1, the CuCl enters another heat recovery heat exchanger HX2 where it recovers heat from the oxygen produced from the decomposition reaction. The CuCl leaves heat exchanger HX2 at state 7-2 and then gains heat from heat exchangers HX5 and HX6, which simultaneously perform the intercooling of multi-stage compression in the mercury heat pump. The two phase fluid at state 7-4 is eventually transformed into a saturated vapor at state 8 as it gains heat from the mercury heat pump through last heat exchanger HX7.

After the CuCl is fully converted to a saturated vapor at state 8, it enters a three compressor multistage compression device. The first compression stage takes place in compressor is C1 (state 8 to state 9) and is followed by intercooling (state 9 to state 10) through heat exchanger HX3. The second compression stage of CuCl vapor takes place im compressor C2 (state 10 to state 11) and

is followed by an intercooling in HX4 (state 11 to state 12). The high temperature of the superheated vapor is intercooled by a subcooled stream 16 which has a lower temperature than the compressed vapor but higher pressure then the evaporator. The stream 16 route is an excess CuCl route that is technically added to achieve multistage compression intercooling. The pressure increase across each compressor are equivalent, i.e., $\Delta P_{c1} = \Delta P_{c2} = \Delta P_{c3}$.

After multi stage compression, the CuCl vapor exits the last compression stage C3 with a pressure equivalent to the stream at state 16. This stream is originally an excess CuCl subcooled liquid that was expanded from the liquid saturation line at 1 bar pressure after leaving the reactor. The hot temperature vapor at state 13 and the subcooled liquid at state 16-2 are mixed in the mixer and depart as a saturated liquid at state 14. Note that the saturation temperature of the mixer pressure is equivalent to the temperature of the excess CuCl we intend to inject into the reactor (e.g. P_{mixer}=P16= P_{sat} @ T_{15}).

The saturated liquid at state 14 leaving the mixer is pumped to the reaction pressure of the copper oxychloride decomposition reactor (1 bar), and leaves at state 15 and is injected into the reactor as an excess CuCl thermal energy source for Cu_2OCl_2 (stream 1) decomposition. The endothermic reaction in the reactor takes place as follows:

$$Cu_2OCl_2 \xrightarrow{\text{Heat from (stream 15) CuCl}} \frac{1}{2}O_2 + 2CuCl$$

The decomposition can be achieved with a reaction temperature range greater than 773K (greater than 500°C) and the temperature of excess CuCl at stream 15 is higher than that. The excess CuCl leaves mixed with the CuCl produced from the reaction at state 3 while the oxygen (O_2) produced via the reaction leaves the reactor at state 2. Streams leaving the reactor have the temperature of the reactor and the sensible heat of the produced CuCl at state 4 and the produced O_2 at state 2 are recovered by the CuCl stream at state 7 in the evaporator as explained previously. The produced CuCl is then sent to the Cu-Cl cycle for hydrogen production.

The excess CuCl is recirculated, while the CuCl to be evaporated and compressed is expanded from state 5 to state 7 (the lowest heat pump pressure), and the CuCl to be used for intercooling is expanded from state 6 to state 16, which is at an intermediate pressure.

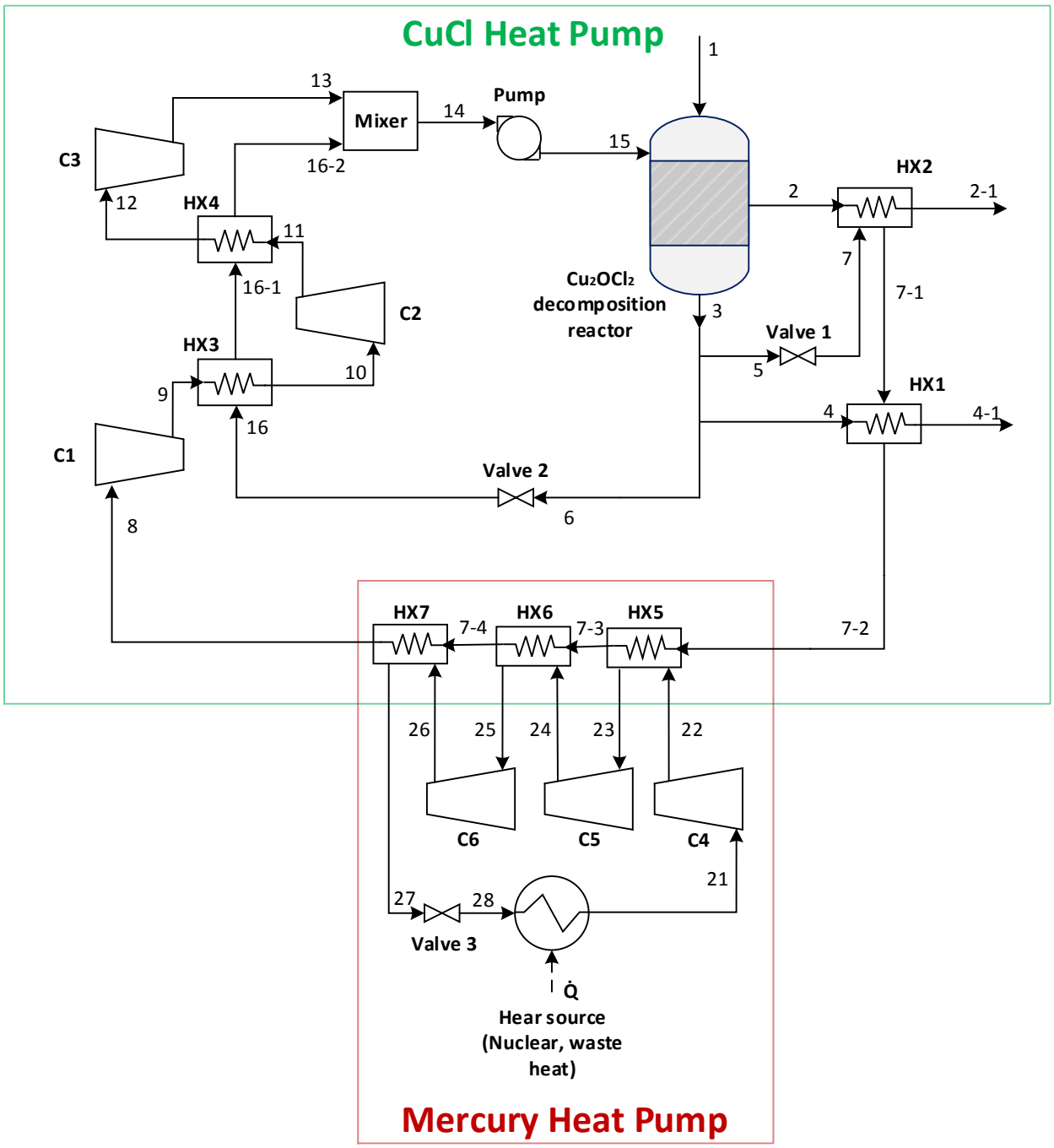

Figure 2.1. A schematic diagram of the proposed Cuprous Chloride – Mercury Cascaded Heat Pump (CuCl-Hg).

2.2 System Two: Cuprous Chloride – Biphenyl Cascaded Heat Pump (CuCl-$(C_6H_5)_2$)

The second cascaded heat pump proposed in this work is the cuprous chloride – biphenyl heat pump CuCl-$(C_6H_5)_2$ and it is shown in Figure 2.2. The function of this heat pump is similar to the heat pump previously discussed except that the bottom heat pump operates with biphenyl as a working fluid.

The two-phase mixed biphenyl at state 25 gains heat as it flows through the heat exchanger, recovering heat from the low temperature heat source and exits as a saturated liquid at state 26. Prior to compression, the saturated liquid at state 26 is superheated further by an internal heat recovery heat exchanger HX6. The heat is recovered from the stream at state 23, which then exits the heat exchanger HX5 which is responsible for evaporating the CuCl in the CuCl heat pump evaporator.

Heat exchanger HX6 is necessary due to the retrograde nature of the biphenyl. If the saturated vapor is pressurized in the compressor, it becomes a two-phase vapor-liquid fluid that eventually damages the compressor. However, preheating the biphenyl will assure that it remains a vapor during compression.

The superheated biphenyl leaves HX6 at state 27 and is compressed by compressor C4 to state 22 which is used to evaporate the CuCl through heat exchanger HX5. For clarification, Table 2.1 shows the temperature, pressure, and mole flow rate of the state points calculated from Aspen Plus. Thermodynamic properties such as molar enthalpy and molar entropy will be presented when as results in later chapters.

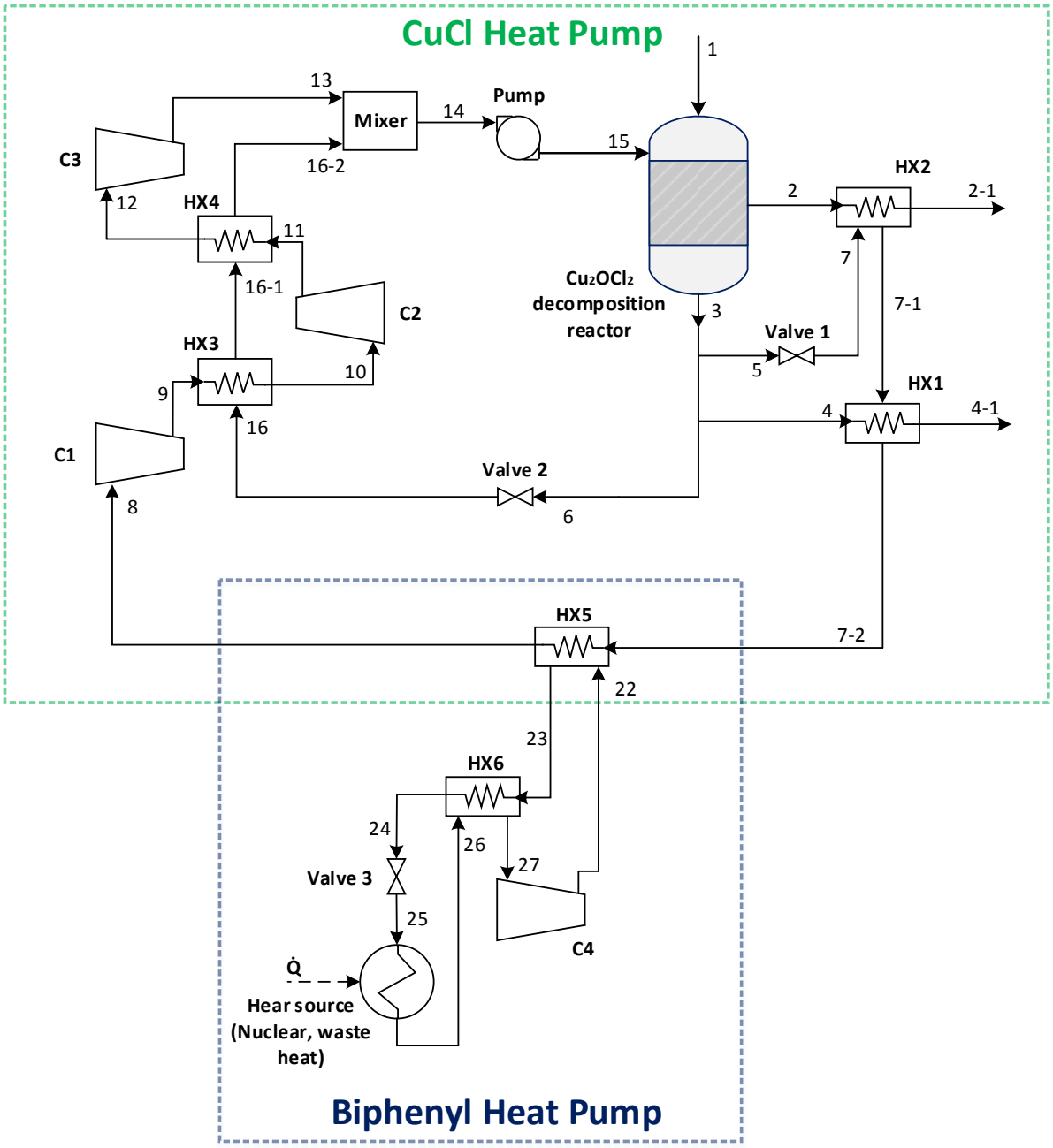

Figure 2.2. A schematic diagram of the proposed Cuprous Chloride – Biphenyl Cascaded Heat Pump ($CuCl\text{-}(C_6H_5)_2$).

Table 2.1. Temperature, pressure, and mole flow rate for heat pumps state points for (a) CuCl Heat Pump, (b) Mercury heat pump, and (c) Biphenyl heat pump.

(a) CuCl Heat Pump			
State	**T (K)**	**P (bar)**	**ṅ (mol/s)**
1	675.00	1.0000	0.788
2	850.00	1.0000	0.394
3	850.00	1.0000	19.075
4	850.00	1.0000	1.575
5	850.00	1.0000	0.389
6	850.00	1.0000	17.111
7	754.65	0.0002	0.389
7-1	754.65	0.0002	0.389
7-2	754.65	0.0002	0.389
7-3	754.65	0.0002	0.389
7-4	754.65	0.0002	0.389
8	754.65	0.0002	0.389
9	1549.18	0.0036	0.389
10	950.00	0.0036	0.389
11	1126.75	0.0071	0.389
12	950.00	0.0071	0.389
13	1052.17	0.0105	0.389
14	950.00	0.0105	17.500
15	950.00	1.0000	17.500
16	850.00	0.0105	17.111
16-1	858.90	0.0105	17.111
16-2	861.52	0.0105	17.111

(b) Mercury Heat Pump			
State	**T (K)**	**P (bar)**	**ṅ (mol/s)**
21	568.96	0.30	0.916
22	1565.14	2.93	0.916
23	760.00	2.93	0.916
24	1021.13	5.56	0.916
25	760.00	5.56	0.916
26	910.34	8.20	0.916
27	760.84	8.20	0.916
28	568.96	0.30	0.916

(c) Biphenyl Heat Pump			
State	T (K)	P (bar)	ṅ (mol/s)
22	800	30	2.37
23	760.61	30	2.37
24	646.28	30	2.37
25	561.56	2	2.37
26	561.57	2	2.37
27	726.07	2	2.37

Chapter 3: Model Development and Analyses

This chapter is specified to discuss and explain the physical properties, energy, and exergy thermodynamic analyses relevant to the proposed cascaded heat pumps. At the beginning we will explain the thermophysical properties used to obtain the state points of the pure substances involved in the heat pumps. Then we will explain the thermodynamic analysis and balance equations from the aspect of first law of thermodynamics and second law of thermodynamics. After that, the exergoeconomic analyses tools, cost flow rate balance equations, and equating of streams cost per exergy unit according to fuel and product rules are presented and discussed.

3.1 Thermophysical properties of pure substances

Giving some detail about the thermophysical properties of pure substances used in the analyses is of great importance, especially with an existence of data discrepancy for some pure substances involved in our systems modeling and analyses. Besides the fact that mercury temperature-dependent properties have been calculated with the ideal gas equation of state in Aspen Plus and such values need to be compared with values of properties calculated empirically for quality control.

3.1.1 Cuprous chloride (CuCl)

The thermophysical properties of CuCl used in Aspen Plus that are in concern and related to thermodynamic analysis are as follow:

1- The heat capacity used for CuCl in gas and liquid phases are both obtained from Engineering Equation Solver (EES) software (fChart, 2015) through the curve fitting tool to match Aspen Plus correlation (3.1) which is inserted in the TABPOLY thermodynamic methods specification sheet in Aspen Plus. That is,

$$\mathrm{Cp}\ \left(\frac{\mathrm{kJ}}{\mathrm{kmolK}}\right) = a_1 + a_2 T + a_3 T^2 + a_4 T^3 + \frac{a_5}{T} + \frac{a_6}{T^2} + \frac{a_7}{\sqrt{T}} + a_8 \ln T \qquad (3.1)$$

The coefficients obtained for the liquid phase through EES curve fitting are:

$a_1 = 0.276685135, a_2 = -0.000201376, a_3 = 9.13 \times 10^{-8}, a_4 = -1.56 \times 10^{-11},$

$a_5 = -130.881994$ and $a_6 = 36115.8377.$

The reference enthalpy and entropy are adjusted to be at 696 K, as it is the minimum liquid temperature with available properties in EES, then $h^{o}_{liquid,969K} = -118.554\ kJ/mol$ and $s^{o}_{liquid,969K} = 0.1566\frac{kJ}{molK}$ for a 696-1685 K temperature range .

The ideal gas heat capacity coefficients obtained from EES curve fitting and used in the Aspen Plus TABPOLY specification sheet are

$a_1 = 0.036534634, a_2 1.32462 \times 10^{-6}, a_3 = -3.95 \times 10^{-10}, a_4 = 6.99 \times 10^{-14},$

$a_5 = 0.407417915$ and $a_6 = -303.301646.$

The reference enthalpy and entropy are also adjusted for the gas phase to be at 696 K, so that $h^{o}_{gas,969K} = 105.635\ kJ/mol$ and $s^{o}_{gas,969K} = 0.2682\frac{kJ}{molK}$ for a 696-1685 K temperature range. The melting point of CuCl is 703K (430°C), its boiling point is 1763K (1212°C), and its critical temperature is 2435K (2162°C) according to The Design Institute for Physical Properties (DIPPR) (Rowley et al., 2004).

2- The thermodynamic method used in Aspen Plus for CuCl is IDEAL, which considers the compound to behave as an ideal gas and an ideal liquid. The calorimetric properties are calculated in simulation by means of the ideal gas equation of state. Zamfirescu et al. (2011) explain how ideal gas equation of state are suitable for our calculation as the vapor phase are all existing in very low pressure in the CuCl heat pump and the liquid CuCl is only temperature dependent. The variation of vapor specific enthalpy with respect to pressure at isothermal conditions is negligible (i.e. $(\frac{\partial h}{\partial P})_T = 0$) while pressure dependence is considered in the molar entropy calculation

$$s(T,P) = s(T,P_0) + RT\ln(\frac{P_0}{P}) \quad (3.2)$$

3.1.2 Biphenyl $(C_6H_5)_2$

Biphenyl is an option in our work for being a working fluid in a bottom heat pump to upgrade heat from the low temperature source to the CuCl heat pump evaporator. It is an aromatic retrograde hydrocarbon that can be produced industrially through fossil fuel distillation and occurs in naturally within natural gas and crude oil. The thermophysical properties of biphenyl and many of its physical characteristics are obtained and understood from DIPPR (Rowley et al., 2004) and

they are contained in Aspen Plus databank. Biphenyl has a normal boiling point temperature of 529 K (256°C) which makes it suitable as a working fluid for high temperature heat pumps, as in our case. The critical temperature of biphenyl is about 773 K (500°C) which is greater than the temperature range we want to achieve in the heat sink, the CuCl evaporator. Nevertheless, the critical temperature is of great importance in the equation of state used to relate temperature, pressure and volume and for the thermodynamic properties calculations using the Peng-Robinson equation of state. Biphenyl is also stable up to 873K (600°C) temperatures. The DIPPR thermophysical properties of biphenyl are shown in Table 3.1.

Table 3.1. Thermophysical properties of biphenyl.

Properties	**Biphenyl**
Chemical formula	$(C_6H_5)_2$
Molecular mass (kg/kmol)	154.2
Melting point (°C)	69.05°C (342.05 K)
Normal boiling point (°C)	256°C (529 K)
Autoignition temperature (°C)	540°C (813 K)
Flash point (°C)	113°C (386 K)
Critical temperature (°C)	500°C (773 K)
Critical pressure (bar)	33.8
Critical volume (m/kmol)	0.497
Critical compressibility	0.261
Acentric factor	0.40287
References	(Rowley et al., 2004) (Zamfirescu et al., 2009)

The Peng-Robinson equation of state (Peng and Robinson, 1976, Koretsky, 2004) is aproperiate for calculating the state point properties of any fluids realted to natureal gas processing, including biphenyl. The Peng robinson equation general form is

$$P = \frac{RT}{v-b} - \frac{a\alpha(T)}{v(v+b)+b(v-b)} \tag{3.3}$$

where

$$a = 0.45724 \frac{R^2 T_c^2}{P_c} \tag{3.4}$$

$$b = 0.07780 \frac{RT_c}{P_c} \tag{3.5}$$

$$\alpha(T) = [1 + k\left(1 - \sqrt{\frac{T}{T_c}}\right)]^2 \tag{3.6}$$

$$k = 0.37464 + 1.54226\ \omega - 0.26992\ \omega^2 \tag{3.7}$$

and where P is the pressure, R=8314.472 kJ/molK is the universal ideal gas constant, T is the temperature, v is the specific volume, T_c is the critical temperature, P_c is the critical pressure, and ω is the eccentric factor. Critical properties needed here and the eccentric factor are shown in Table 3.1.

3.1.3 Copper Oxychloride (Cu_2OCl_2)

Zamfirescu et al. (2010) collected thermophysical properties of copper compound involved in the copper chlorine hydrogen production thermochemical cycle considered here. They collected various properties of Cu_2OCl_2 from the literature, and they found some disagreements in the experimental specific heat measurements between Kawashima et al. (2007) and Parry (2008). Zamfirescu et al. (2010) also developed temperature-dependent property correlations, from which we are using the properties of Cu_2OCl_2 in the analysis of the copper oxychloride reactor. The value of the enthalpy of formation entered in Aspen Plus is $\Delta_f h^o = -384.65 \pm 2.5$ kJ/mol and the value of the Gibbs free energy of formation is $\Delta_f g^o = -369.7$ kJ/mol. The specific heat correlation they developed and used here is

$$Cp\ \left(\frac{kJ}{mol.K}\right) = a + bT + cT^2 + dT^3 \tag{3.8}$$

where

$$a = 53.716657, b = 0.334033497, c = -0.00052212794, d = 2.9995 \times 10^{-7}$$

The specific heat values for the CuCl and Cu_2OCl_2 are used by Aspen Plus to obtain other properties including, specific enthalpy, specific entropy, specific Gibbs free energy, and specific exergy.

3.1.4 Mercury (Hg)

Mercury is one of the two working fluids used in the bottom heat pump that upgrades heat from the low temperature heat source to the temperature of the CuCl evaporator in the top cycle heat pump. Mercury exists as a metal liquid in ambient conditions, its boiling point is 630 K (357°C), its critical temperature is 1750 K (1477°C), and its critical pressure is 17.2 bar. Mercury is suggested for use as a top cycle in a cascaded power generation Rankine cycle (Dincer and Zamfirescu, 2014). The IDEAL thermodynamic method in Aspen Plus is used for the calculation of mercury thermodynamic properties. As it is difficult to enter equation of states other than the ones included in Aspen Plus, a comparison between the calculated saturated pressure, enthalpy of vaporization, and entropy of vaporization is made with data of Sugawara et al. (1962) for a quality check of the ideal method. These comparison are shown in Tables 3.2, 3.3, and 3.4. It can be seen that the differences between the values calculated with the Aspen Plus IDEAL method and experimental calculations of Sugawara et al. (1962) are low (<5%) for the temperature range of interest 250°C-500°C.

In open literature, it has been found that mercury has never been tested in a lab scale as a heat pump working fluid, but it has been tested as a Rankine cycle working fluid (Gutstein et al., 1975). Therefore, as another quality check, the ideal gas thermodynamic method assumption made for mercury is compared with the experimental results by means of turbine power output. In Gutstein et al. (1975), a mercury turbine with an efficiency of 56% is used to expand a vapor mercury of 1724 kPa (250 psia) pressure, 677^{0}C (1250^{0}F) temperature, and 1.5 kg/s (11800 lb/h) mass flowrate to a turbine outlet pressure of 96.5 kPa (14 psia) to generate a 64 kW shaft power. This experimental condition is simulated in Aspen Plus and the power output is found to be 4.5% different (67 kW) from the experimental power output, see Table 3.5.

Table 3.2 Comparison between saturation pressure calculated by Aspen Plus and experimental vapor pressure measured by Sugawara et al. (1962)

	Saturated Pressure		
T	P_{sat} by Sugawara et al. (1962)	P_{sat} by Aspen Plus	Difference
°C	kg/cm^2	kg/cm^2	%
200.000	0.024	0.024	0.098
250.000	0.101	0.101	0.118
300.000	0.336	0.335	0.171
350.000	0.916	0.914	0.286
400.000	2.148	2.138	0.479
450.000	4.471	4.438	0.734
500.000	8.457	8.373	0.994
550.000	14.800	14.614	1.255
600.000	24.290	23.929	1.487
650.000	37.800	37.154	1.709
700.000	56.260	55.176	1.926
750.000	80.640	78.913	2.141
800.000	112.000	109.301	2.410

Table 3.3 Comparison between evaporation enthalpy values calculated by Aspen Plus with values calculated from experimental measurements by Sugawara et al. (1962).

	Saturated evaporation enthalpy		
T	Δh_{evap} by Sugawara et al. (1962)	Δh_{evap} by Aspen Plus	Difference
°C	kcal/kg	kcal/kg	%
200.000	71.824	74.130	3.211
250.000	71.434	72.999	2.190
300.000	71.045	71.838	1.117
350.000	70.630	70.647	0.024
400.000	71.180	69.423	2.469
450.000	69.660	68.162	2.150
500.000	69.060	66.863	3.181
550.000	68.350	65.521	4.139
600.000	67.500	64.133	4.988
650.000	66.510	62.694	5.737
700.000	65.360	61.199	6.366
750.000	64.010	59.642	6.824
800.000	62.490	58.016	7.160

Table 3.4 Comparison between evaporation entropy values calculated by Aspen Plus with values calculated from experimental measurements by Sugawara et al. (1962).

	Saturated evaporation entropy		
T	Δs_{evap} by Sugawara et al. (1962)	Δs_{evap} by Aspen Plus	Difference
°C	kcal/kgK	kcal/kgK	%
200.000	0.152	0.157	3.245
250.000	0.136	0.140	2.224
300.000	0.124	0.125	1.124
350.000	0.113	0.113	0.011
400.000	0.104	0.103	1.100
450.000	0.096	0.094	2.197
500.000	0.089	0.086	3.289
550.000	0.083	0.079	4.330
600.000	0.077	0.073	5.197
650.000	0.072	0.068	6.004
700.000	0.067	0.063	6.717
750.000	0.063	0.058	7.252
800.000	0.058	0.054	7.669

Table 3.5. Comparison between experimental and Aspen Plus mercury turbine power output.

	Experimental (Gutstein et al., 1975)	**Aspen Plus**	**Difference %**
Mass flow rate	1.5 kg/s (11800 lb/hr)	1.5 kg/s (11800 lb/hr)	-
Inlet temperature	677^0C (1250^0F)	677^0C (1250^0F)	-
Inlet pressure	1724 kPa (250 psia)	1724 kPa (250 psia)	-
Outlet temperature	354^0C (669^0F)	354^0C (669^0F)	-
Outlet pressure	96.5 kPa (14 psia)	96.5 kPa (14 psia)	-
Isentropic efficiency	55 %	55 %	-
Power output	64 kW	67 kW	4.5

3.2 Thermodynamic Analysis

A thermodynamic analysis considers several balances condition stemming from the first and second laws of thermodynamics. These include a mass, energy, entropy and exergy balances. The first balance condition is the mass balance. The energy balance stems from the conservation of energy principle according to the first law of thermodynamics. The entropy balance stems from the non-conservation of entropy principle of the second law of thermodynamics. The exergy

balances stems from the first and second laws of thermodynamics; exergy is a non-conserved quantity.

In our analyses, we utilize steady state versions of these balances since, as will be stated, the overall heat pump processes are assumed to be at steady state. Also, we consider rate balance here.

3.2.1 Mass rate balance equation

The mass rate balance (mass conservations) for a control volume can be expressed as the difference between the outlet and inlet mass flow rate being equal to the rate of mass accumulation:

$$\sum_{in} \dot{m}_{in} - \sum_{out} \dot{m}_{out} = \frac{dm_{cv}}{dt} \quad (3.9)$$

where $\dot{m}$ is the mass flow rate and $\frac{dm_{cv}}{dt}$ is the rate of mass accumulation within the control volume. For a steady state process with no accumulation rate of mass within control volume, equation (3.9) can be written as

$$\sum_{in} \dot{m}_{in} = \sum_{out} \dot{m}_{out} \quad (3.10)$$

3.2.2 Energy rate balance equation

The energy rate balance for a control volume considers all forms of energy (e.g. flow energy, thermal energy, mechanical energy). It states that the energy rate leaving the system and the energy rate entering the system is equivalent to the rate of energy accumulation within the control volume.

$$\dot{Q} - \dot{W} = \frac{dE_{cv}}{dt} \quad (3.11)$$

where $\dot{Q}$ is heat flow input rate to the control volume, $\dot{W}$ is the work output rate, and $\frac{dE_{cv}}{dt}$ is the rate of energy accumulation within the system. In equation (3.11) heat flowing out of the system and work done on the control volume are negative. For steady state, we can write:

$$\dot{Q}_{in} + \dot{W}_{in} + \sum \dot{m}_{in} h_{in} = \dot{Q}_{out} + \dot{W}_{out} + \sum \dot{m}_{out} h_{out} \quad (3.12)$$

Note that in both equation (3.11) and equation (3.12) kinetic energy and potential energy are neglected.

3.2.3 Entropy rate balance equation

The entropy rate balance at steady state can written as follows:

$$\frac{\dot{Q}_{in}}{T} + \sum \dot{m}_{in} s_{in} + \dot{S}_{gen} = \frac{\dot{Q}_{out}}{T} + \sum \dot{m}_{out} s_{out} \quad (3.13)$$

where $\dot{S}_{gen}$ is the entropy generation rate within the control volume.

3.2.4 Exergy rate balance equation

The exergy balance equation for a control volume at steady state can be written as:

$$\dot{Ex}^{Q}_{in} + \dot{W}_{in} + \sum \dot{m}_{in}\, ex_{in} = \dot{Ex}^{Q}_{out} + \dot{W}_{out} + \sum \dot{m}_{out} ex_{out} + \dot{Ex}_{destruction} \quad (3.14)$$

where $\dot{Ex}^{Q}$ is the thermal exergy flow rate which can be calculated by multiplying heat flow rate by the Carnot factor:

$$\dot{Ex}^{\dot{Q}} = \dot{Q}(1 - \frac{T_o}{T}) \quad (3.15)$$

Also, $\dot{Ex}_{destruction}$ is the exergy destruction rate, which can be related to the entropy generation in equation (3.13) by multiplying it by the reference temperature

$$\dot{Ex}_{destruction} = \dot{S}_{gen} T_o \quad (3.16)$$

Here, "ex" denotes the specific exergy. T in equation (3.15) is the temperature of the boundary where heat transfer is occurring. A convenient quick approximation of the boundary temperature in case of heat exchangers, for example, is to take the average temperature of all streams entering and leaving the heat exchanger. The molar exergy can be expressed as

$$ex = ex_{phys} + ex_{ch} \quad (3.17)$$

where ex_{phys} is the molar physical exergy, which is concerned with the exergy content as it reaches mechanical and thermal equilibrium with the environment (e.g. dead state). ex_{ch} is the molar chemical exergy which is concerned with chemical constituents concentrations. Chemical exergy is neglected if stream constituents do not chemically change. Molar physical and chemical exergy can be expressed respectively as

$$ex_{i-phys} = (h_i - h_o) - T_o(s_i - s_o) \quad (3.18)$$

$$ex_{i-chem} = \sum x_n \, ex_{ch}^n + RT_o \sum x_n \ln(x_n) \quad (3.19)$$

where h_i is the molar enthalpy of the stream, h_o is the molar enthalpy of the stream at ambient conditions, T_o is the ambient temperature, s_i is the molar entropy of the stream, s_o is the molar entropy of the stream at ambient conditions, ex_{ch}^n is the chemical exergy of a particular species, x_n is the mole fraction of the particular species, and $R = 8314.472 \frac{kJ}{mol\,K}$ is the universal gas constant.

3.3 Application of Thermodynamic Analysis on Systems

In this section of the context the thermodynamic models defined earlier in section 3.2 of this chapter are going to be applied on the system's components. Both heat pumps include similar components which are mainly compressors/pumps, valves, heat exchangers, heat sources, and the copper oxychloride decomposition reactor.

It is important to explicitly write the assumptions made regarding the heat pumps analyzed

1- All heat pumps operate in steady flow state.

2- Compressors and pumps are adiabatic and run with a practical efficiency of 85% in the base case (Srinivas et al., 2007).

3- The endothermic reaction of copper oxychloride is considered to be stoichiometric.

4- Pressure drops are considered to be zero along pipe lines and control volume components.

5- For the base case, the ambient temperature and pressure are taken to be 25°C and 1 bar.

The rest of this section will be dedicated to general set of balance equations for the heat pumps components.

3.3.1 Heat exchangers

All of the heat exchangers in both configurations are considered to be countercurrent flow heat exchangers. Their balance equations are all the same and written as the follow:

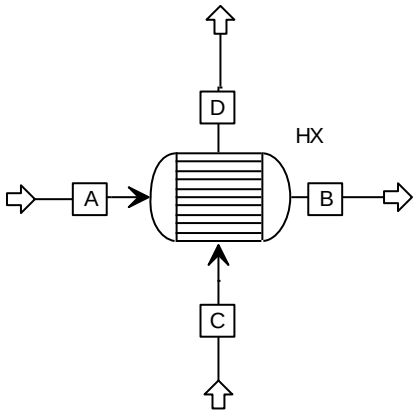

Mass balance:

$$\dot{m}_A = \dot{m}_B \quad (3.20)$$

$$\dot{n}_A = \dot{n}_B \quad (3.21)$$

Energy balance:

$$\dot{n}_A h_A + \dot{n}_C h_C = n_B h_B + \dot{n}_D h_D \quad (3.22)$$

Entropy balance:

$$n_A s_A + \dot{n}_C s_C = \dot{n}_B s_B + \dot{n}_D s_D + \dot{S}_{gen} \quad (3.23)$$

Exergy balance:

$$\dot{n}_A ex_A + \dot{n}_C ex_C = \dot{n}_D ex_D + \dot{n}_B ex_B + \dot{E}x_{destruction} \quad (3.24)$$

3.3.2 Copper oxychloride decomposition reactor

The decomposition reactor undergoes an endothermic reaction in which the copper oxychloride Cu_2OCl_2 decomposes into O_2 and product CuCl. The heat is provided by the high temperature excess CuCl fed into the reactor. Note that CuCl (B) flowing out of the reactor is a mixture of the heat pump excess CuCl (A) and the produced CuCl. The thermodynamic balance equations governing this component are written as the follows:

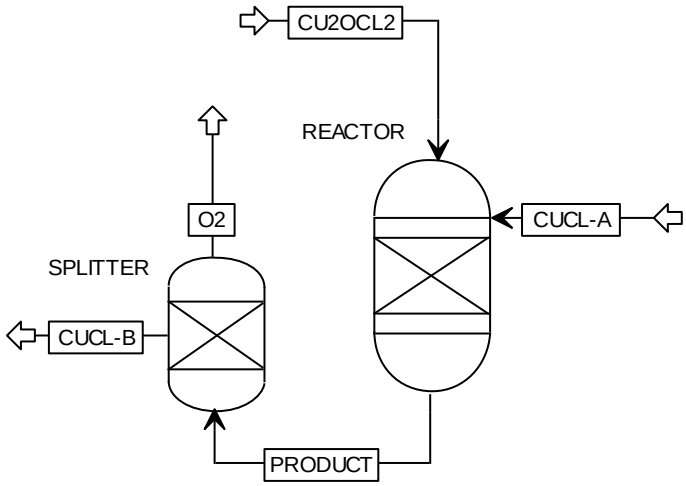

Stoichiometry / Mass balance:

$$Cu_2OCl_2 \xrightarrow{\dot{Q}by\ CuCl-A} \frac{1}{2}O_2 + 2CuCl \tag{3.25}$$

$$\dot{m}_{CuCl-A} + \dot{m}_{Cu_2OCl_2} = \dot{m}_{O_2} + \dot{m}_{CuCl-B} \tag{3.26}$$

Energy balance:

$$\dot{n}_{Cu_2OCl_2}h_{Cu_2OCl_2} + \dot{n}_{CuCl-A}h_{CuCl-A} = \dot{n}_{CuCl-B}h_{CuCl-B} + \dot{n}_{O_2}h_{O_2} \tag{3.27}$$

Entropy balance:

$$\dot{n}_{Cu_2OCl_2}s_{Cu_2OCl_2} + \dot{n}_{CuCl-A}s_{CuCl-A} = \dot{n}_{CuCl-B}s_{CuCl-B} + \dot{n}_{O_2}s_{O_2} + \dot{S}_{gen} \tag{3.28}$$

Exergy balance:

$$\dot{n}_{Cu_2OCl_2}ex_{Cu_2OCl_2} + \dot{n}_{CuCl-A}ex_{CuCl-A} + \dot{E}x_{destruction} = \dot{n}_{CuCl-B}ex_{CuCl-B} + \dot{n}_{O_2}ex_{O_2} \tag{2.29}$$

3.3.3 Compressor

The compressor helps to compresses the vapor phase of the working fluids through a mechanical power supply. As the vapor is compressed, it is temperature is elevated which makes it suitable in heating applications similar to our case.

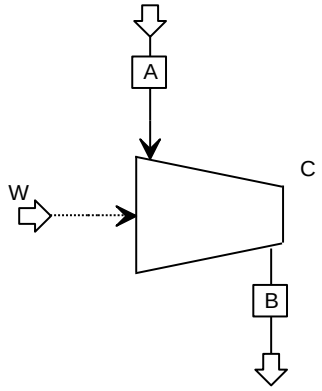

Mass balance:

$$\dot{m}_A = \dot{m}_B \tag{3.30}$$

$$\dot{n}_A = \dot{n}_B \tag{3.31}$$

Energy balance:

$$\dot{n}_A h_A + \dot{W} = \dot{n}_B h_B \tag{3.32}$$

Entropy balance:

$$\dot{n}_A s_A = \dot{n}_B s_B + \dot{S}_{gen} \tag{3.33}$$

Exergy balance:

$$\dot{n}_A ex_A + \dot{W} = \dot{n}_B ex_B + \dot{E}x_{destruction} \tag{3.34}$$

3.3.4 Expansion valves

Expansion valves are isenthalpic components in which the specific enthalpy of the inlet stream and outlet stream are equal. The usage of expansion valve is very necessary in such heating application as it causes the pressure drop so that heat can be added by the source temperature we are interested to amplify to the heat sink stage. Its balance equations are written as follows:

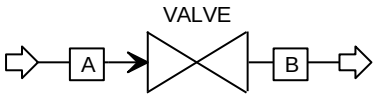

Mass balance:

$$\dot{m}_A = \dot{m}_B \tag{3.35}$$

$$\dot{n}_A = \dot{n}_B \tag{3.36}$$

Energy balance:

$$h_A = h_B \tag{3.37}$$

Entropy balance:

$$\dot{n}_A s_A = \dot{n}_B s_B + \dot{S}_{gen} \tag{3.38}$$

Exergy balance:

$$\dot{n}_A ex_A = \dot{n}_B ex_B + \dot{E}x_{destruction} \tag{3.39}$$

3.3.5 Heat recovery

The heat recovery diagram symbolizes heat addition of heat to out evaporator for the sake of turning a two phase (liquid-vapor) fluid to a saturated vapor to be compressed. The heat recovery symbol is only added in the mercury heat pump and biphenyl heat pump as they are in the bottom cycle and responsible of recovering the heat to be upgraded. Below are the heat recover governing equation of states.

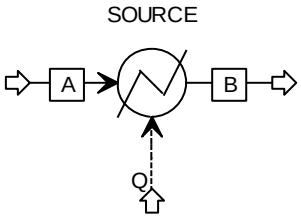

Mass balance:

$$\dot{m}_A = \dot{m}_B \tag{3.40}$$

$$\dot{n}_A = \dot{n}_B \tag{3.41}$$

Energy balance:

$$\dot{n}_A h_A + \dot{Q} = \dot{n}_B h_B \tag{3.42}$$

Entropy balance:

$$\dot{n}_A s_A + \frac{\dot{Q}}{T} = \dot{n}_B s_B + \dot{S}_{gen} \tag{3.43}$$

Exergy balance:

$$\dot{n}_A ex_A + \dot{Q}(1 - \frac{T_o}{T}) = \dot{n}_B ex_B + \dot{Ex}_{destruction} \tag{3.44}$$

3.3.6 Evaluation parameters

The main evaluation parameters of the heat pump are the energetic and exergetic coefficient of performances which are generally defined as

$$COP_{en} = \frac{\sum \dot{Q}_{out}}{\sum \dot{W}_{in}} \tag{3.45}$$

$$COP_{ex} = \frac{\sum \dot{Q}_{out}\left(1-\frac{T_o}{T}\right)}{\sum \dot{W}_{in}} \tag{3.46}$$

For the CuCl heat pump and the overall cascaded heat pump COPs

$$\dot{Q}_{out} = \dot{Q}_{oxydecom.} = h_{O_2}\dot{n}_{O_2} + h_{CuCl}\dot{n}_{CuCl} - h_{Cu_2OCl_2}\dot{n}_{Cu_2OCl_2} \tag{3.47}$$

where T is the temperature of the boundary where heat transfer occurs. For the reactor, the heat transfer boundary is the surface of the solid copper oxychloride and it is considered to have a temperature similar to the reaction temperature $T=T_3=T_4=T_5=T_6$. This assumption is similar to the one made by Zamfirescu et al. (2011). The exergetic COP is equivalent to the multipication of the desired heat output $\sum \dot{Q}_{out}$ and the Carnot factor, $\left(1 - \frac{T_o}{T}\right)$, which considers the irreversibility of the finite temperature difference and the approach of the the boundary temperature to the dead

state reference temperature. Other useful parameters to be considered are the recovery ratio for each of the sensible heat recovered from the produced O_2 and CuCl in HX1 and HX2, and the heat recovered from the bottom cycle through the cascading heat exchangers. These ratios tell us how many percent each of the sensible heat recovered from these two products and the heat obtained from the bottom heat pump are contributing to the overall evaporation of CuCl in (stream 7).

For CuCl-mercury:

$$X_s = \frac{\dot{Q}_{HX_1} + \dot{Q}_{HX_2}}{\dot{Q}_{HX_1} + \dot{Q}_{HX_2} + \dot{Q}_{HX_5} + \dot{Q}_{HX_6} + \dot{Q}_{HX_7}} \tag{3.48}$$

$$X_{bottom} = \frac{\dot{Q}_{HX_5} + \dot{Q}_{HX_6} + \dot{Q}_{HX_7}}{\dot{Q}_{HX_1} + \dot{Q}_{HX_2} + \dot{Q}_{HX_5} + \dot{Q}_{HX_6} + \dot{Q}_{HX_7}} \tag{3.49}$$

And for CuCl-biphenyl

$$X_s = \frac{\dot{Q}_{HX_1} + \dot{Q}_{HX_2}}{\dot{Q}_{HX_1} + \dot{Q}_{HX_2} + \dot{Q}_{HX_5}} \tag{3.50}$$

$$X_{bottom} = \frac{\dot{Q}_{HX_5}}{\dot{Q}_{HX_1} + \dot{Q}_{HX_2} + \dot{Q}_{HX_5}} \tag{3.51}$$

where X_s is the sensible heat recovery ratio, and X_{bottom} is bottom heat pump recovery ratio.

One more thing to explain is the options of vapor compression pressure difference across each compressor. The base case taken for the system is that the pressure increase across each compressor is equivalent (e.g. $\Delta P_{c1} = \Delta P_{c2} = \Delta P_{c3}$). Four cases are studied regarding the pressure increase distribution which are

Case 1: $[\Delta P_{c1} < \Delta P_{c2} < \Delta P_{c3}]$

$$\Delta P_{c1} = \frac{\Delta P_{c2}}{2} = \frac{\Delta P_{c3}}{4} \tag{3.52}$$

Case 2: $[\Delta P_{c1} = \Delta P_{c2} > \Delta P_{c3}]$

$$\frac{\Delta P_{c1}}{2} = \frac{\Delta P_{c2}}{2} = \Delta P_{c3} \tag{3.53}$$

Case 3: $[\Delta P_{c1} = \Delta P_{c2} < \Delta P_{c3}]$

$$\Delta P_{c1} = \Delta P_{c2} = \frac{\Delta P_{c3}}{2} \quad (3.54)$$

Case 4: $[\Delta P_{c1} > \Delta P_{c2} > \Delta P_{c3}]$

$$\frac{\Delta P_{c1}}{4} = \frac{\Delta P_{c2}}{2} = \Delta P_{c3} \quad (3.55)$$

The parameter defined to see the difference between these cases and the base case as the ratio of their COP difference with the base case over the base case COP

$$COP^{*} = \frac{COP_{i} - COP_{base}}{COP_{base}} \quad (3.56)$$

3.4 Exergoeconomic Analysis

Exergoeconomic analysis considers both costs and exergy in the economic analysis to achieve optimum a system with optimum performance and cost. Such is based on the convention that distribution of costs should be on the exergy thermodynamic quantity to achieve proper costing and scientifically and economically optimized system capacity and performance (Tsatsaronis and Moran, 1997, Dincer and Rosen, 2007).

The thermodynamic exergy analysis explained in previous sections was an initial step toward exergoeconomic analysis, and the remaining steps to be taken are the economic analysis (e.g. purchase costing, chemical engineering plant cost index (CEPCI) costs adjustment) the costing of streams exergy, and exergoeconomic evaluation through exergoeconomic evaluation tools (e.g. exergoeconomic factor f, relative cost difference RCD, and total cost flow).

3.4.1 Purchase cost estimation

One of the first steps to be done in the economic analysis is the determination of purchase costs of different equipment included in the system to be analyzed. Our cost estimation is made through an equipment capacity-based estimation equation (Turton, 2009) that includes coefficients depending on the equipment type. The equation is written as follows:

$$\log Z = K_1 + K_2 \log(A) + K_3 [\log(A)]^2 \quad (3.57)$$

Z is the estimated cost of equipment purchase in 2001, K_i are coefficients provided by Turton (2009), A is the capacity (e.g. power, volume flow rate, heat transfer areas) on which the estimation

is based. The coefficients in equation (3.53) for different equipment used in heat pump are given in Table 3.5.

The only exception is for the cost estimation of valves which was estimated by equation (3.58) provided by Hamut (2012)

$$Z_{ev} = 12.36\ \dot{m} \tag{3.58}$$

where $\dot{m}$ is the mass flow rate of the stream expanded through the valve.

Equations (3.57) and (3.58) are based on 2001 and 2012 costing, respectively. It is therefore necessary to make an adjustment on the calculated costs to get an updated costs. This can be achieved by using Chemical Engineering Plant Cost Index (CEPCI) in the following way:

$$C_1 = C_2 \frac{\text{CEPCI 1}}{\text{CEPCI 2}} \tag{3.59}$$

where C_1 is the cost of equipment in the year of interest, C_2 is the cost of the equipment available for a particular date, $CEPCI_1$ is the chemical engineering plant cost index for the year in which the equipment cost is to be found, and $CEPCI_2$ is the chemical engineering plant cost index for the available costs (or equation) year. The CEPCI used for 2001, 2010, 2012, and 2015 are 394, 551, 571 (Norwegian University of Science and Technology, 2011), and 560.7 (Chemical engineering online, 2015).

Table 3.6. Equipment coefficients used in equipment purchase cost estimation equation (3.57) by Turton (2009)

Coefficients\Components	Heat exchangers	Compressor	Pumps	Reactor	Mixer
A	Area (m^2)	Power (kW)	Power (kW)	Volume (m^3)	Volume (m^3)
K_1	4.3247	2.2897	3.8696	3.4974	5.0141
K_2	-0.303	1.3604	0.3161	0.4485	-0.4133
K_3	0.1634	-0.1027	0.122	0.1074	0.3224

3.4.2 Exergy cost and cost balance

According to references that discussed exergoeconomic approaches (Bejan et al., 1996; Tsatsaronis and Moran, 1997; Lazzaretto and Tsatsaronis, 2006; Dincer and Rosen, 2007) cost flow rate is equivalent to the multiplication between the flow exergy cost by the thermodynamic exergy flow. Note that all costs presented in this thesis are in US$. In addition, all costs are updated to the year 2015 using the CEPCI equation (3.55) explained above.

$$\dot{C} = c\,\dot{E}x \tag{3.60}$$

$\dot{C}$ stands for the cost flow rate ($/s), c is the cost of exergy ($/kJ), while $\dot{E}x$ is the exergy flow rate (kW). Now exergy flow can be in be in these forms of interest: matter, work and heat:

$$\dot{C}_{matter} = (c\,\dot{E}x)_{matter} \tag{3.61}$$

$$\dot{C}_w = c_w \dot{W} \tag{3.62}$$

$$\dot{C}_q = c_q \dot{Q}(1 - \frac{T_o}{T}) \tag{3.63}$$

where $\dot{C}_{matter}$ is the cost flow rate of matters (e.g. streams), $\dot{C}_w$ is the electric power cost flow, and $\dot{C}_q$ is the heat cost flow. The cost flow rate of streams, work, and heat flowing through a component can either be fuel costs flow rate of product costs flue rate, depending on situation, and they are related to the capital cost as in the following relations

$$\dot{C}_P = \dot{Z}_k + \dot{C}_F \tag{3.64}$$

$$\dot{Z}_k = \frac{Z_k CRF \varphi}{N} . F_m \tag{3.65}$$

$$CRF = \frac{i(1+i)^n}{(1+i)^n - 1} \tag{3.66}$$

where $\dot{C}_P$ is the product cost flow, $\dot{Z}_k$ is the capital cost and maintenance cost per annual operation periods in the unit of seconds, Z_k is the estimated purchase cost of a component using equations (3.57) or (3.58), CRF is the capital recovery factor which depends on interest i, φ is the maintenance factor taken to be 1.06 (Bejan et al., 1996), F_m is the material factor, N is the annual operation in seconds, and n is the operation life time in years. In our work, we are assuming the

base interest rate is 5%, and the heat pump life time is assumed to be 15 years. Now we can write the general form of balance equation for a particular equipment as

$$\sum_{out}(c_{out}\dot{E}x_{out})_k + c_{w,k}\dot{E}x_{w,k} = c_{q,k}\dot{E}x_{q,k} + \sum_{in}(c_{in}\dot{E}x_{in})_k + \dot{Z}_k \quad (3.67)$$

where the mechanical power input cost flow $c_{w,k}\dot{E}x_{w,k}$ is negative for mechanical power consuming devices (e.g. compressors) and the heat cost flow $c_{q,k}\dot{E}x_{q,k}$ is negative if heat is rejected from the component. Although the cost of fuels and cost balance equations may be known, auxiliary equations need to be developed for us to be able to solve the cost balancing. To achieve this fuel and product rules were developed with economic reasoning to fill this insufficiency of unknowns (Lazzaretto and Tsatsaronis, 2006).

The cost flow balance equations are based on equations (3.64) to (3.67) and the following explanation shows the fuel and product cost flow in each component applied according to rules explained in literature (Bejan et al., 1996).

a) Heat exchangers

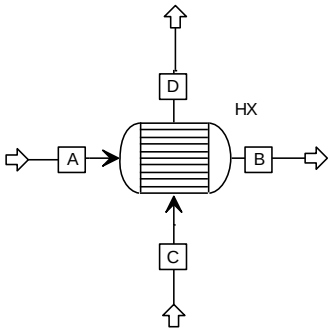

Assuming (A-B) to be hot stream and (C-D) to be cold stream. The fuel and product are determined as follows for heat exchangers:

$$\dot{C}_P = \dot{C}_D - \dot{C}_C \quad (3.68)$$

$$\dot{C}_F = \dot{C}_A - \dot{C}_B \quad (3.69)$$

Auxiliary relation: $c_A = c_B$ (Fuel rule)

b) Reactor

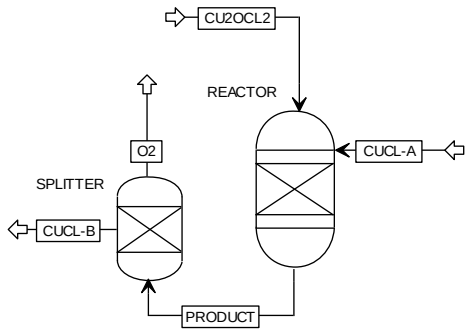

The reactor fuel depends on the variation of the costs flow of the excess CuCl used in heating across the reactor. Product depends on the difference between the Cu_2OCl_2 and its product cross difference. They are written as follows

$$\dot{C}_P = \dot{C}_2 + \dot{C}_4 - \dot{C}_1 \qquad (3.70)$$

$$\dot{C}_F = \dot{C}_{15} - \dot{C}_5 + \dot{C}_6 \qquad (3.71)$$

Auxiliary relation: $c_1 = c_2 + c_4$ (product rule)

Explanation is only numbered for the reactor according to stream numbers*

c) Compressors

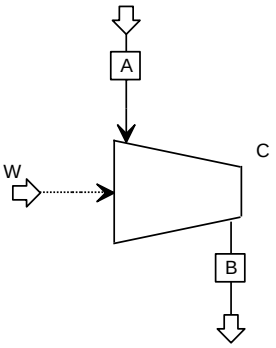

The compressors fuel and product cost flow are entered as follows

$$\dot{C}_P = \dot{C}_B - \dot{C}_A \qquad (3.72)$$

$$\dot{C}_F = \dot{C}_w \qquad (3.73)$$

Auxiliary relation: None

d) Mixer

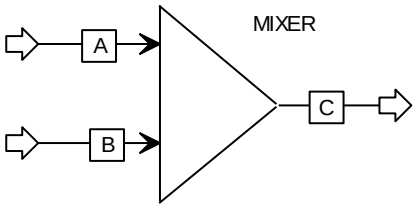

The mixer fuel and product cost flow are entered as follows

$$\dot{C}_P = \dot{C}_C \qquad (3.74)$$

$$\dot{C}_F = \dot{C}_B + \dot{C}_A \qquad (3.75)$$

Auxiliary relation: None

e) Heat source

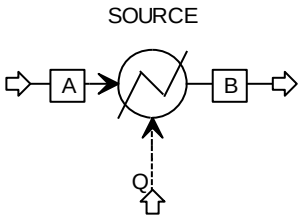

The thermal source from recovered heat has its fuel and product cost flow entered as the following

$$\dot{C}_P = \dot{C}_B \qquad (3.76)$$

$$\dot{C}_F = \dot{C}_q + \dot{C}_A \qquad (3.77)$$

Auxiliary relation: None

f) Valves

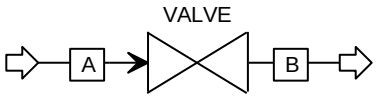

Lastly, the expansion valves fuel and product are expressed similar to the inlet and outlet, respectively

$$\dot{C}_P = \dot{C}_B \quad (3.78)$$

$$\dot{C}_F = \dot{C}_A \quad (3.79)$$

Auxiliary relation: None

The cost of electric power is taken to be 0.11 USD $/kWh (Hydro, 2016) and the cost of thermal power input is taken to be 0.0024 USD $/MJ (Ansari et al., 2010) and updated for 2015.

The hidden cost of exergy destruction of a component k is not included in the cost flow balance equation and it is evaluated by the multiplication of the fuel cost by the exergy destruction rate evaluated in the exergy analysis

$$\dot{C}_{d,k} = c_{f,k}\, \dot{E}x_{destruction,k} \quad (3.80)$$

As the cost of the exergy destruction rate is hidden and not included in the cost flow balance equation, the exergoeconomic tools of evaluation comes into the picture to consider the exergy destruction relative to other costing factors.

3.4.3 Exergoeconomic evaluation parameters

A system can be evaluated exergoeconomically through the exergoeconomic factor, which is the ratio of the capital cost flow over the summation of capital cost flow and exergy destruction cost flow

$$f = \frac{\dot{Z}}{\dot{Z}+\dot{C}_{d,k}} \quad (3.81)$$

Another parameter is the Relative Cost Difference RCD, which shows the percentage of increase (or decrease) in product cost flow with respect to fuel cost flow.

$$\mathrm{RCD} = \frac{c_p - c_f}{c_f} \tag{3.82}$$

Chapter 4: Aspen Plus Simulation and Methodology

Aspen Plus is a chemical process modeling software developed by Aspentech (Aspen Technology, 2015). Aspen Plus is very well known in chemical industries as a reliable process modeling tool due to its rigorous and unique modeling features. Aspen Plus has been used, and can be used, in enhancing process performance, plant upscaling, plant energy consumption reduction, and reducing plant facility installation and operation expenditures. It can also be used as a technical and economic optimization tool for a variety of chemical processes involving substances of different nature and a different chemical properties. As Aspen Plus has been the basis of our thermodynamic analysis, it is proper to briefly present some of the software features and discuss the steps that have been taken to build heat pump systems flowsheet and run the simulation. Aspen Plus has three sections: *Properties, Simulation, and Energy Analysis*. Our work has been restricted to the first two.

4.1 Physical Property Models

Aspen Plus has numerous databanks that contain a massive number of pure components and phase equilibrium data. The data that can be found in Aspen Plus includes, but is not restricted to, conventional chemicals, hydrocarbons, polymers, electrolytes, and solids. Moreover, Aspen Plus has a National Institute of Standards and Technology (NIST) database built-in and has the feature of having the data easily updated.

Components to be used in simulation can be added in the *Component* window once a new simulation is created by the user. The component search feature included in Aspen Plus enables the user to easily and quickly select the intended components, see Figure 4.1. Furthermore, if a chemical substance is not found, Aspen Plus has the feature of allowing the user to create their own chemical component by providing inputs such as its element, bond type, structure drawing, and thermophysical properties etc.

As variation of chemical substances necessitates variation of a proper thermodynamic method that would make the calculated thermodynamic properties of the chemical substances of interest both accurate and reliable, Aspen Plus provides numerous thermodynamic methods for different chemical processes. Once components are selected from the *Components* window and the user clicks *Next*, Aspen Plus directs the user to the methods *Specification* window where the

thermodynamic method can be selected. Note that the user can select more than one thermodynamic method by choosing them in the scroll bar. The chosen thermodynamic methods in concern are then shown under the methods *Selected Methods* folder. It should also be noted that the thermodynamic method left shaded in the methods *Specification* window is going to be the default thermodynamic method in the *Properties* section and the *Simulation* section. The user can specify a particular method for particular process components, as will be explained in the parts related to simulation in this chapter. The *Method Assistant* tool found in the *Home* tab can be used in case the users are not sure which thermodynamic method would be convenient for their simulation interest.

The thermophysical properties to be used can be shown by clicking *Retrieve Parameters* in the *Home* tab and then going to *Parameters >> Pure components >> Review* window under the methods category. Through the *Review* window we can include, view, or modify values such as enthalpy of formation, Gibbs free energy, critical temperature, critical pressure and acentric factor. Moreover, the temperature dependent parameters can also be viewed under the *Pure Components* folder. Example of temperature dependent parameters are different phases' heat capacity, thermal conductivity, and kinematic viscosity of particular substance. More than one temperature dependent parameter can be included (such as correlations with a function of temperature and coefficients a_0, a_2, a_3) under the *Pure Components* window and their selection can be controlled by the thermal switch *THRSWTI*. Further explanation can be found in the Aspen Plus user manual (Aspen Technology, 2015).

Another alternative to enter temperature dependent parameters is by using the *TABPOLY* feature found under the *Properties* folder. *TABPOLY* allows users to enter the coefficient or tabular based temperature dependent parameter values. It also enables the users to change the reference temperature, pressure, enthalpy, entropy, and Gibbs free energy.

4.1.1 Selection of our components and thermodynamic methods

The selection of cuprous chloride (CuCl), copper oxychloride (Cu_2OCl_2), and oxygen (O_2) as components was necessary due to their involvement in the CuCl heat pump. It was also necessary to select working fluids for the bottom heat pump as the CuCl heat pump cycle would not be sufficient to upgrade heat from low temperatures of about 300°C to higher temperatures

accommodating the Cu_2OCl_2 decomposition. The selection of suitable working fluids for the bottom heat pump was not pre-determined.

A selection criteria was that a bottom heat pump working fluid would have a normal boiling point near 300°C. The normal boiling point is defined as the fluid evaporation temperature at an absolute pressure of 1 atm. The importance of the normal boiling point is that it determines the pressure of the evaporator. The higher a normal boiling point temperature is, the more vacuum (e.g. sub-atmospheric) the evaporator needs to be to accommodate lower source temperatures to its evaporator.

The critical temperature is another essential criteria to be considered while selection of a heat pump working fluid. The critical temperature should be higher than the sink temperature and, in our case, the critical temperature of the bottom heat cycle should be higher than the temperature of the CuCl heat pump evaporator. The critical pressure of a working fluid is also essential in the selection of the working fluid. Utilizing a low critical pressure working fluids allow us to obtain a better safety and cheaper construction. Nevertheless, the heat pump evaporator is likely to be in vacuum (e.g. sub-atmospheric) if the critical pressure of its working fluid is very low.

Working fluids like mercury (Hg) and biphenyl ($(C_6H_5)_2$) were found to be suitable for the bottom heat pump. Their thermophysical properties explained in Section 3.1 meets the temperature and pressure criteria demonstrated above.

The chemical components of interest (e.g. O_2, CuCl, Cu_2OCl_2, Hg, and $(C_6H_5)_2$) were searched and added from the *Components* window. After component selection, the *IDEAL* and *PENG-ROB* thermodynamic methods, which respectively correspond to ideal gas equation of state and Peng and Robinson equation of state, were added to the *Selected Methods*. The method *IDEAL* was used for CuCl, Hg, and O_2, while the method *PENG-ROB* was used for biphenyl. Figure 4.2 shows the *Methods* selection window and the *Selected Methods* folder.

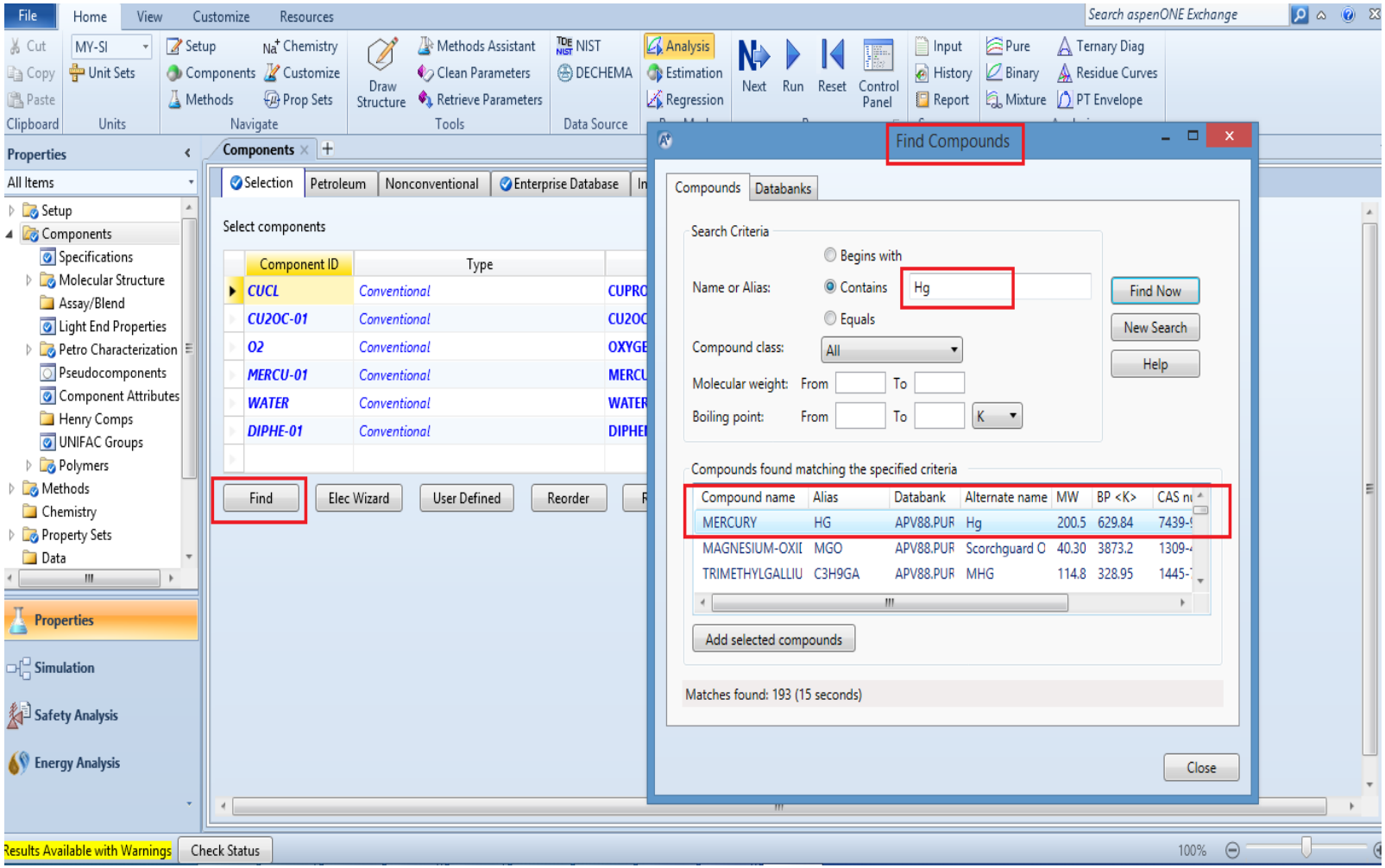

Figure 4.1. Components window and components search tool. Mercury is searched as an example.

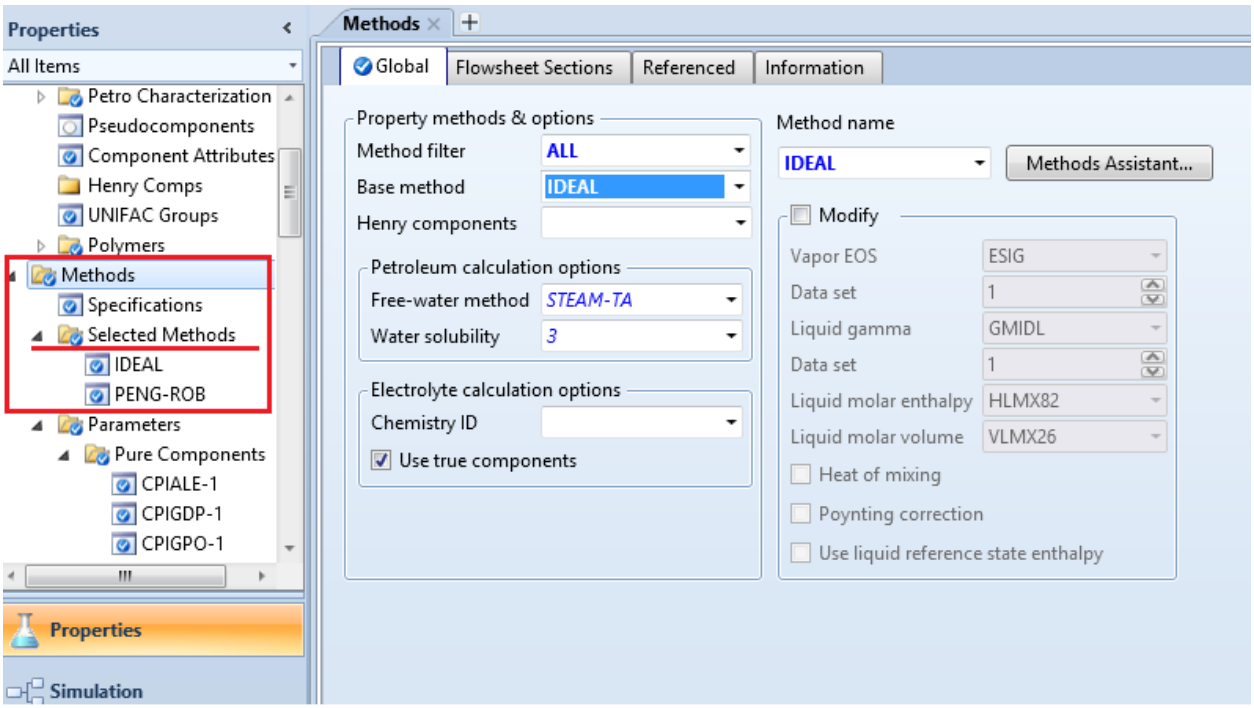

Figure 4.2. *Methods* and *Selected Methods*. Recall that the shaded base method in the *Methods* window is the default method in flowsheet, if not changed.

The *TABPOLY* tool shown in Figure 4.3 was used to enter CuCl heat capacity for both liquid and ideal gas, from which state parameters such as molar enthalpy and molar entropy are calculated. Moreover, the reference enthalpy and entropy were changed as has been explained in Section 3.1. The solid heat capacity of Cu_2OCl_2 was entered using a suitable form of polynomial in the *Pure Components Parameters* folder based on Zamfirescu et al. (2010) formulation. No changeds were made on the available property data for Hg, $(C_6H_5)_2$ and O_2.

After setting the proper thermodynamic parameters for the substances of interest, we can move to the simulation section to create the flowsheet.

4.2 Simulation Flowsheet

The user can start preparing the simulation flowsheet in the *Simulation* section after the chemical components, thermodynamic models, and thermodynamic properties are all set in the *Properties* section. If the *Properties* section is not properly set, the simulation immediately notifies of an error, when executed. Process component blocks, such as compressors, heat exchangers, valves, reactors, and vessels can be found in the *Model Palette*.

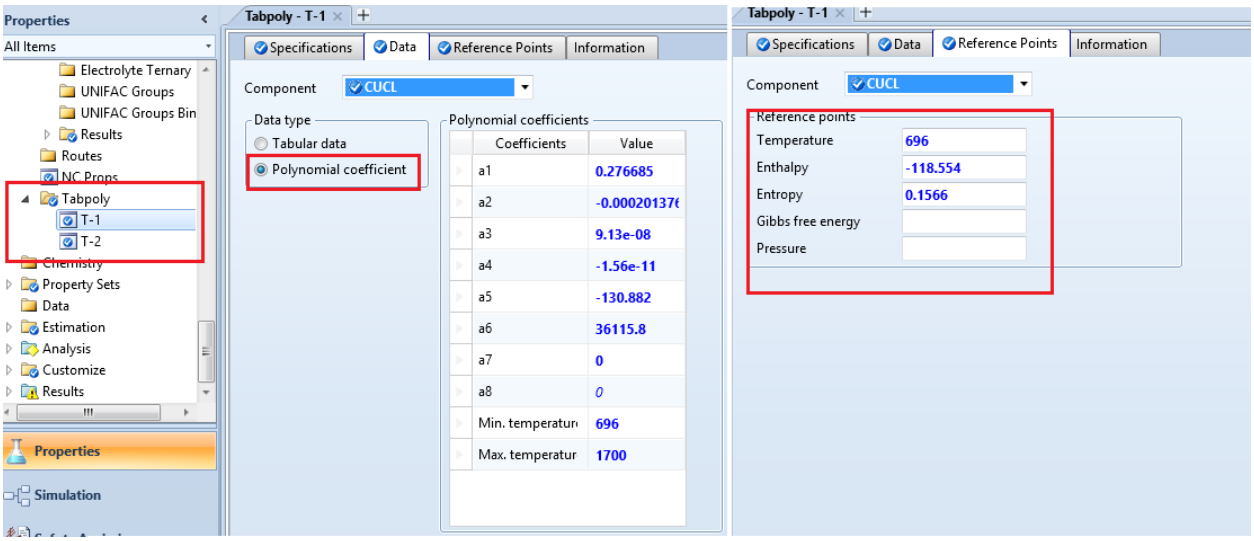

Figure 4.3. An example of utilizing the *TABPOLY* tool to enter the CuCl heat capacity of liquid. It is observed that coefficients were added and reference points were adjusted.

The user can select the blocks of interest and have them connected with each other using the *Material* stream lines. Specifications of selected blocks must be insert by the user. For instance, if placing a heat exchanger block in the flowsheet, the users must specify values such as hot/cold outlet temperature, hot/cold outlet vapor fraction, temperature approach, or degree of sub-cooling. If specifications are not entered for selected blocks, a *Required Input Incomplete* highlighted in red will be shown in the bottom left corner. As for *Material* streams, only the streams entering the system should be defined by the user in terms of temperature, pressure, constituents, and flow rate, while the intermediate and output streams are calculated by Aspen Plus. The user now can set the appropriate thermodynamic methods for each block according to the substances of entering and leaving streams. For example, HX5 in the CuCl-biphenyl heat pump has biphenyl, which corresponds to the *PENG-ROB* method, as its hot stream, and CuCl, which corresponds to the *IDEAL method,* as its cold stream. This can be set in the *Model* window under the *Results Summary* folder, see Figure 4.4.

The *Flowsheeting Options* folder consists of essential tools to build interactive relationships between the streams and blocks. The *Design Spec* tool, for instance, supports the user to meet a particular target (e.g. particular outlet temperature, output production flow rate, vapor fraction) by varying a specified input in either blocks or streams. Another very essential *Flowsheeting Options* tool is the *Calculator*. By using the calculator, the user can build relationships between blocks and streams (e.g. make all isentropic efficiencies equal to each other,

or let a hot stream outlet temperature specification in a heat exchanger block be equal to a saturated temperature corresponding to a particular compressor outlet). More details can be found in the Aspen Plus user manual (Aspen Technology, 2015).

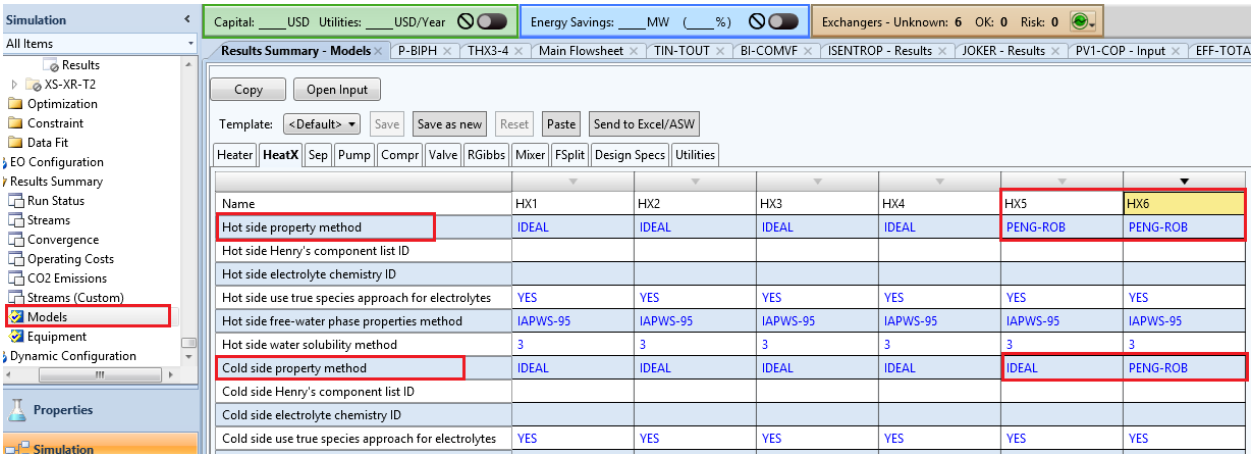

Figure 4.4. An example of setting the appropriate thermodynamic model for a particular block (e.g. HX5) streams in the *Models* window.

The *Flowsheeting Options* folder consists of essential tools to build interactive relationships between the streams and blocks. The *Design Spec* tool, for instance, supports the user to meet a particular target (e.g. particular outlet temperature, output production flow rate, vapor fraction) by varying a specified input in either blocks or streams. Another very essential *Flowsheeting Options* tool is the *Calculator*. By using the calculator, the user can build relationships between blocks and streams (e.g. make all isentropic efficiencies equal to each other, or let a hot stream outlet temperature specification in a heat exchanger block be equal to a saturated temperature corresponding to a particular compressor outlet). More details can be found in the Aspen Plus user manual (Aspen Technology, 2015).

4.2.1 Building the heat pumps flow sheet.

The heat pumps were built block by block starting from the copper oxychloride reactor. The simulation was run after each block stage was built to guarantee that all streams and blocks converge without error. The first heat pump modeled in the flowsheet was the CuCl heat pump. After the CuCl heat pump was fully modeled without errors in its simulation, two Aspen files were created for each of the mercury cascading and biphenyl cascading.

When the mercury heat pump was being modeled, one compressor was initially added with one heat exchanger to transfer heat from the mercury heat pump (condensing) to the CuCl heat pump (evaporation). However, due to the high temperature obtained when the simulation was run (>2000 K), it was realized that a single compression was not sufficient and multistage compression with intercooling must be considered, similar to the CuCl heat pump multistage compression. After trial and error, a multistage compression of three compressors with intercooling was considered to be an acceptable final configuration to raise heat from the heat source to the CuCl heat pump evaporator using the mercury heat pump. Cascading CuCl-mercury coupling with a third heat pump was not necessary. Nevertheless, considering a third heat pump would only be required in case the operation of the mercury heat pump is needed to be above the atmospheric pressure. The same approach was taken when the biphenyl heat pump was being built in Aspen Plus, the inclusion of one heat pump cycle (biphenyl) with one compressor could achieve our heat upgrading target.

In both systems, an RSTOIC reactor model, which stands for a stoichiometric reaction, was used for the copper oxychloride reactor. The *Heat duty* in the *RSTOIC* reactor *Specifications* was set to be zero. That is because the copper oxychloride reactor was assumed not to have any source of heat (adiabatic) apart from the heat provided by the excess CuCl (stream 15) injected to the reactor. Moreover, for compressors and valves, *Compr* and *Valve* models in *Pressure Changers* model palette were used, respectively. For heat exchangers, *HeatX* model was selected. *Shortcut Method* was selected in the *HeatX Specifications* window as heat exchangers calculation approach. For splitting and mixing, *Fsplit* model and *Mixer* model were used, respectively.

Finally, Table 4.1 and Table 4.2 show the relationships made between streams and blocks using the *Design Spec* and *Calculator* tools, respectively. Note, it is necessary sometimes to adjust the execution sequence of the *Design Spec*s and *Calculator*s in the *Sequence tab* to avoid errors and to acknowledge the sequence module execution of the software. The flowsheets built for the CuCl-mercury heat pump and the CuCl-biphenyl heat pump are shown in Figure 4.5 and Figure 4.6, respectively.

Table 4.1. *Variables* set by Aspen Plus *Design Spec* tool to achieve specified operating targets.

	Variable	Target
1	Stream 1 mole flow rate	850 K outlet temperature of streams leaving the copper oxychloride decomposition reactor.
2	Stream 5/6 splitter fraction.	Convergence of tear stream 15.
3	HX6 cold stream outlet approach in biphenyl heat pump.	Convergence of tear stream 22.

Table 4.2. The purpose of using the *Calculator* tool in Aspen Plus in achieving particular design purposes.

Calculator No.	Purpose
1	Making the outlet pressure of valve 2 equals to the saturation pressure of stream 15 temperature, T_{15}.
2	Making the pressure increase across each of the compressors C1, C2, and C3 equal. $\frac{P_{\text{stream 16}} - P_{\text{stream 8}}}{3} = \Delta P_{c1} = \Delta P_{c2} = \Delta P_{c3}$ Note: Same approach was taken to equate pressure increase across each compressor in the mercury multistage compression.
3	Equating compressors isentropic efficiencies: $\eta_1=\eta_2=\eta_3=\eta_4=\eta_5=\eta_6$.
4	Equating temperature approaches of HX1 and HX2.
5	Equating hot stream outlet temperatures of HX3 and HX4.
6	Equating hot-cold temperature approaches of HX1 and HX2.

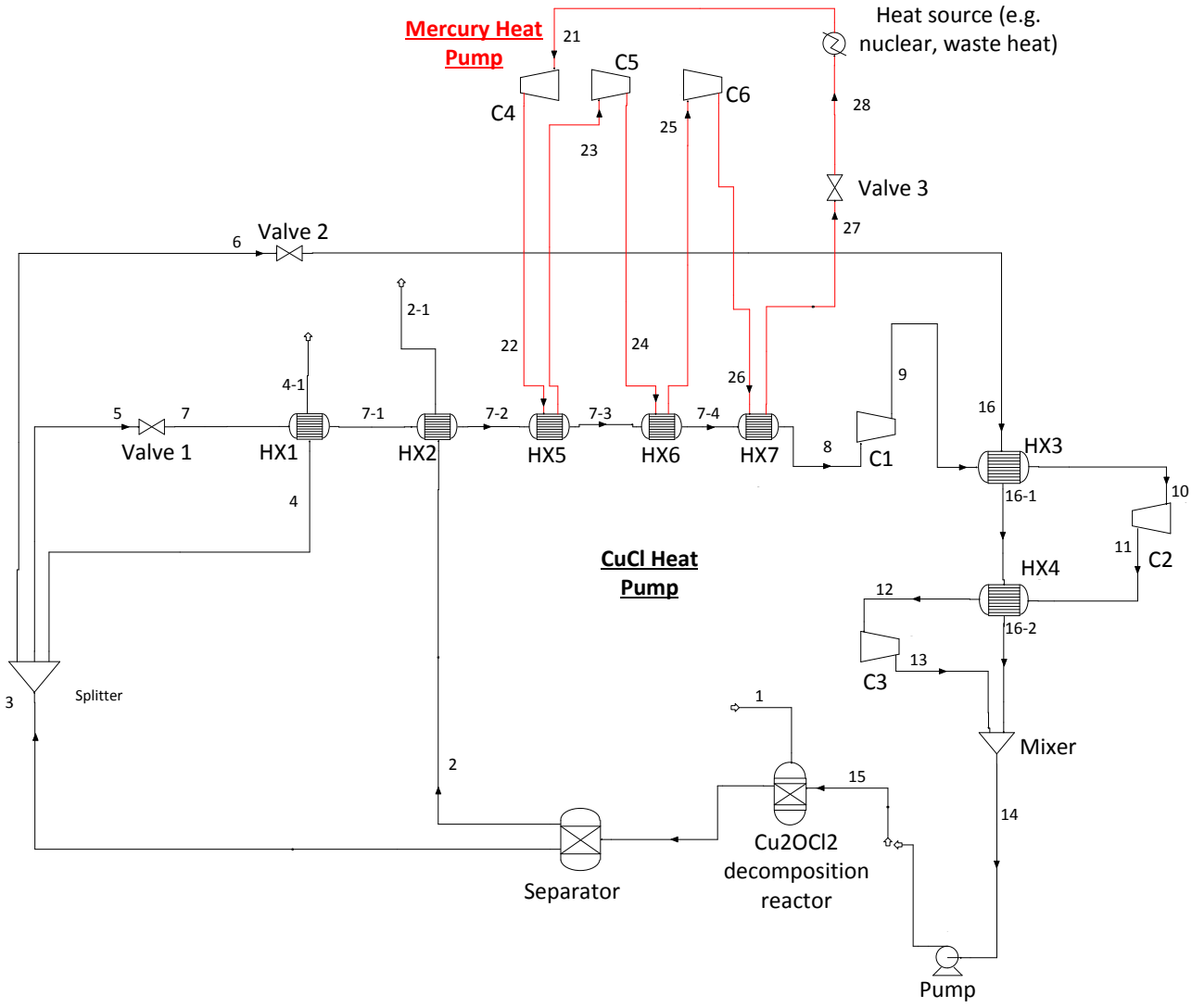

Figure 4.5. Aspen Plus flowsheet built for the CuCl-mercury heat pump.

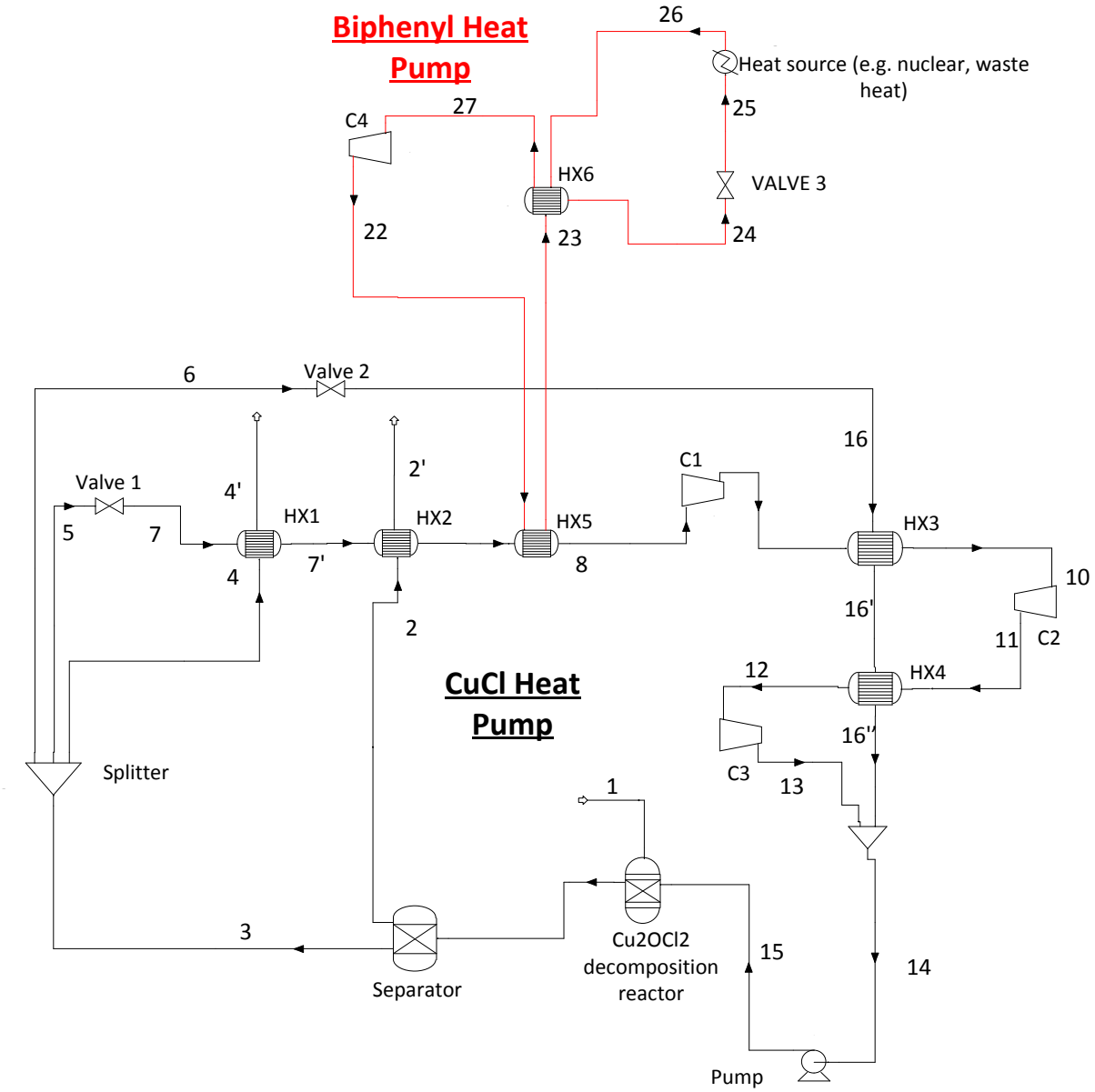

Figure 4.6. Aspen Plus flowsheet built for the CuCl-biphenyl heat pump.

Chapter 5: Results and Discussion

Thermodynamic analyses from energy and exergy points of view, and exergoeconomic analysis are carried out to study the performance of the systems and its costing. For both systems, we are selected significant design and operating parameters such as compressor isentropic efficiencies, temperature of CuCl fed into the reactor, reaction temperature (i.e. temperature of products leaving the reactor), heat exchanger approach temperature, and heat exchanger degree of intercooling, evaporator pressure, and ambient temperature.

Table 5.1. State points of the base case showing temperature, pressure, molar enthalpy, molar entropy, for each of (a) CuCl heat pump, (b) mercury heat pump, (c) biphenyl heat pump

(a) CuCl Heat Pump					
State	**T (K)**	**P (bar)**	**h (kJ/mol)**	**s (kJ/molK)**	**ṅ (mol/s)**
1	675.00	1.0000	-337.096	0.052	0.79
2	850.00	1.0000	17.551	0.033	0.39
3	850.00	1.0000	-109.368	0.169	19.08
4	850.00	1.0000	-109.368	0.169	1.58
5	850.00	1.0000	-109.368	0.169	0.39
6	850.00	1.0000	-109.368	0.169	17.11
7	754.65	0.0002	-109.368	0.166	0.39
7-1	754.65	0.0002	-87.835	0.184	0.39
7-2	754.65	0.0002	-84.754	0.186	0.39
7-3	754.65	0.0002	-45.304	0.218	0.39
7-4	754.65	0.0002	-32.509	0.228	0.39
8	754.65	0.0002	107.823	0.342	0.39
9	1549.18	0.0036	137.812	0.345	0.39
10	950.00	0.0036	115.144	0.327	0.39
11	1126.75	0.0071	121.802	0.328	0.39
12	950.00	0.0071	115.144	0.321	0.39
13	1052.17	0.0105	118.989	0.322	0.39
14	950.00	0.0105	-103.647	0.175	17.50
15	950.00	1.0000	-103.647	0.175	17.50
16	850.00	0.0105	-109.368	0.169	17.11
16-1	858.90	0.0105	-108.854	0.169	17.11
16-2	861.52	0.0105	-108.702	0.169	17.11

(b) Mercury Heat Pump					
State	**T (K)**	**P (bar)**	**h (kJ/mol)**	**s (kJ/molK)**	**ṅ (mol/s)**
21	568.96	0.3000	66.946	0.122	0.92
22	1565.15	2.9300	87.653	0.125	0.92
23	760.00	2.9300	70.917	0.110	0.92
24	1021.13	5.5600	76.345	0.110	0.92
25	760.00	5.5600	70.917	0.104	0.92
26	910.34	8.2000	74.042	0.105	0.92
27	760.84	8.2000	14.509	0.028	0.92
28	568.96	0.3000	14.509	0.030	0.92

(c) Biphenyl Heat Pump					
State	**T (K)**	**P (bar)**	**h (kJ/mol)**	**s (kJ/molK)**	**ṅ (mol/s)**
22	800.00	30.0000	311.807	-0.102	2.37
23	760.61	30.0000	280.231	-0.143	2.37
24	646.28	30.0000	226.149	-0.220	2.37
25	561.56	2.0000	226.149	-0.215	2.37
26	561.57	2.0000	240.385	-0.190	2.37
27	726.07	2.0000	294.467	-0.106	2.37

ASPEN Plus chemical processing simulation software is used in the analyses. Thermodynamic methods and properties of substances used in the analyses, as described in chapter 3. CuCl properties are calculated using previously mentioned specific heat of equation (3.1). The Ideal gas equation of state is also used for mercury, and the Peng-Robinson equation of state for biphenyl.

The base cases state points, for both CuCl-Mercury and CuCl-Biphenyl heat pumps, are shown in Table 5.1. The Tis diagrams of CuCl-mercury and CuCl-biphenyl heat pumps base cases are shown in Figure 5.1 and Figure 5.2, respectively.

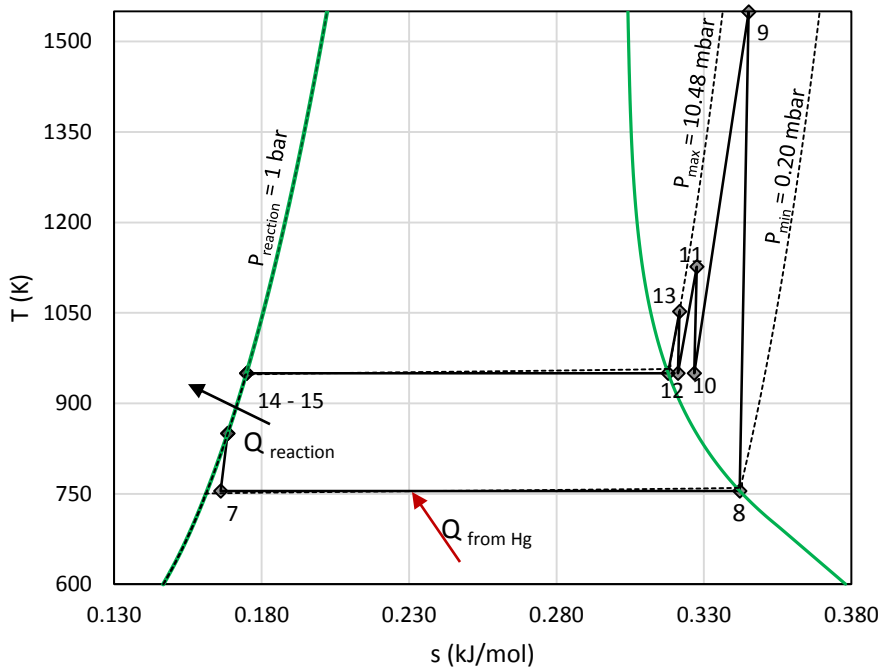

(a)

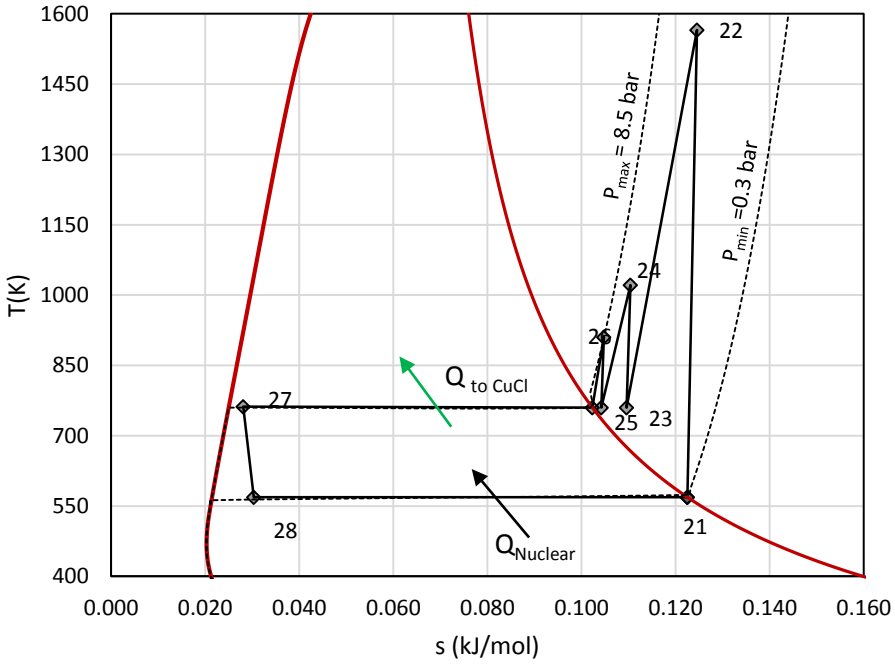

(b)

Figure 5.1. T- s diagrams of (a) cuprous chloride (CuCl) and (b) mercury (Hg) cascaded heat pump.

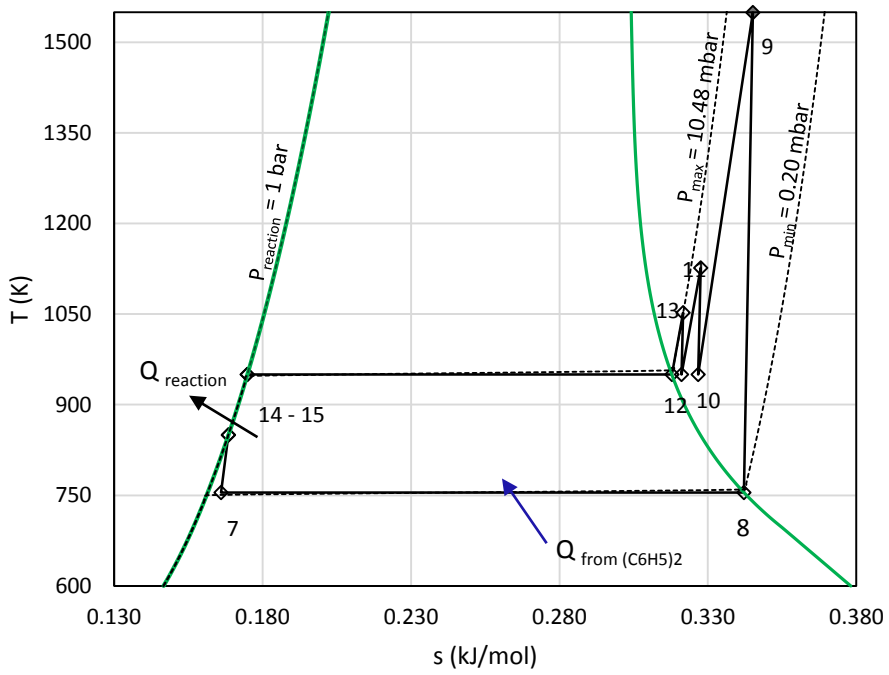

(a)

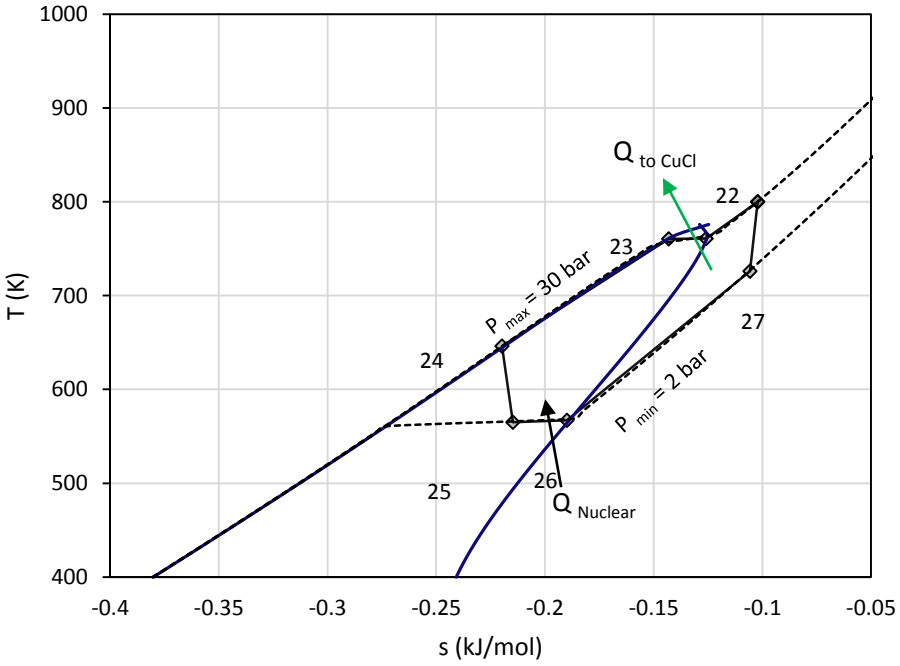

(b)

Figure 5.2. T-s diagrams of the (a) cuprous chloride (CuCl) and (b) biphenyl ($(C_6H_5)_2$) cascaded heat pump.

5.1 Results of the Sole CuCl Heat Pump

5.1.1 Effect of the temperature of excess CuCl fed to copper oxychloride reactor on CuCl heat pump performance

The CuCl heat pump proposed suggests that the heat input required by the copper oxychloride decomposition endothermic reaction is provided by the excess CuCl (stream 15) fed into the reactor. Thus it is important to investigate the effects of T_{15} on the performance of each heat pump and the cascaded heat pump configurations. Firstly, we will be considering the effect of T_{15} variation on the CuCl mole flow rates.

Figure 5.3 shows the variation of the mole flow rates with respect to T_{15}, namely for stream 3, 6 and 5 (see systems' description). The flow rates are presented as ratios to stream 4, the CuCl produced from oxychloride decomposition and supplied to the copper chlorine (Cu-Cl) thermochemical hydrogen production cycle. It is seen from the figure that the increase of T_{15} decreases the mole flow rate of stream 3, indicating that less mole flow rate of excess CuCl is needed to achieve the enthalpy flow required to decompose copper oxychloride. This decrease is also noticed in stream 6 mole flow rate, which is used for the multistage compression intercooling through HX3 and HX4. This also indicates that more CuCl are produced from copper oxychloride decomposition to be supplied for hydrogen production. It is important to restate that the reactor is modeled as a stoichiometric endothermic reaction. Furthermore, the decrease of all ratios indicates that more copper oxychloride are added to balance the enthalpies and achieve an adiabatic flame temperature within the practical reaction temperature range (775-850 K.) Moreover, it is shown that only nearly 23% of CuCl produced is equal to the flow rate of CuCl to be vaporized and compressed in the CuCl heat pump (stream 6). In addition to that, it is interesting to note that such adjustment of flows guarantees having a saturated liquid when stream 6 and compressed vaporized CuCl of stream 5 are mixed in the mixer.

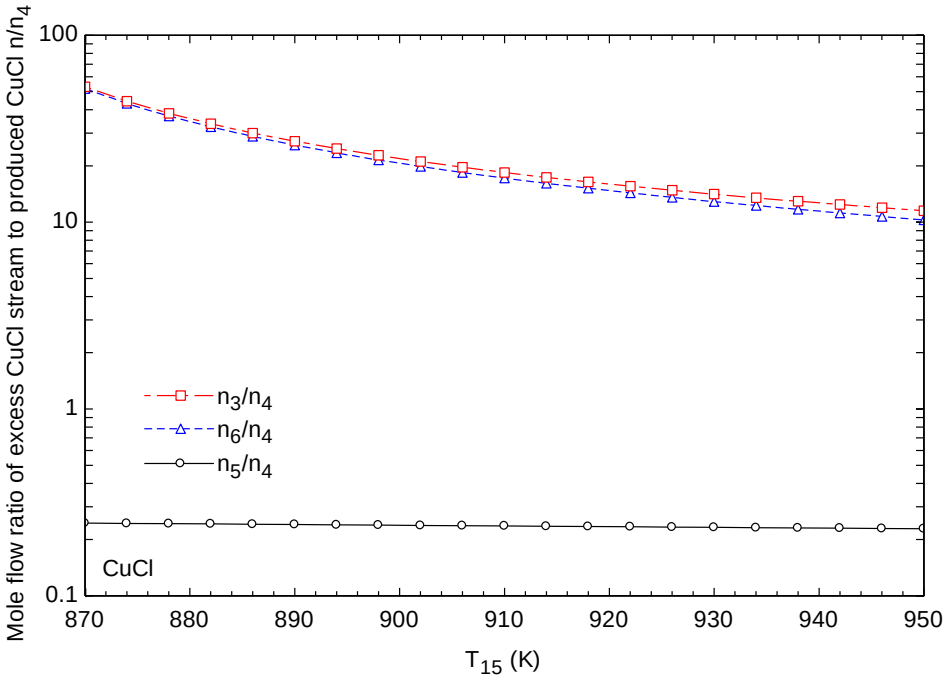

Figure 5.3. The effect of excess CuCl feed temperature on the excess CuCl mole flow rate with respect to the mole flow rate of CuCl produced n_4.

As it is shown that the mole flow rates of the stream varies with respect to $T_{15,}$ the enthalpy flow rate will also vary and effect the amount of heat recovered from oxygen (through HX2) and CuCl (through HX1) produced from the copper oxychloride decomposition. It is observed in Figure 5.4 that the increase of excess CuCl temperature supplied to decomposition reaction will increase the sensible heat recovered from O_2 and CuCl products. This is explained by the fact that the increase of T_{15} will increase the amount of Cu_2OCl_2 supplied and decomposed in the reactor. Thus, more CuCl and O_2 are produced and more of its heat are recovered before they are sent to other processes. At an isentropic efficiency of 75%, the sensible heat recovery ratio increases from 11.4% to 12.2% in an 870-950K temperature range. Moreover, Figure 5.4 shows that decrease in compressors isentropic efficiency increases X_s. This inversely proportional relationship between X_s and isentropic efficiency is due to the high temperature of vapor leaving compressors with low isentropic efficiency and, therefore, low excess CuCl is needed to operate heat pump supply of heat. This low flow rates of CuCl are compensated by an increase in the supply of Cu_2OCl_2 mole flow rate to maintain the practical adiabatic flame temperature of the endothermic reaction. Note that as isentropic efficiency of compressors decrease, X_s becomes more sensible to T_{15} (e.g. slope increases).

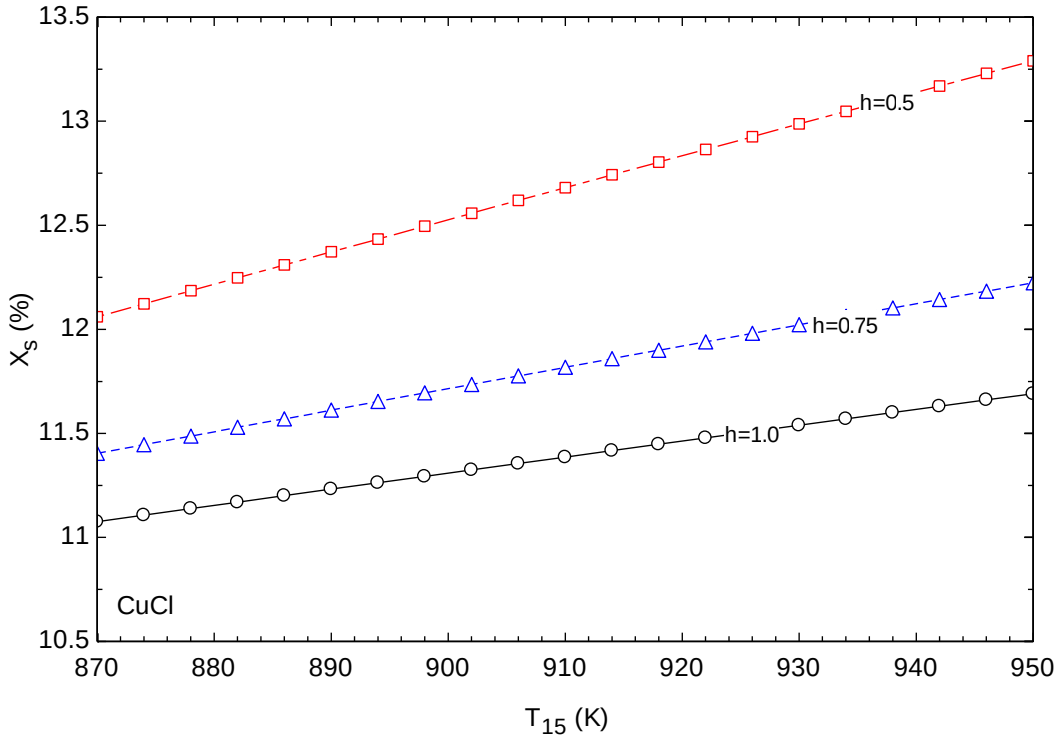

Figure 5.4 Variation of O_2 and produced CuCl sensible heat recovery ratio with excess CuCl feed temperature for different isentropic efficiencies.

The ratio of heat recovered from bottom heat pump (either mercury or biphenyl heat pumps cascaded with CuCl heat pump) to overall heat needed to evaporate stream 7 CuCl, that is to be compressed, behaves totally opposite to the sensible heat recovery ratio. As shown in Figure 5.5, bottom heat pump recovery ratio X_{bottom} decrease as T_{15} increases and as isentropic efficiency decreases. X_{bottom} simply drops because X_s will increase, a portion of heat to evaporate CuCl in stream 7 will be provided by O_2 and CuCl leaving the system to other processes. The explanation is the same for the behavior of the ratio with respect to the isentropic efficiencies. For an isentropic efficiency of 75%, X_{bottom} decreases by 1%. For a theoretical isentropic efficiency of 100%, X_{bottom} only decreases by 0.5%. However, for the lowest isentropic efficiency of 50%, X_{bottom} will drop by 4%, low isentropic efficiency makes the heat recovery ratios more sensitive to the excess CuCl feed temperature.

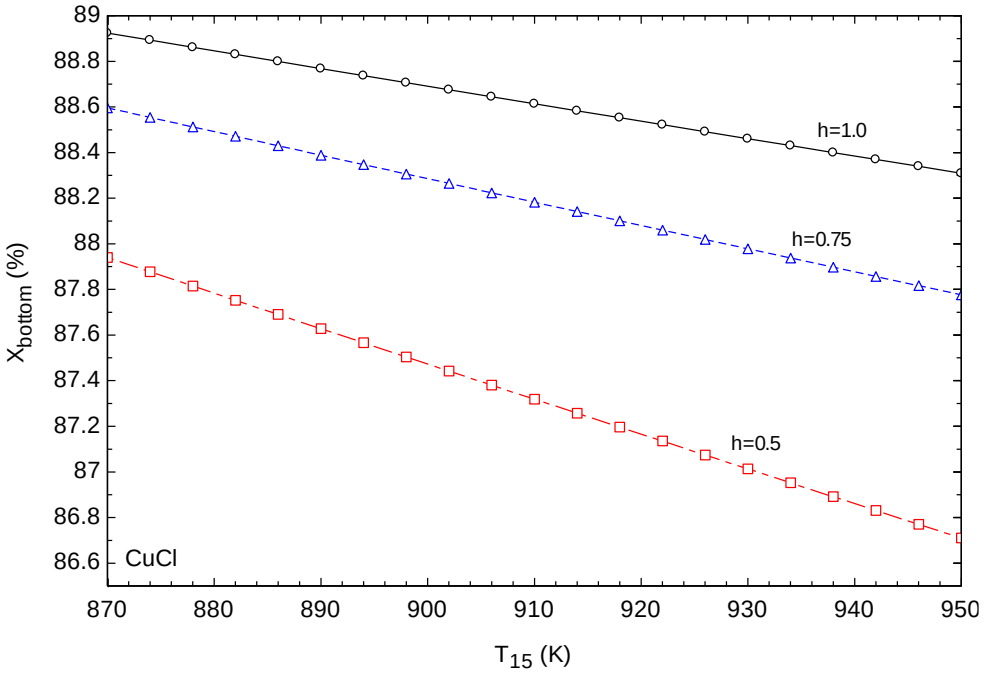

Figure 5.5. Variation of bottom heat pump supplied heat recovery ratio with excess CuCl feed temperature for different isentropic efficiencies.

5.1.2 Effect of copper oxychloride reaction temperature on heat recovery ratios

The heat recovery ratios, both sensible from the reaction products and from the bottom heat pump, seems to be more sensitive to the reaction temperature than to the temperature of stream 15. For a 75% isentropic efficiency, Figure 5.6 shows that the increase of sensible heat recovery ratio from O_2 and CuCl leaving the heat pump is from 12.3% to about 21%. This is simply because the endothermic reaction products will leave the reactor with the reaction temperature, and its increase will create more room for heat to be recovered from the CuCl at stream 7 before it is sent to thermochemical hydrogen production cycle, or the O_2 sent to any other useful process. The effect of isentropic efficiency on Xs is similar to that observed in Figure 5.4.

X_{bottom} in Figure 5.7 decreases with the increase of reaction temperature. In contrast with the relationship between X_{bottom} and temperature of stream 15, X_{bottom} is highly sensitive to reaction temperature. As the product leaving the reactor are having a high temperature, more heat will be recovered from O_2 and CuCl leaving the system, and more flow enthalpy will be associated with stream 5 before it expands to the evaporator at state 7. Therefore more heat will be needed to have

stream 7 reaching the vapor phase. For an isentropic efficiency of 75%, X_{bottom} drops by about 9% in the 850-930K reaction temperature range.

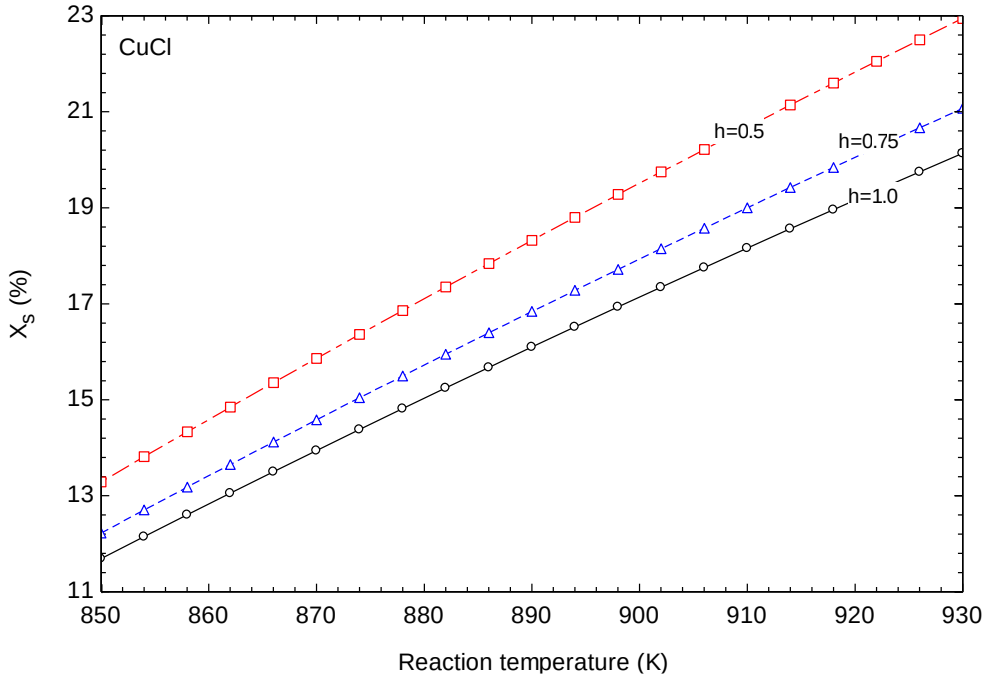

Figure 5.6. Variation of produced CuCl sensible heat recovery ratio with copper oxychloride reaction temperature (reactor outelt temperature) for different isentropic efficiencies.

5.1.3 Effects of heat exchanger temperature approach and degree of intercooling on heat pumps performance

Figure 5.8 shows the decrease of sensible heat recovery ratio X_s with the increase of the temperature approaches in HX1 and HX2 simultaneously (i.e. the approach of O_2 and CuCl temperature to the temperature of stream 7 to be heated.) In a 75% isentropic efficiency, X_s decreases from 12.8% at 1K approach to 17.8% at 20 K approach. Similar to X_s variations with other parameters shown in Figure 5.4 and Figure 5.6, X_s increases with the decrease of isentropic efficiencies as more CuCl and O_2 are going to be produced from copper oxychloride decomposition (i.e. more heat is recovered).

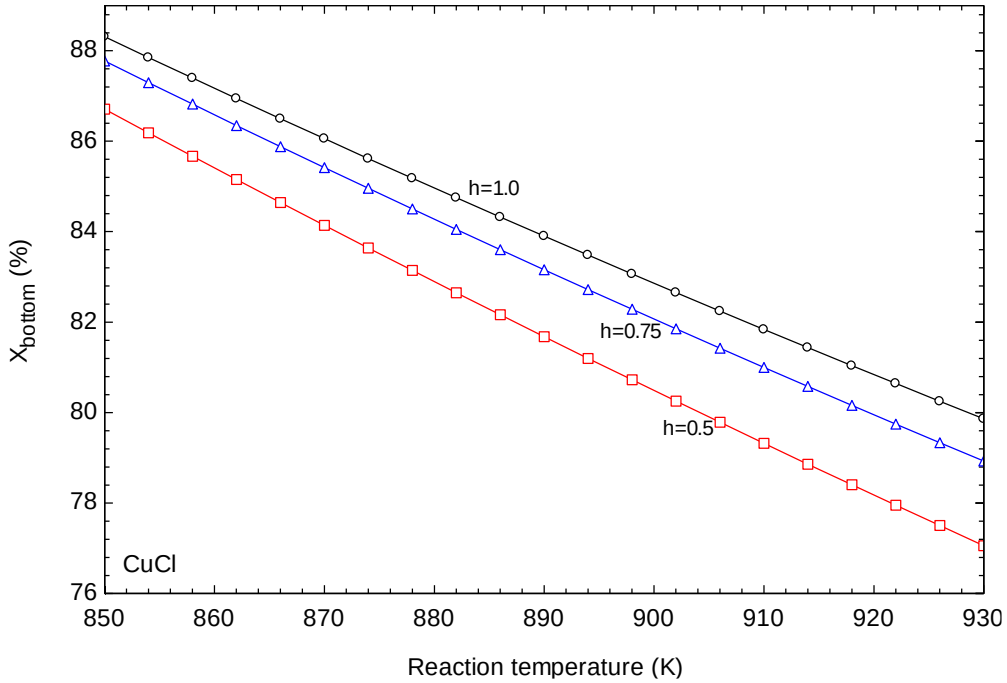

Figure 5.7. Variation of bottom heat pump supplied heat recovery ratio with reaction temperature (reactor outlet temperature) for different isentropic efficiencies.

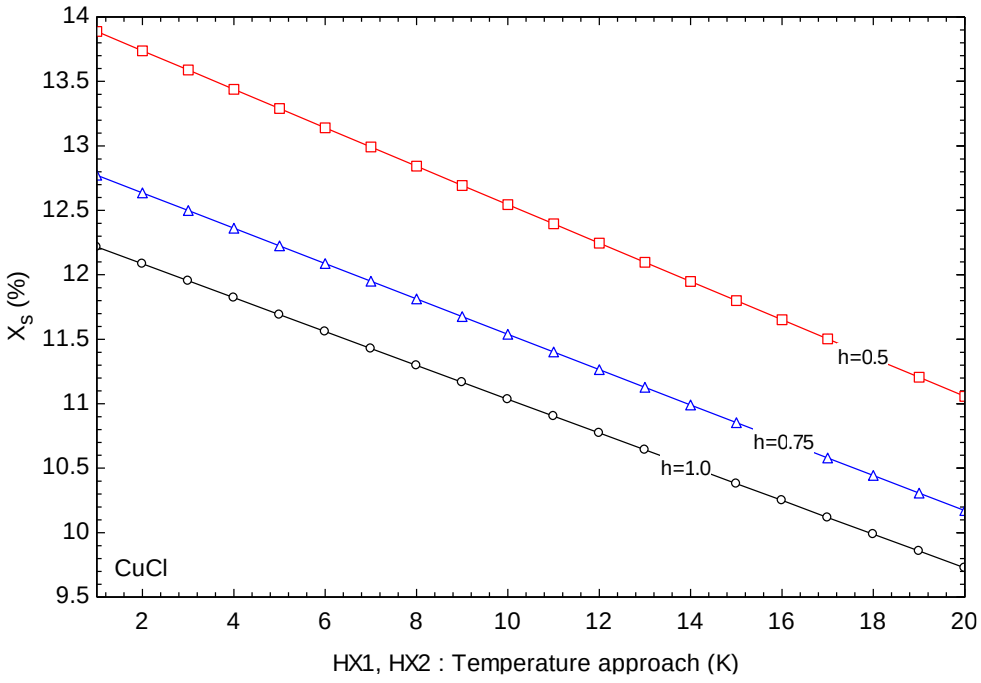

Figure 5.8. Variation of produced CuCl and O_2 sensible heat recovery ratio with HX1 and HX2 temperature approach.

Figure 5.9 shows the response of X_{bottom} to decrease in temperature of approach temperature in HX1 and HX2. As expected, the decrease in temperature approach in these heat exchangers will

create more need of heat from the bottom heat pump to achieve evaporation of stream 7 in the CuCl heat pump. In temperature approach ranging between 1-20K, X_{bottom} increases by 2.6% for system compressors having 75% isentropic efficiency.

The energetic and exergetic COP of CuCl heat pump is investigated in Figure 5.10 with respect to increase in HX3 and HX4 intercooling temperature outlet. It is seen that if the gas phase of CuCl is cooled to as low as possible of intercooling temperature, the energetic and exergetic COPs increase. For the base case temperature of excess CuCl supplied to reactor (950 K), maximum energetic and exergetic COPs of 6.4 and 4.1 can be achieved if the gas phase is intercooled to a temperature of 920 K between compression stages. These COPs drop as intercooling temperature increases (degree of intercooling reduces). Furthermore, Figure 5.10 shows that as T_{15} is decreased, energetic and exergetic COPs become more sensitive to intercooling temperature in HX3 and HX4. In a 920-1100 K of intercooling temperature range, energetic and exergetic COPs drop by 0.24 and 0.17 for a T_{15} equals to 950K, but the COPs drop by 0.74 and 0.5 for a T_{15} equals to 875 K.

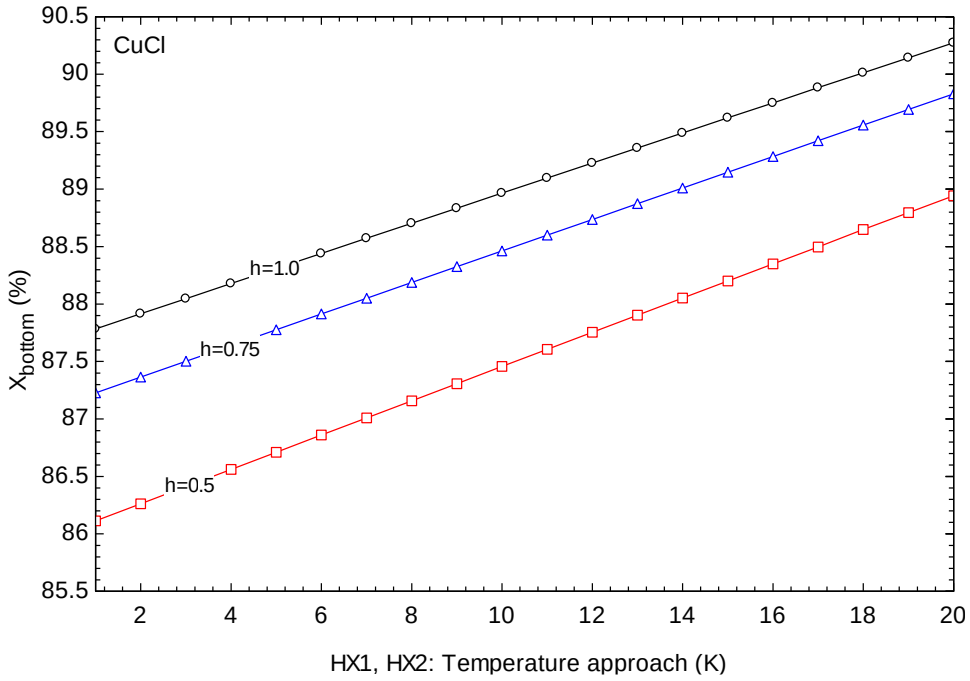

Figure 5.9. Variation of bottom heat pump supplied heat recovery ratio with HX1 and HX2 temperature approach.

5.1.4 Effect of evaporator pressure on CuCl heat pump performance

Figure 5.11 shows that the energetic and exergetic COPs of the CuCl heat pump will respectively increase from 4.5 and 2.93 at 0.05 mbar evaporator pressure to 10.7 and 6.9 at 1 mbar evaporator pressure. The reason behind this increase is that less power will be consumed in the compression of the saturated vapor at state 8 to a superheated vapor at state 13.

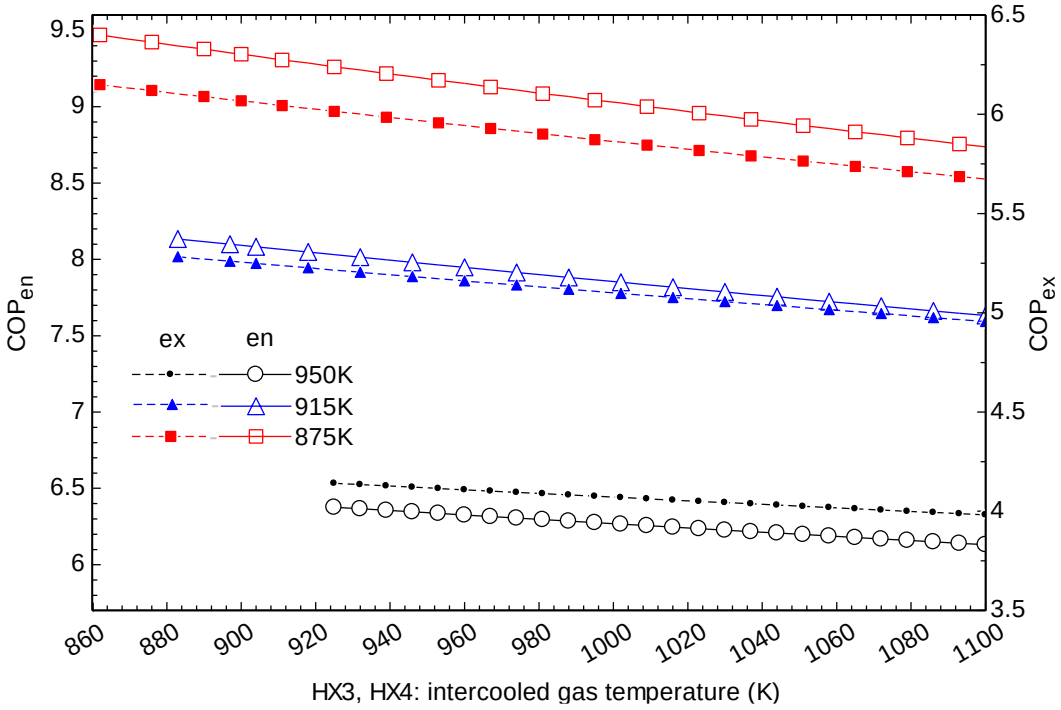

Figure 5.10. Variations in energetic and exergetic COPs of CuCl heat pump with HX3 and HX4 outlet intercooling temperature of the CuCl vapor.

5.1.5 Effect of compressors pressure increasing options on CuCl heat pump performance

The contribution of each compressor in increasing the pressure of CuCl vapor in multistage compression may be a crucial factor to be considered in heat pump performance enhancement. The options of pressure increase in each compressor, which are case 1: $[\Delta P_{c1} < \Delta P_{c2} < \Delta P_{c3}]$; case 2: $[\Delta P_{c1} = \Delta P_{c2} > \Delta P_{c3}]$; case3: $[\Delta P_{c1} = \Delta P_{c2} < \Delta P_{c3}]$; and case 4: $[\Delta P_{c1} > \Delta P_{c2} > \Delta P_{c3}]$, are compared to the base case pressure increase option $[\Delta P_{c1} = \Delta P_{c2} = \Delta P_{c3}]$. In Figure 5.12 a comparison is made for the CuCl heat pump alone. It is shown that pressure increasing option in case 1 gives a 4% higher COP (6.59) than base case COP (6.34). Case 3 (6.47) comes at the second place with about 2% increase while case 2 and case 4 worsen the CuCl heat pump performance to lower than 1.5% and 4%, respectively.

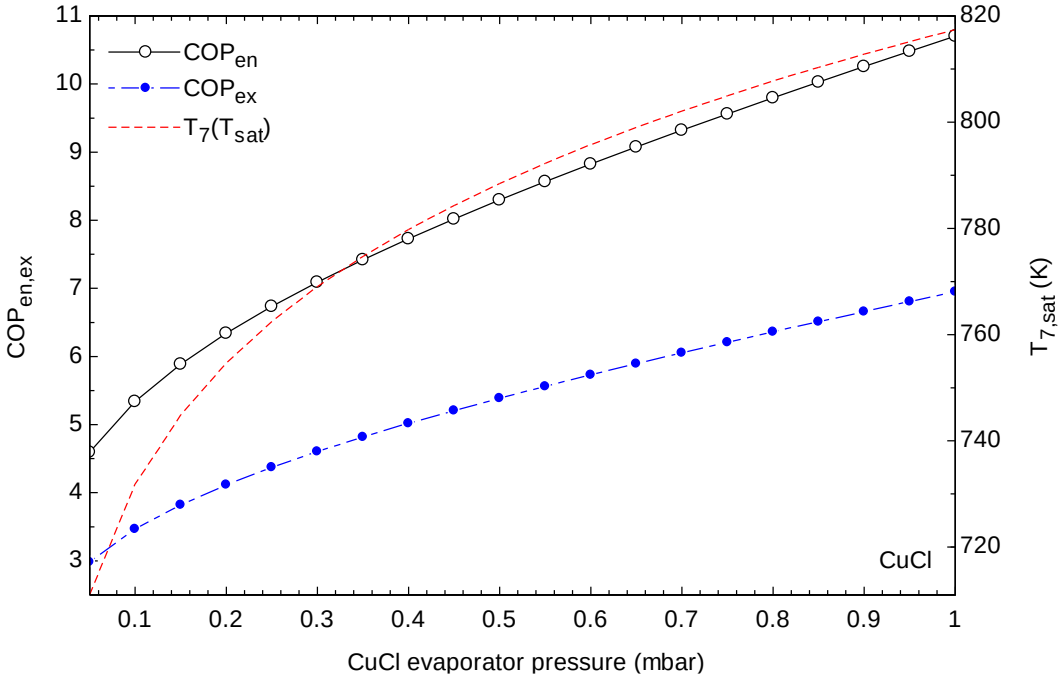

Figure 5.11. Variations in energetic and exergetic COP of CuCl heat pump with its evaporator pressure (Valve 1). Only source temperatures greater than the saturation temperature can be utilized.

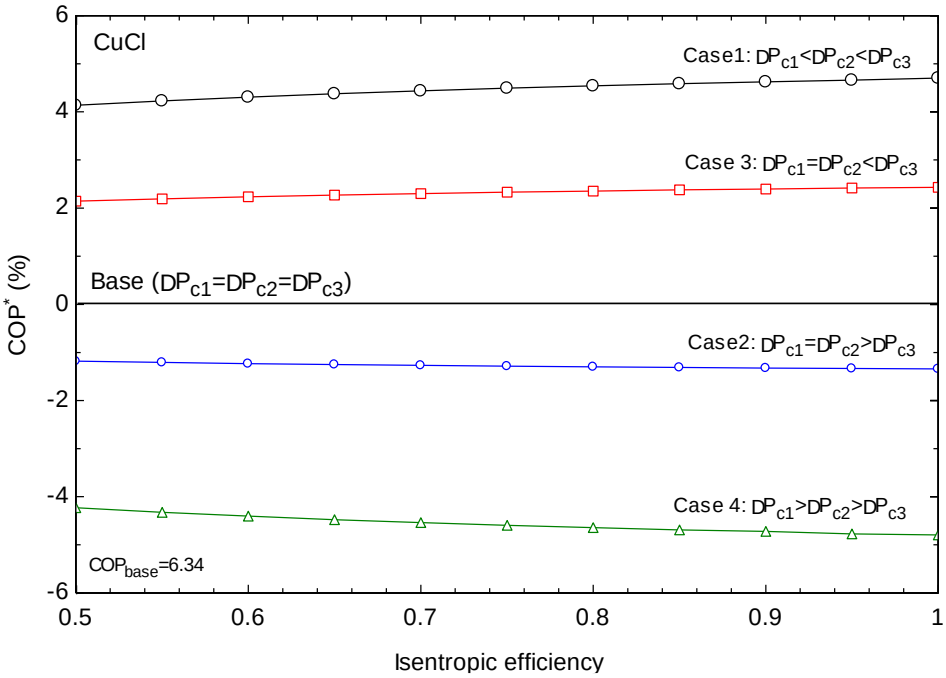

Figure 5.12. The effect of isentropic efficiency of compressors on the COPs of different multistage compression options relative to base COP for CuCl heat pump.

5.2 Results of the Sole Mercury Heat Pump and CuCl-Mercury Cascaded Heat Pumps

5.2.1 Effect of intercooling heat exchanger temperature approach on mercury based heat pumps

The effect of HX5 and HX6 intercooling temperature (approach of hot inlet to the temperature of stream 7) on energetic and exergetic COPs when mercury is operating alone and when it is coupled with the CuCl is presented in Figure 5.13. The degree of intercooling is important for the compressors performance and to avoid high temperature compressors outlet that materials cannot withstand. Figure 5.13 shows that both energetic and exergetic COPs increase as the temperature approach of the heat exchangers decrease. Each of the single mercury COPs, energetic and exergetic, increases by 0.25 in a 0-250 K temperature approach range. The cascaded heat pump COPs seems much less sensitive to the heat exchangers temperature approach in the same range (0.02 difference between COPs at 0K and 250 K). The difference between the energetic and exergetic COPs for the cascaded CuCl-mercury heat pump is far greater than their difference in the single mercury heat pump.

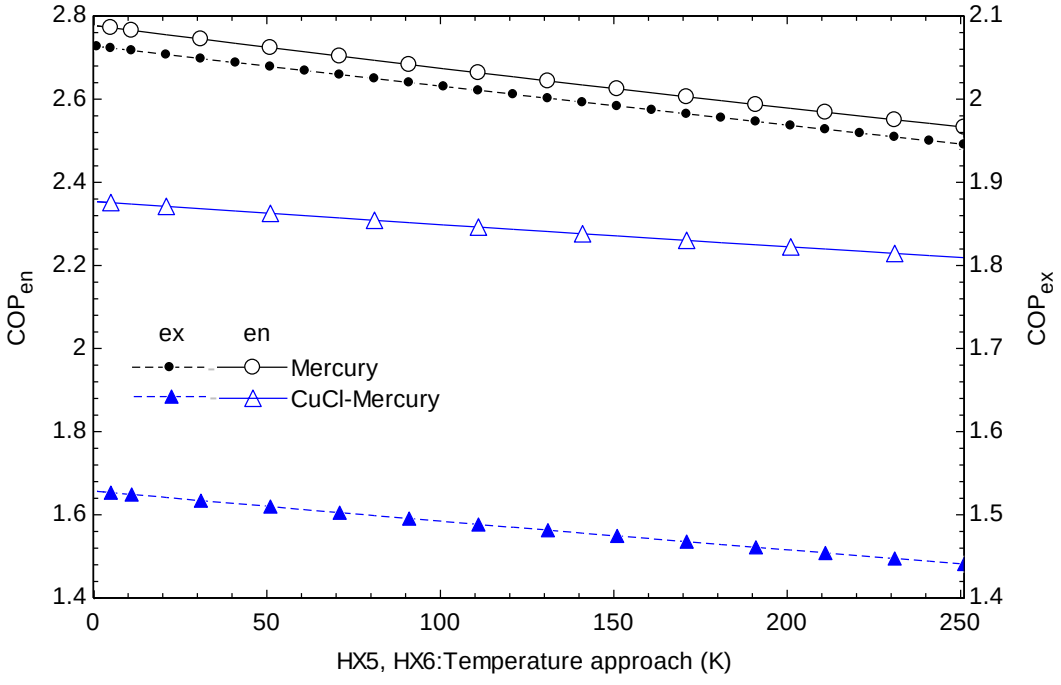

Figure 5.13. Variation in energetic and exergetic COPs of single mercury with HX5 and HX6 hot fluid temperature approach.

5.2.2 Effect of evaporator pressure on mercury-based heat pumps performance

The base case for the bottom heat pumps are set to accommodate a 573 K (300°C) source temperature, which is the temperature of common nuclear power plants we are considering as heat sources, and this is achieved by setting the pressure of the evaporator of the bottom to 0.3 bar in the case of mercury (saturation temperature of 569 or 296°C) and 2 bar in case of biphenyl (saturation temperature of 561 K or 288°C). The COPs of mercury bottom heat pumps, solely and cascaded with CuCl heat pump, are investigated to understand their performance for lower temperature heat sources.

Figure 5.14 shows single mercury heat pump energetic and exergetic COPs behavior in a 0.05-0.3 bar pressure range for the mercury evaporator. Both the energetic and exergetic COPs increase in higher evaporator pressure, which is limited to heat source temperature higher than saturation temperature corresponding to the pressure of evaporator at that instant. Energetic COP at a pressure of 0.05 bar (1.4, suitable for source temperatures greater than 500 K, 227°C) is about 50% lower than energetic COP at pressure of 0.3 bar (2.77, suitable for source temperatures greater than 570 K, 297°C).

The energetic and exergetic COPs of the CuCl-mercury cascaded heat pumps shown in Figure 5.15 agrees with Figure 5.14 except for the fact that the heat pumps coupling leads to lower COPs, energetic and exergetic COPs for cascaded case are respectively 0.42 and 0.57 lower than the sole-mercury heat pump energetic and exergetic COPs. In a pressure range of 0.05-0.3 bar (source temperature higher than a range of 500 K (227°C)-570 K (297°C)) the cascaded CuCl-mercury heat pump COPs energetically rise by 0.88 and exergetically rise by 0.55.

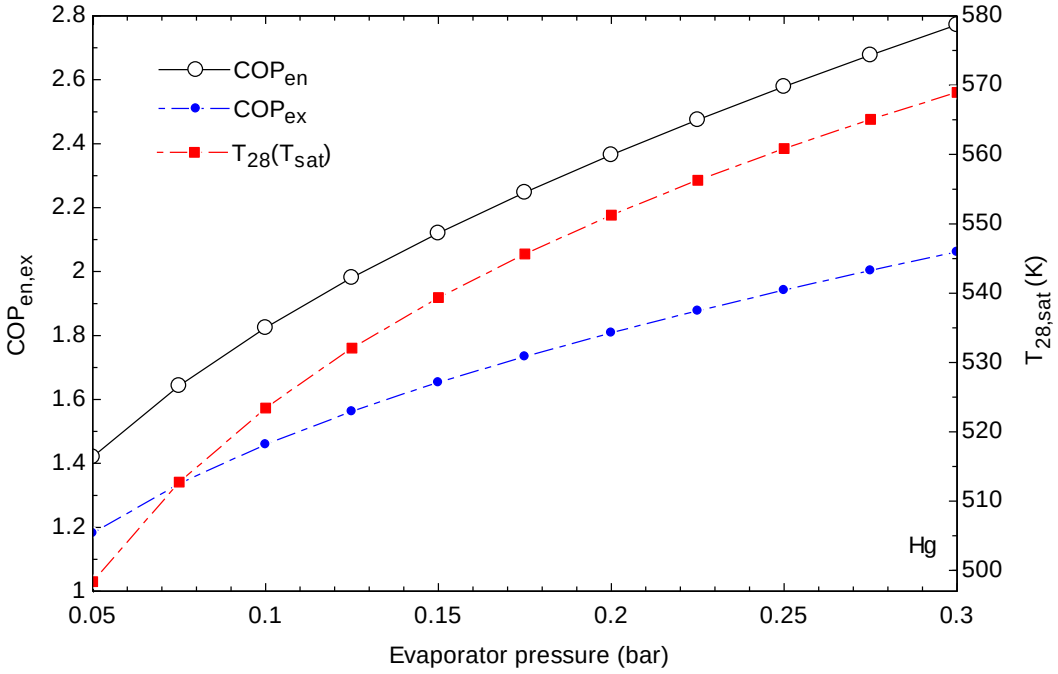

Figure 5.14. Variations in energetic and exergetic COPs of sole mercury heat pump with its evaporator pressure. Only source temperatures greater than the saturation temperature can be utilized.

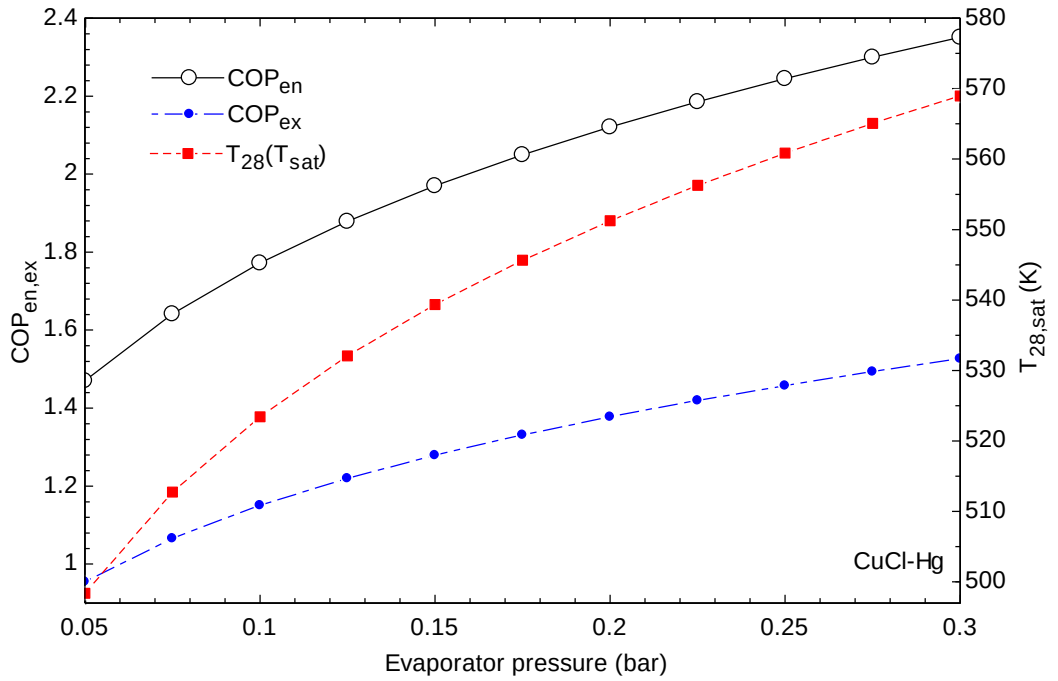

Figure 5.15. Variations in energetic and exergetic COPs of cascaded CuCl-mercury heat pumps with mercury heat pump evaporator pressure. Only source temperatures greater than the saturation temperature can be utilized.

In contrast to the performance enhancement of the CuCl heat pump with the increase of it evaporator pressure shown in Figure 5.11, bottom mercury heat pump cycle will experience a drop in its energetic and exergetic COPs as shown in Figure 5.16. The reason behind such a decrease in COPs is that as the pressure of the CuCl heat pump (stream 7 to 8) evaporator increases, high temperature working fluid in the bottom cycle condenser will be expected to evaporate the fluids in the top cycle evaporator. That high temperature source provided by the bottom mercury heat pump cycle cannot be obtained unless its heat sink pressure (i.e. condenser pressure) is raised, which will eventually lead to more power consumption and COPs to drop.

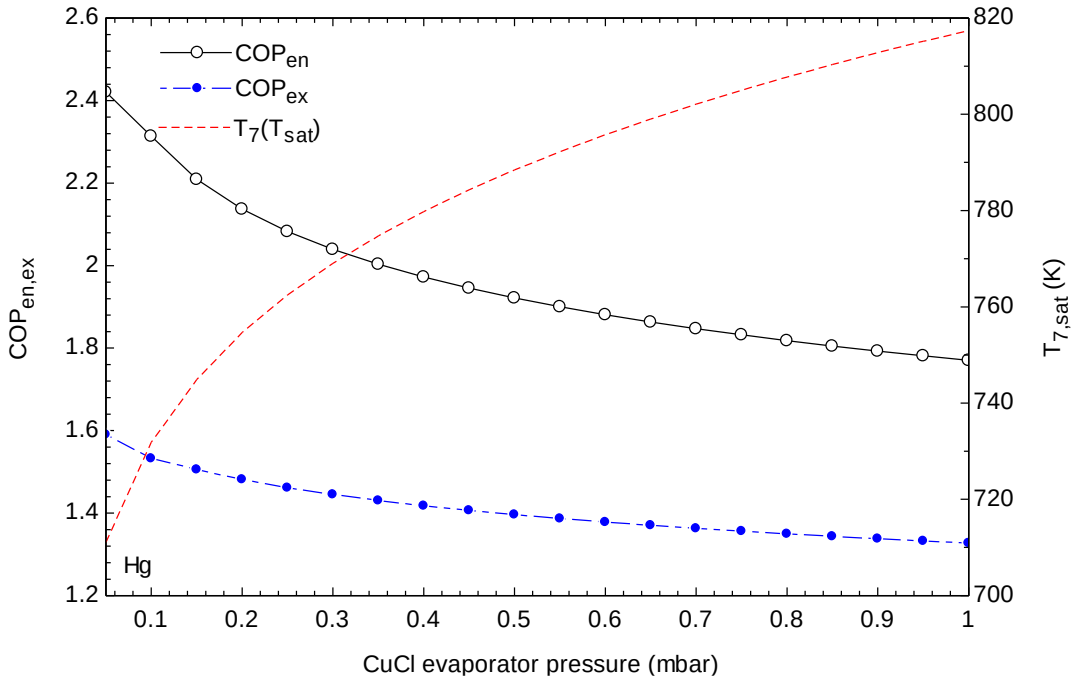

Figure 5.16. Variations in energetic and exergetic COPs of mercury heat pump with respect to CuCl evaporator pressure (valve 1 outlet pressure). Only source temperatures greater than the saturation temperature can be utilized.

Nevertheless, a good optimization of the cascaded system can achieve a cascaded heat pump welling to produce greater unit of heat per unit of electric power input. In the CuCl evaporator pressure range of 0.02-0.3 mbar, both energetic and exergetic COPs of the CuCl-mercury cascaded heat pumps becomes greater than unity (2.1-1.7), as shown in Figure 5.17.

5.2.3 Effect of compressors pressure increasing options in CuCl heat pump on performance of mercury and CuCl-mercury heat pumps

The mercury based heat pumps performances are investigated using the CuCl heat pump pressure increase options presented previously in section 5.1.5. Cases are - case 1: $[\Delta P_{c1} < \Delta P_{c2} < \Delta P_{c3}]$; case 2: $[\Delta P_{c1} = \Delta P_{c2} > \Delta P_{c3}]$; case3: $[\Delta P_{c1} = \Delta P_{c2} < \Delta P_{c3}]$; and case 4: $[\Delta P_{c1} > \Delta P_{c2} > \Delta P_{c3}]$, which are aa compared to the base case pressure increase option $[\Delta P_{c1} = \Delta P_{c2} = \Delta P_{c3}]$.

Similar to the COP of the single CuCl heat pump, in Figure 5.18 case 1 is found to have the highest COP but this time with an increase that varies from 1.43% to 0.8% in a 0.5 to 1 isentropic efficiency range. Case 3 comes as the second preferred option, while case 2 and case 4 options give a COP lower than the base operation COP. For a cascaded CuCl-Mercury heat pumps, Case 1 remains to be the first preferred option in multistage compression, case 3 is the second preferred, case 2 and case 4 are inconvenient if compared to case base case. Case 1 COP (2.33) is 1.5% higher than base case COP (2.22), and case 3 (2.23) is nearly 0.5 higher, see Figure 5.19.

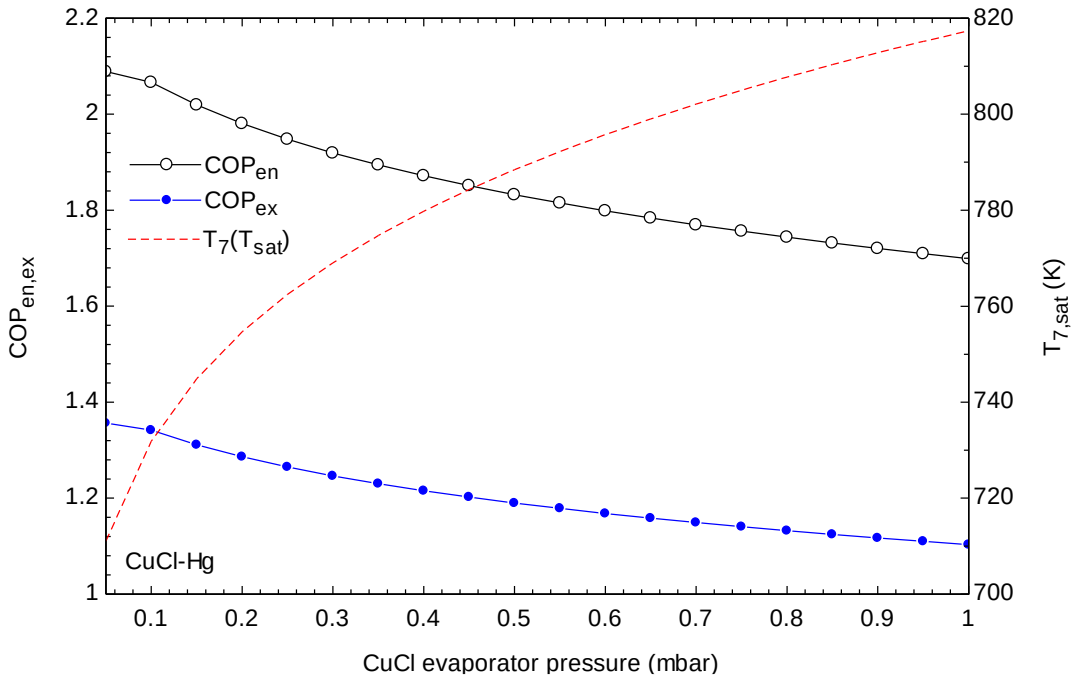

Figure 5.17. Variations in energetic and exergetic COPs of CuCl-mercury heat pump with respect to CuCl evaporator pressure (valve 1 outlet pressure). Only source temperatures greater than the saturation temperature can be utilized.

5.3 Results of the Sole Biphenyl Heat Pump and CuCl-Biphenyl Cascaded Heat Pumps

5.3.1 Effect of evaporator pressure on biphenyl-based heat pump performance

In Figure 5.20 and Figure 5.21, the evaporator pressure in the biphenyl heat pump is varied from 0.1 bar (suitable for heat source temperatures greater than 465 K (192°C)) to a pressure of 4 bar (suitable for heat source temperatures greater than 601 K (328°C)). In Figure 5.19, the energetic and exergetic COPs of the sole biphenyl heat pump increase from values below unity (COP_{en}=0.85, COP_{ex}=0.52) at 0.1 bar to 2.53 and 1.55, respectively, at a pressure of 4 bar. Moreover, the exergetic COP of the sole biphenyl heat pump is 39% lower than the energetic COP.

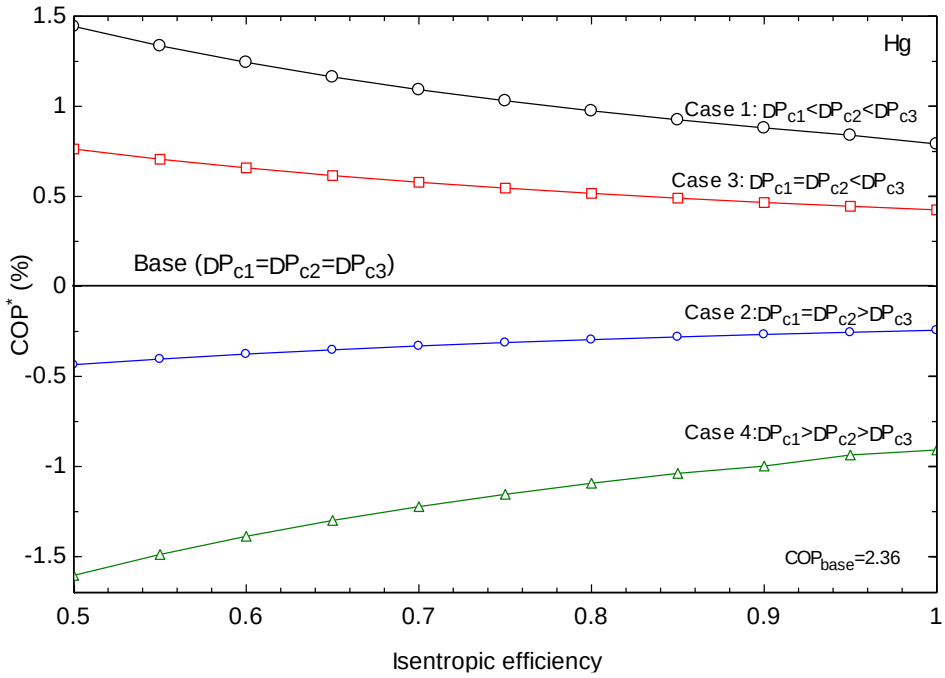

Figure 5.18. The effect of isentropic efficiency of compressors on the COPs of different multistage compression options relative to base COP for mercury heat pump.

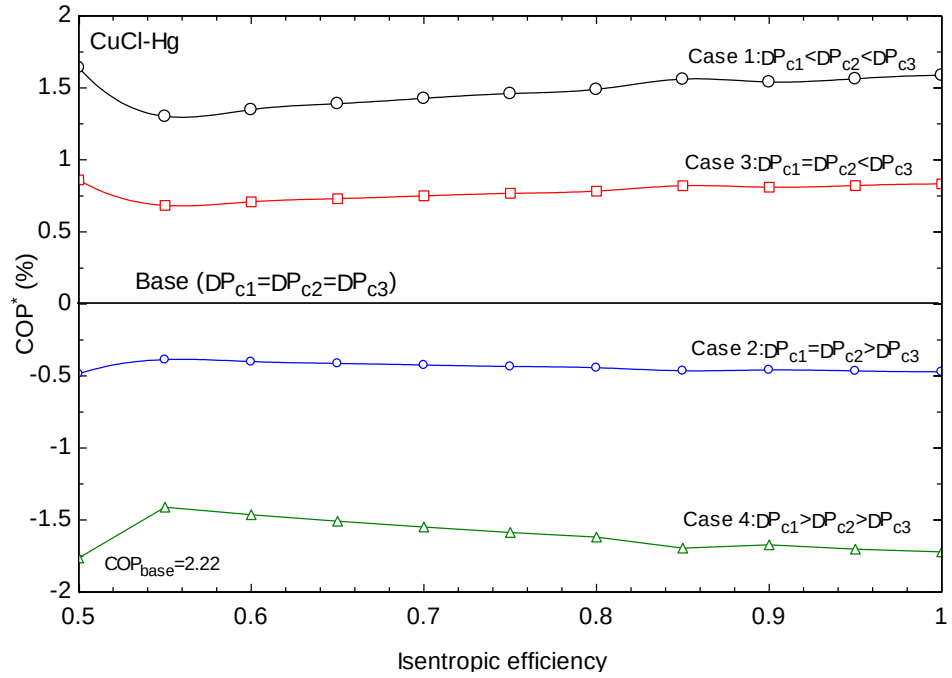

Figure 5.19. The effect of isentropic efficiency of compressors on the COPs of different multistage compression options relative to base COP for CuCl-mercury cascaded heat pump.

Figure 5.21 shows that, at the lowest pressure of 0.1 bar, the CuCl-biphenyl cascaded heat pump has a lower overall energetic COP (0.52) than the sole biphenyl heat pump (0.85). Its exergetic COP (0.62), however, is greater compared to the exergetic COP (0.52) of the single heat pump.

In contrast to the improvement in the CuCl heat pump with the increase of its evaporator pressure, as shown in Figure 5.11, bottom biphenyl heat pump cycle will experience a drop in its energetic and exergetic COPs as shown in Figure 5.22. The reason behind such decrease in the performance of the biphenyl heat pump is that as the evaporator pressure of the CuCl heat pump (stream 7 to 8) increases, high temperature working fluids in the bottom cycle condenser will be expected to evaporate the fluids in the top cycle evaporator. That high temperature source should be provided by the bottom biphenyl heat pump to the CuCl heat pump evaporator cannot be obtained unless the biphenyl heat sink pressure is raised, which will eventually lead to more power consumption and COPs to drop. The CuCl-biphenyl cascaded heat pump will witness a similar drop in energetic and exergetic COPs for the same reason as shown in Figure 5.23.

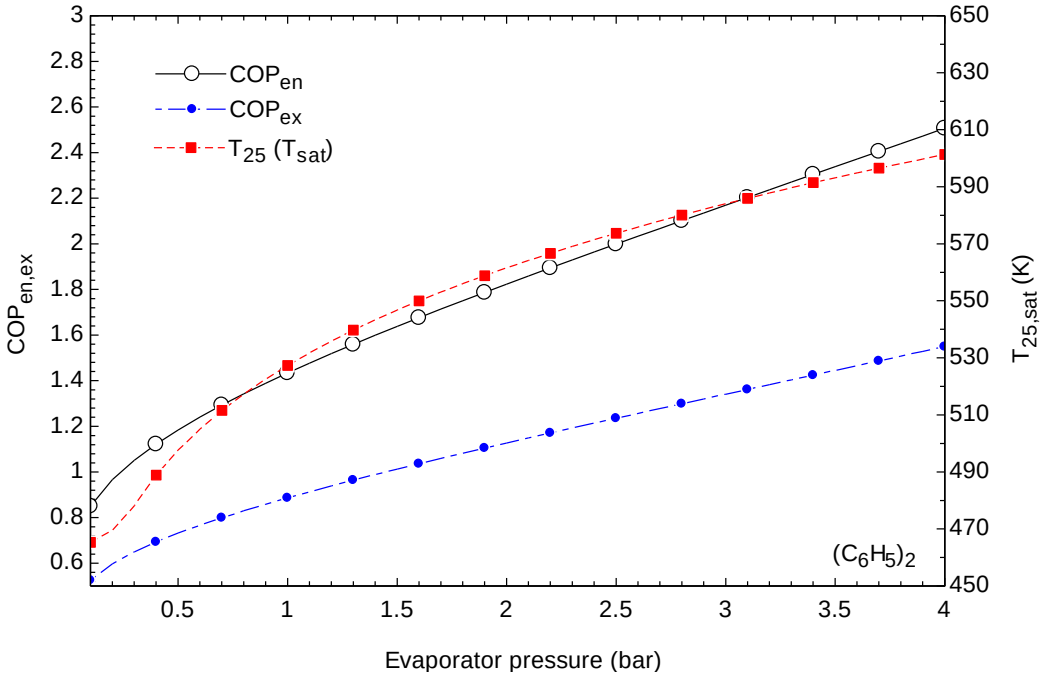

Figure 5.20. Variations in energetic and exergetic COPs of sole biphenyl heat pump with its evaporator pressure. Only source temperatures greater than the saturation temperature can be utilized.

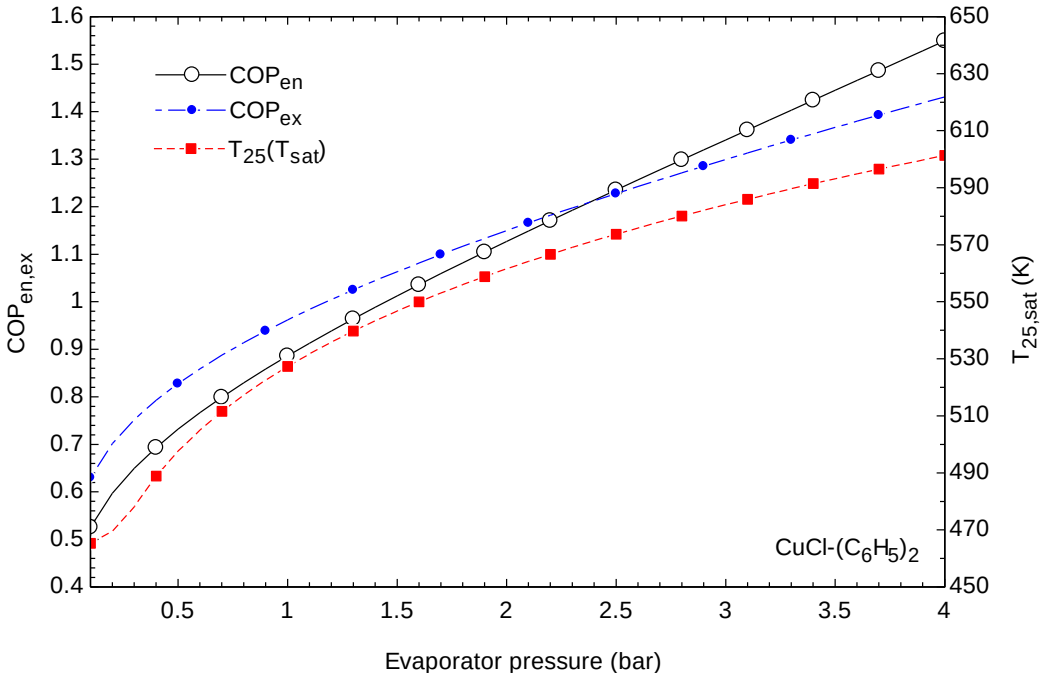

Figure 5.21. Variations of energetic and exergetic COPs of CuCl-biphenyl cascaded heat pump with biphenyl evaporator pressure. Only source temperatures greater than the saturation temperature can be utilized.

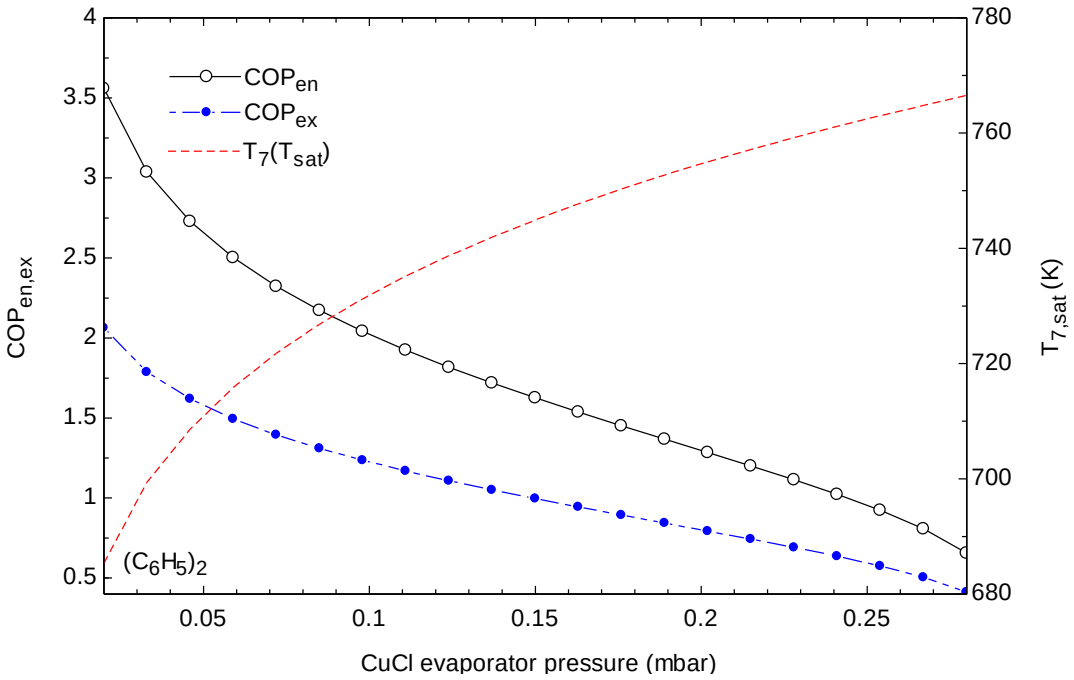

Figure 5.22. Variations in energetic and exergetic COPs of biphenyl heat pump with CuCl evaporator pressure (valve 1). Only source temperatures greater than the saturation temperature can be utilized.

5.3.2 Effect of biphenyl compressor outlet temperature on biphenyl related heat pumps

The temperature of biphenyl leaving the compressor is investigated in this section as it is related to the heat pump COP through the biphenyl compressor power requirement. Figures 5.24 and 5.25 indicate that an increase of the biphenyl temperature at the compressor outlet increases the energetic and exergetic COPs for the single biphenyl heat pump and the CuCl cascaded heat pumps. The energetic COP of both the single biphenyl heat pump and the cascaded heat pump increase from 0.45 and 0.54 at an outlet temperature of 765 K to 1.9 and 1.8 at an outlet temperature of 830 K, respectively. In addition, the exergetic COP of the sole biphenyl heat pump and the cascaded heat pump increase by 1.5 and 0.82, respectively. Note that the exergetic performance of CuCl-biphenyl coupled heat pump is energetically and exergetically better than that of the single functioning biphenyl heat pump for most compressor outlet temperature ranges. This increase in COP is explained by the fact that temperature is high enough to only require low flow rates of biphenyl to evaporate CuCl in the top heat pump cycle. Therefore, as less mole flow rate is requires

at high compressor outlet temperature, less power consumption will be achieved by the biphenyl compressor, see Figures 5.24 and 5.25.

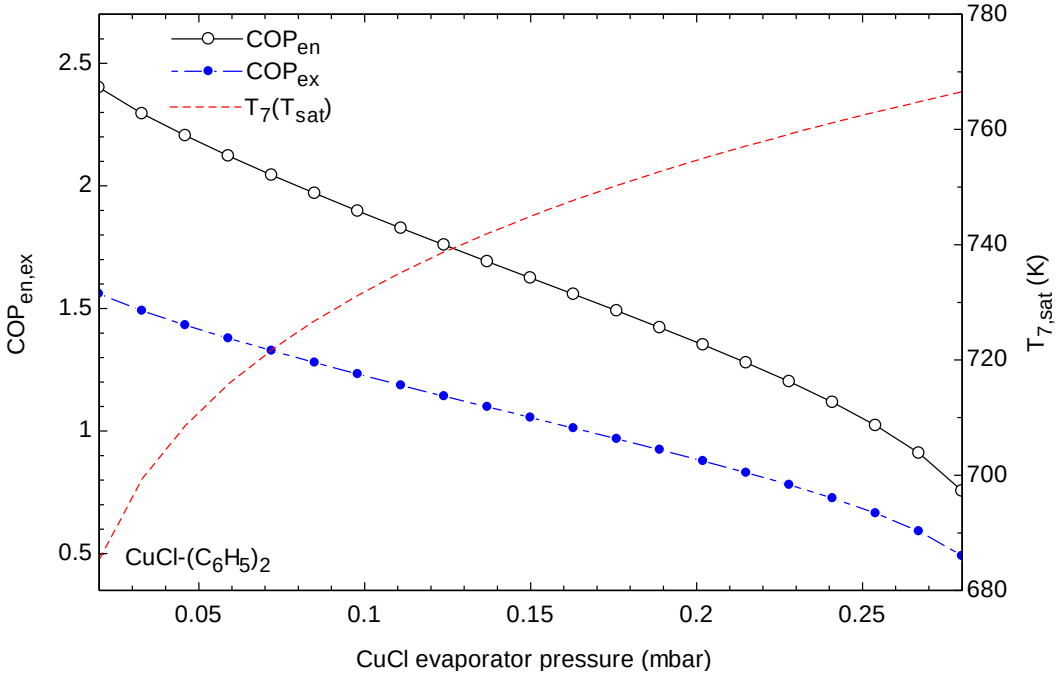

Figure 5.23. Variations in energetic and exergetic COPs of cascaded CuCl-biphenyl heat pumps with to CuCl evaporator pressure (valve 1 outlet pressure).

5.4 Comparative Results of Proposed Heat pumps

5.4.1 Effect of isentropic efficiency of compressors on performance of heat pumps

Compressors are considered to be main components in heat pumps involving vapor compression. In both configurations, compressors are used and their isentropic efficiencies are varied to assess performance parameters. In the base (reference) case, 85% isentropic efficiency is considered for all compressors in both configurations, sole and cascaded, mercury based and biphenyl related. The increase in compressors isentropic efficiency lower its power requirement to achieve desired compression vapors, and theoretically explains the increase of vapor compression heat pumps and refrigeration cycles coefficient of performances COPs. Isentropic efficiencies variation takes place simultaneously for all compressors.

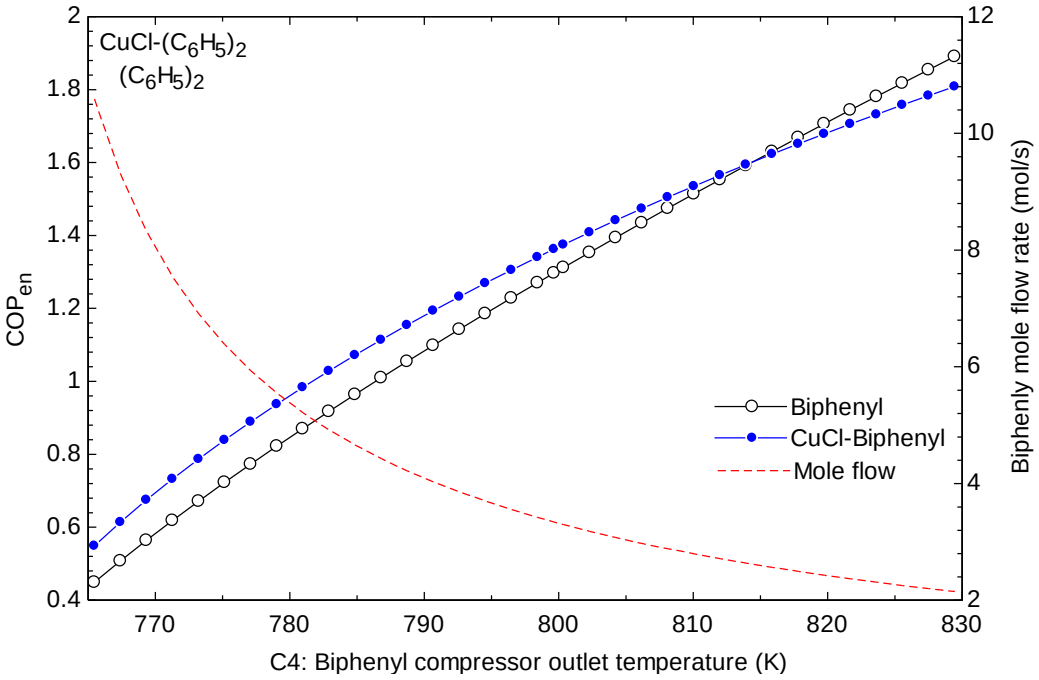

Figure 5.24. Variation of energetic COP of biphenyl and cascaded CuCl-biphenyl heat pumps with biphenyl compressor C4 outlet temperature.

The first evaluation parameters considered are the energetic and exergetic coefficient of performances (COP_{en}, COP_{ex}) for the CuCl heat pump shown in Figure 5.26. It is observed that the increase of isentropic efficiency enhances the performance of the CuCl heat pump for various temperatures of CuCl (T_{15}) fed to the copper oxychloride decomposition reactor. In the base case in which the excess CuCl temperature fed into reactor is 950 K, the coefficient of performance of the CuCl heat pump rises from 2.71 to 4.76 as the isentropic efficiency increases from 0.5 to 1.0, representing an approximate increase of 2 units of heat production per unit of electrical power supply. Also, as the temperature of the CuCl carrying reaction heat is decreased to a lower operational level (recall that temperature of copper oxychloride reactor should be in an operation temperature range of 775-850 K), the overall energetic and exergetic coefficient of performances increase and become more sensitive to isentropic efficiency of compressors (i.e. increase of slope).

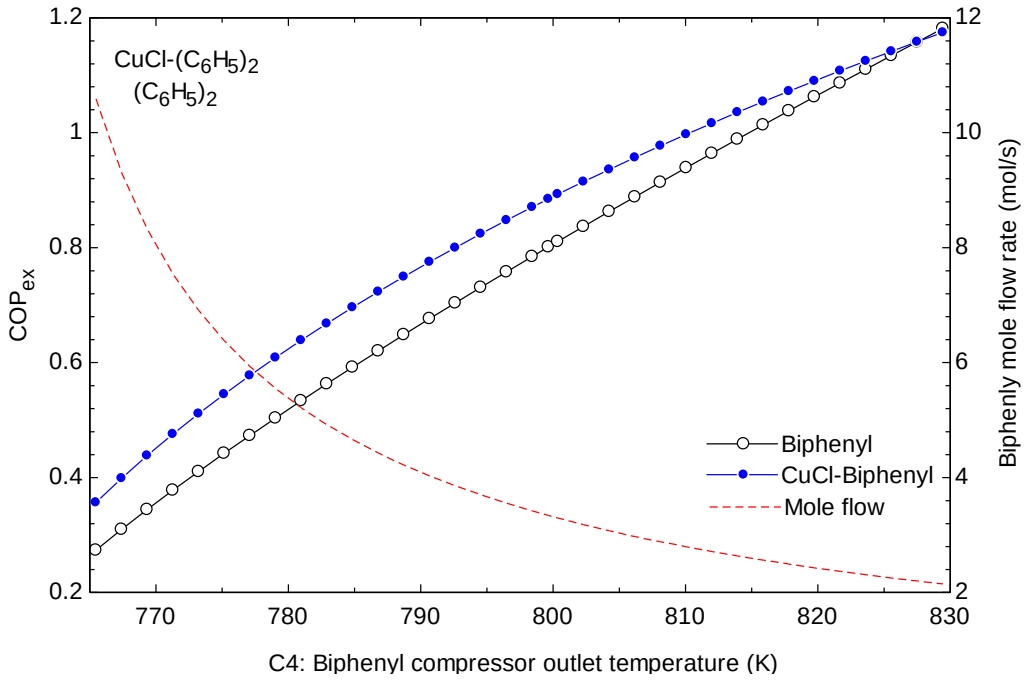

Figure 5.25. Variation of exergetic COP of biphenyl and cascaded CuCl-biphenyl heat pumps with biphenyl compressor C4 outlet temperature.

On the other hand, Figures 5.27 and 5.28 shows the response of the energetic and exergetic COPs respectively for the mercury heat pump, the mercury-CuCl cascaded heat pump, the biphenyl heat pump, and the biphenyl-CuCl cascaded heat pump to changes in isentropic efficiency of its compressors. Again, all COPs, energetic and exergetic, rise with increasing of compressor isentropic efficiency. Nevertheless, the response to an isentropic efficiency increase of both the biphenyl single heat pump and the CuCl-biphenyl cascaded heat pump is low compared to that for the mercury heat pump and the CuCl-mercury cascaded heat pump. In Figures 5.27 and 5.28, the increase of energetic and exergetic COPs for the biphenyl heat pump alone and CuCl-biphenyl cascaded heat pump does not exceed 0.2 for a 0.5 to 1 isentropic efficiency range (i.e. the CuCl-biphenyl cascaded COP varies from 1.6 to 1.8 energetically, and 1 to 1.2 exergetically). Both the single mercury heat pump and the CuCl-mercury cascaded heat pump exhibit notable increases in energetic and exergetic COPs at high isentropic efficiencies (i.e. energetically and exergetically, the COP of CuCl-mercury cascaded heat pump increases from 1.3 to 2.5 and from 0.8 to 1.65, respectively, for a 0.5 to 1 isentropic efficiency rise).

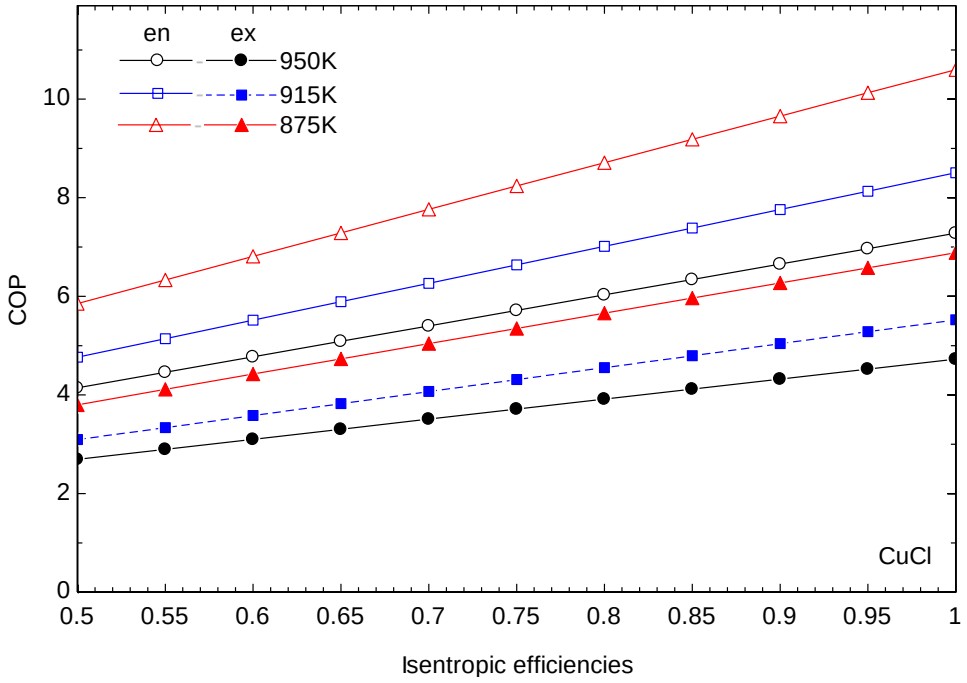

Figure 5.26. Effect of isentropic efficiency of compressors on energetic and exergetic coefficients of performance for several values of temperature of CuCl feed (T_{15}) to reactor.

5.4.2 Effect of the temperature of excess CuCl (T_{15}) fed to the copper oxychloride reactor on performance

It is understood now that the decrease of T_{15} is associated with increase in mole flow rate of excess CuCl (See Figure 5.3). Figure 5.29 shows the energetic COPs of mercury and biphenyl single heat pumps when each of them is cascaded with the CuCl heat pump, with increasing temperature of excess CuCl fed to copper oxychloride reactor, T_{15}. The energetic COP of the mercury single heat pump increases from about 0.6 at 870 K to 2.8 at 950 K. Over the same temperature range, the COP of single biphenyl heat pump increases from 0.4 to 1.8 while the COPs for the cascaded mercury and biphenyl configurations respectively increase from 0.6 to 2.2 and from 0.4 to 1.75. Heat pumps in sole operation have better performance at temperatures greater than 915 K for mercury and 935 K for biphenyl, while at lower T_{15} values, cascaded configurations exhibit better performance.

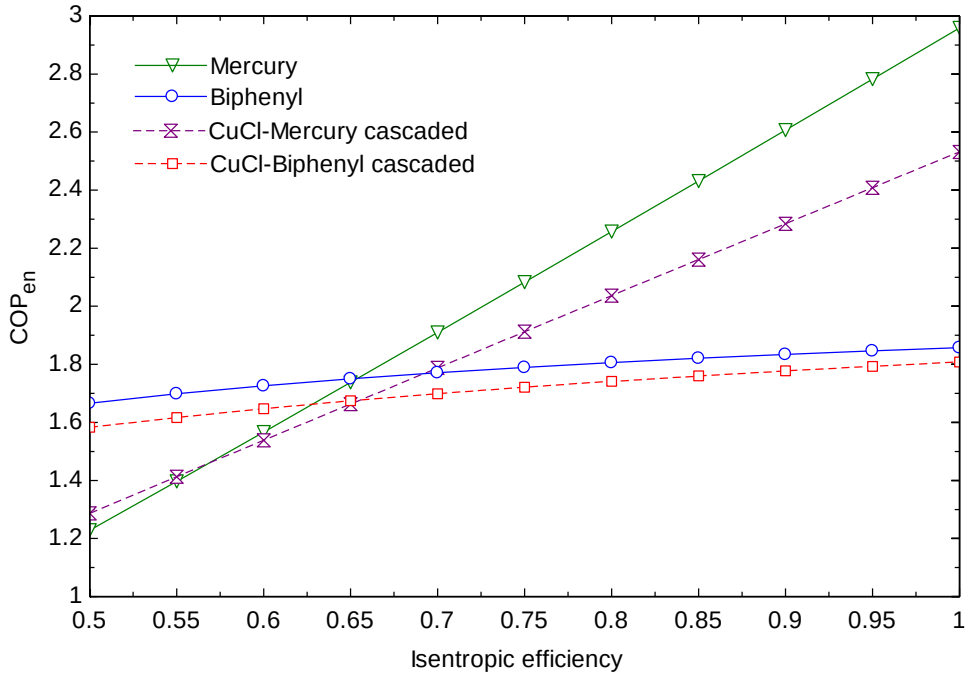

Figure 5.27. Effect of isentropic efficiency of compressors on energetic coefficients of performance of single and cascaded heat pumps.

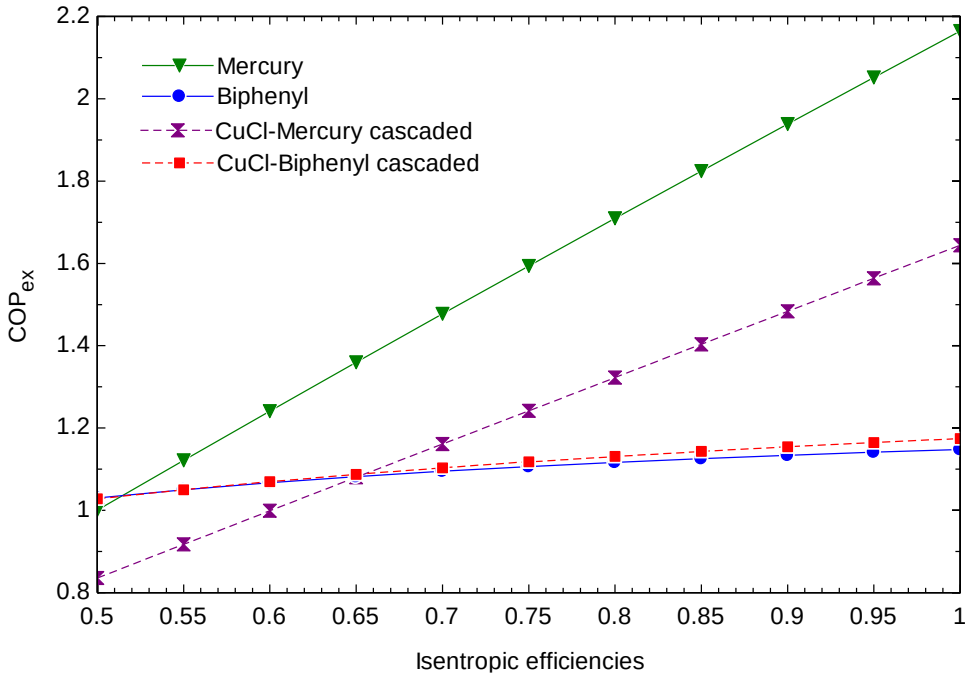

Figure 5.28. Effect of isentropic efficiency of compressors on exergetic coefficients of performance of single and cascaded heat pumps.

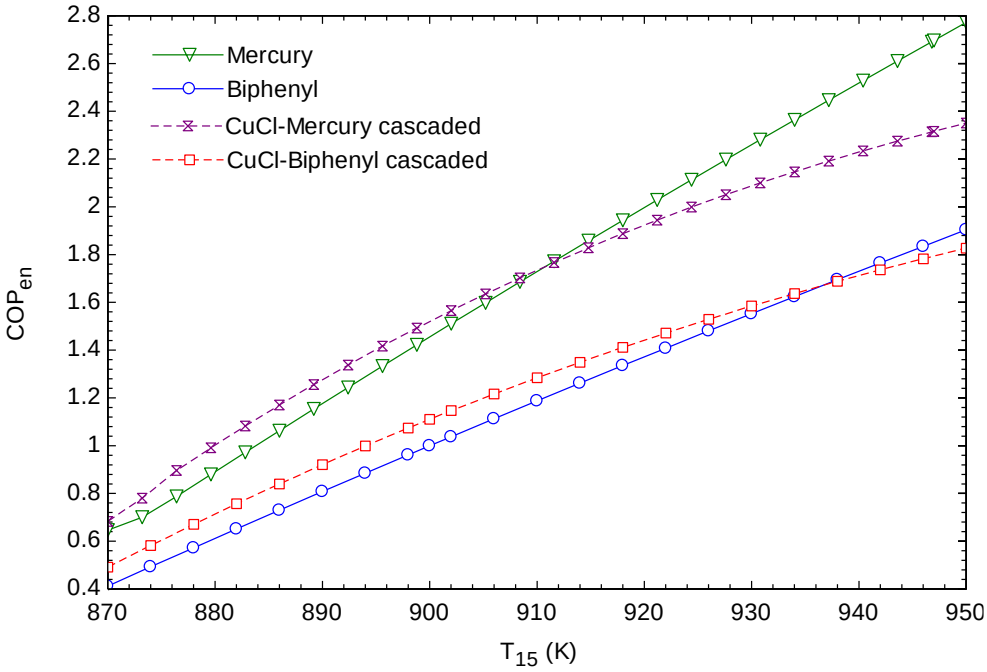

Figure 5.29. Effect of excess CuCl feed temperature (T_{15}) on the energetic COP of single and cascaded heat pumps.

Figure 5.30 shows the effect of T_{15} on the exergetic COP. In contrast to energetic COP, the exergetic COP for the cascaded configurations exhibit better performance than single heat pumps throughout the T_{15} range (870 K (597°C) to 950 K (677°C)). Nevertheless, the exergetic COP is less than the exergetic COP due to the consideration of ambient temperature in reassessing the quality of heat provided by excess CuCl to the endothermic reaction. The exergetic COP of the cascaded mercury system increases from 0.66 to 2.34, which is not excessively low compared to the energetic COP for the same configurations. The biphenyl heat pump cascaded with the CuCl heat pump achieves an exergetic COP of 0.3 to 1.2 over the same temperature range of T_{15}.

5.4.3 Effect of evaporator pressure and temperature on systems performance.

The decrease in the energetic performance of the cascaded heat pump with the increase of the CuCl evaporator pressure is shown in Figure 5.31. Interestingly, the biphenyl based heat pumps have the greatest COPs at the minimum CuCl evaporator pressure investigated. At the lowest CuCl evaporator pressure of 0.02 mbar, the biphenyl heat pump has an energetic COP greater than 3.5 compared to the sole mercury heat pump of which its energetic COP does not exceed 2.5. The CuCl-biphenyl heat pump energetic COP (2.4) is also greater than the CuCl-mercury heat pump

energetic COP (2.1) at a CuCl evaporator pressure of 0.02 mbar. Nevertheless, mercury based heat pumps start to have energetic COPs greater than biphenyl based heat pumps beyond a CuCl evaporator pressure of 0.08 mbar. Figure 5.32 shows the variation of the exergetic COP of the mercury and the biphenyl based heat pumps with the CuCl evaporator pressure. The behavior of the exergetic COP of the heat pumps is the same but with lower values. In both Figure 5.31 and Figure 5.32, it is noticed that the COPs of the biphenyl based heat pumps is more sensitive that the COPs of the mercury based heat pumps.

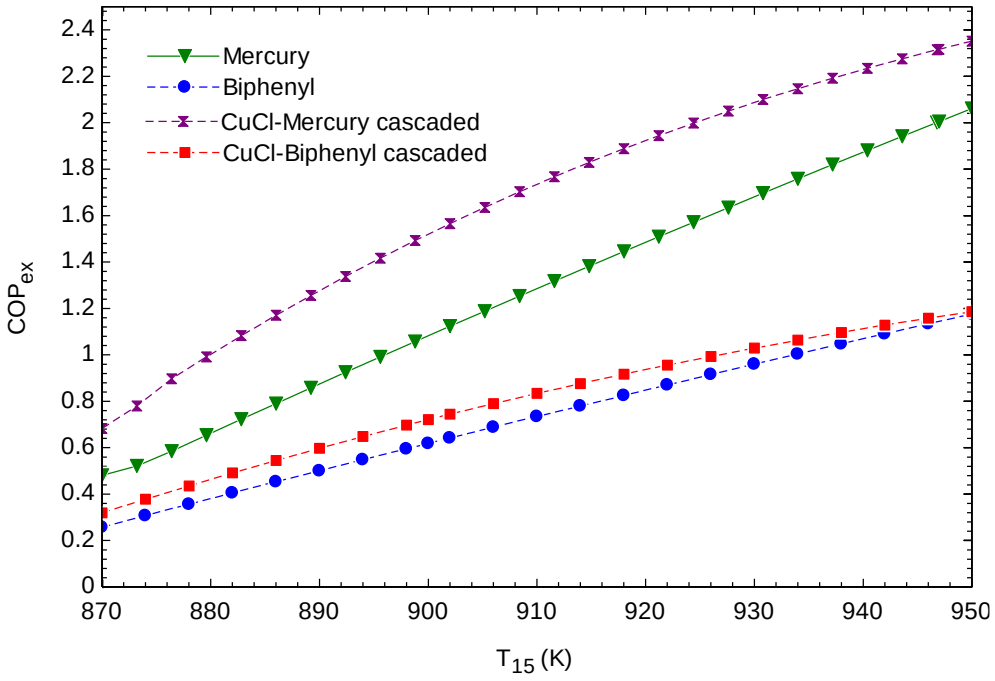

Figure 5.30. Variation of exergetic COPs of the single and cascaded heat pumps with excess CuCl feed temperature (T_{15}).

For comparison between the mercury based and the biphenyl based heat pumps from their evaporators' point of view, the energetic and exergertic COPs variation of the heat pumps with their evaporators temperature is shown in Figure 5.33 and Figure 5.34, respectively. It is seen that the mercury based heat pumps accommodate a shorter temperature range compared to the biphenyl based heat pumps (mercury lowest evaporator temperature is 500 K (227^0C), for biphenyl it is 465 K (192^0C)). Simulating lower evaporator temperatures and pressures causes errors for both mercury and biphenyl based heat pumps. Moreover, the energetic and exergetic COPs of the mercury based heat pumps are greater than the energetic and exergetic COPs in the biphenyl based heat pumps. The biphenyl based heat pumps evaporator can operatre in above atmospheric

pressures. As long as the exergetic COPs are lower than the energetic COPs, a unity and greater exergetic COPs can be achieved in all the mercury based heat pumps at an evaporator temperature equal to or greater than 505 K (232^0C). All biphenyl based heat pumps will be unity or greater in an evaporator temperature equal to or greater than 544 K (271^0C).

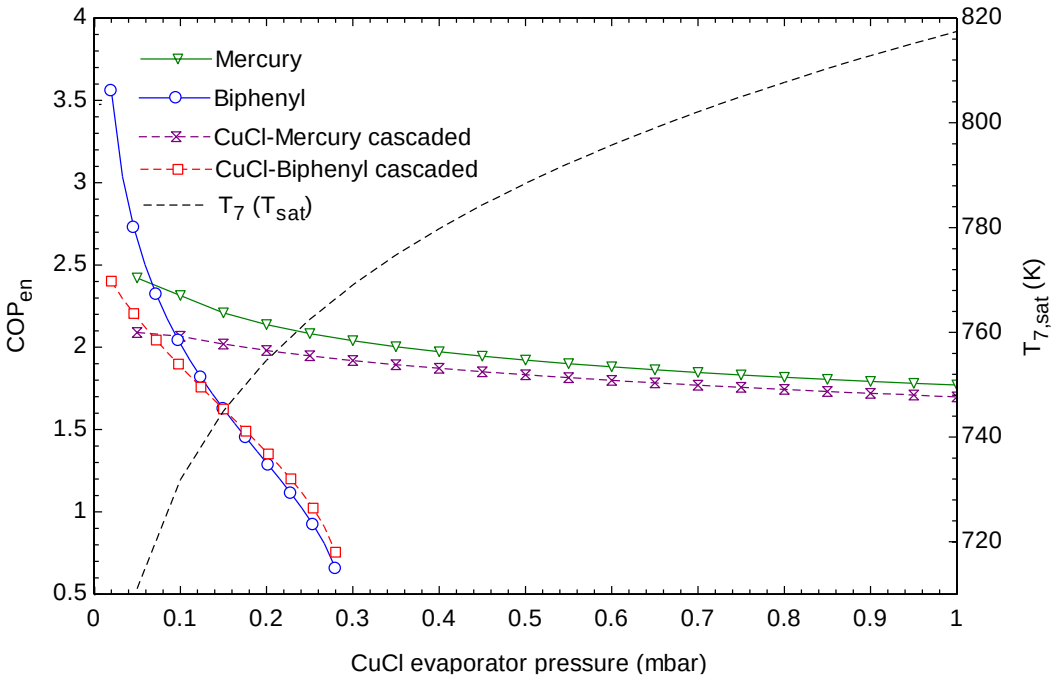

Figure 5.31. Variation of energetic COP of the mercury based and the biphenyl based heat pumps with the CuCl evaporator pressure.

5.4.4 Energy and exergy analysis results

Figure 5.35 shows the heat input rate, mechanical power input, and heat output rate for each single heat pump and the cascaded configurations. It is seen that the CuCl heat pump consumes the minimum amount of electric power input (15.74 kW) followed by the mercury heat pump (36.16 kW) as a bottom heat pump and its biphenyl counterpart (40.97 kW). Heat upgrading is achieved in both cascaded configurations as the thermal output rate (heat rate requirement to achieve reaction temperature of the reactor) outweighs the mechanical power requirements. Notice that the single bottom heat pumps are designed to achieve a 75 kW heat output rate, which is heat input rate for the CuCl heat pump evaporator.

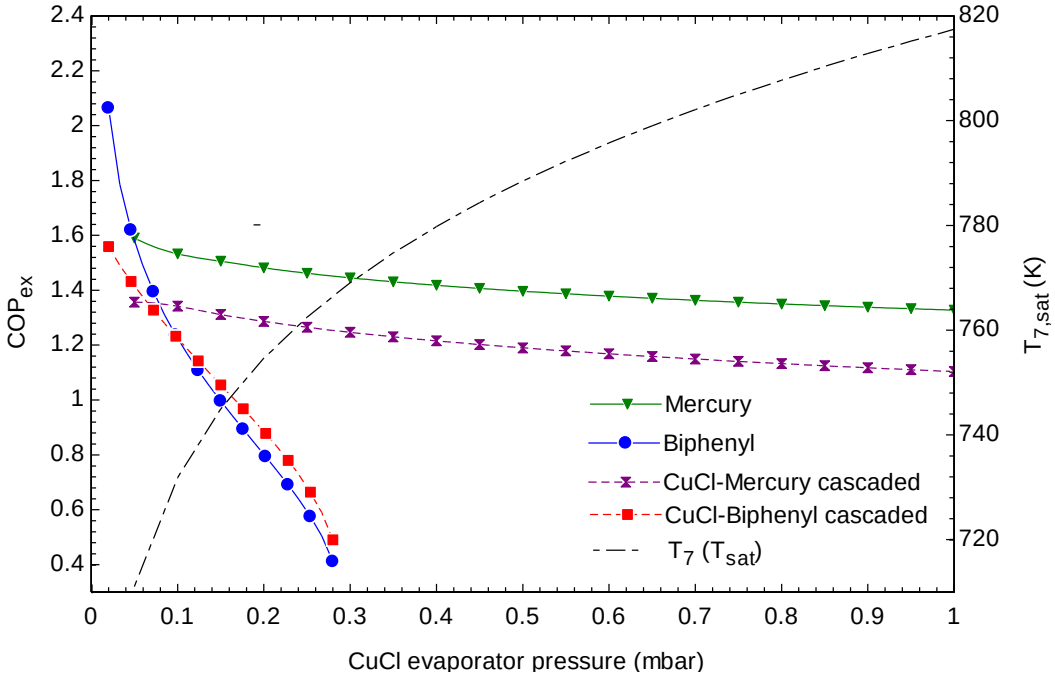

Figure 5.32. Variation of exergetic COP of the mercury based and the biphenyl based heat pumps with the CuCl evaporator pressure.

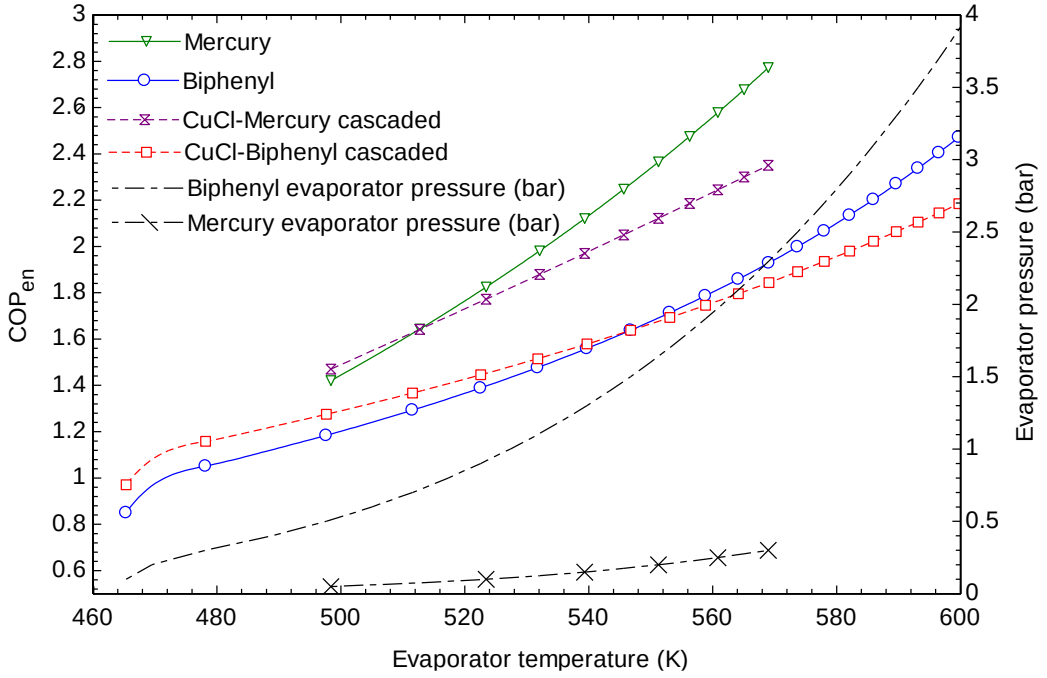

Figure 5.33. Variation of the energetic COP of the mercury based and the biphenyl based heat pumps with their evaporator temperature.

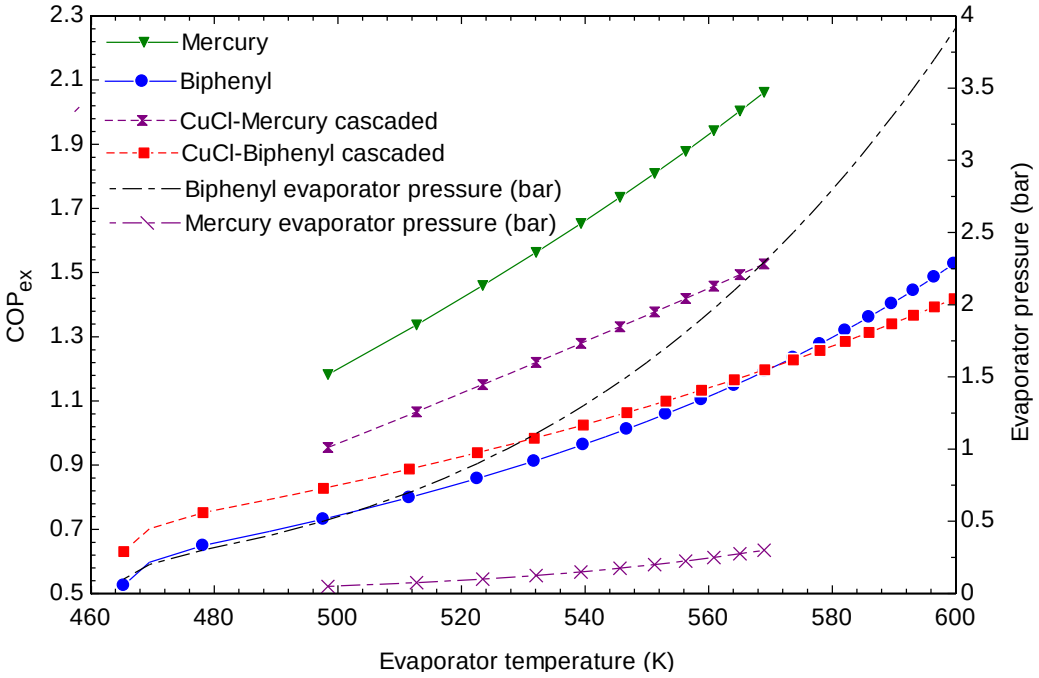

Figure 5.34. Variation of the exergetic COP of the mercury based and the biphenyl based heat pumps with their evaporator temperature.

According to Figure 5.36, single heat pumps have high energetic and exergetic COPs without cascading. As bottom heat pumps, the mercury heat pump achieve higher COPs (energetic 2.06, exergetic 1.53) compared to the biphenyl heat pump (energetic 1.83, exergetic 1.13). In addition, the cascaded heat pump that includes mercury as the bottom cycle also achieves higher energetic (1.93) and exergetic (1.25) COPs compared to the CuCl-biphenyl energetic (1.76) and exergetic (1.15) coefficient of performance.

Besides having the lowest COP, Figure 5.37 shows that the CuCl-biphenyl configuration has the highest exergy destruction rate (86.3 kW) while that for the CuCl-mercury configuration is nearly 2 kW lower (84.6 kW). Figure 5.37 also shows that in both configurations the majority of the exergy destruction rate occurs in the copper oxychloride decomposition reactor (37.6 kW for both configurations) and the heat exchangers (mercury 33.2 kW, biphenyl 30.4). Note that, even though the CuCl-mercury heat pump has six compressors, three in the CuCl heat pump and three in the mercury heat pump, the compressors have a lower total exergy destruction rate (1.5 kW) than the total exergy destruction rate occurring in the CuCl-biphenyl compressors (3.0 kW).

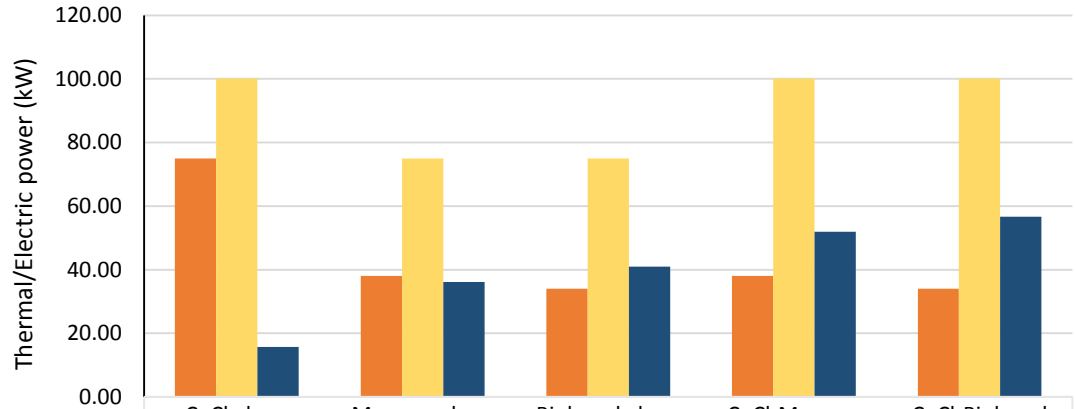

	CuCl alone	Mercury alone	Biphenyl alone	CuCl-Mercury	CuCl-Biphenyl
Q in - kW	75.00	38.00	34.00	38.00	34.00
Q out - kW	100.13	75.00	75.00	100.13	100.13
W in - kW	15.74	36.16	40.97	51.90	56.70

Figure 5.35. Heat input rate, mechanical power input, and heat output rate in each single and cascaded heat pump.

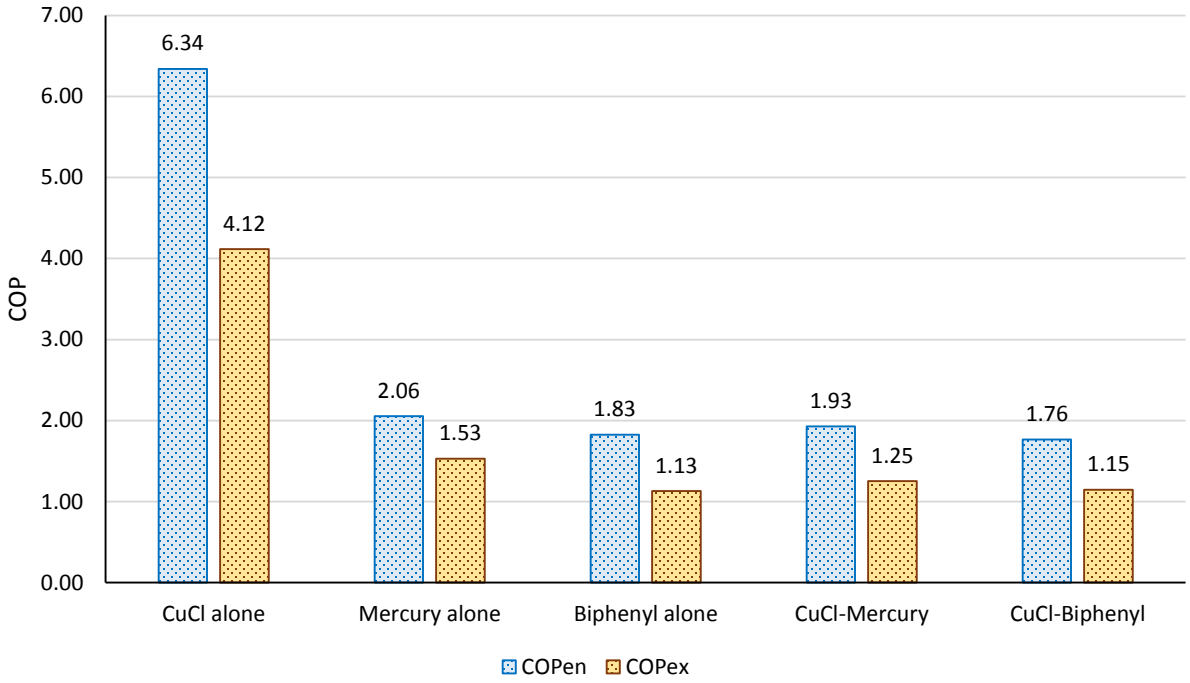

Figure 5.36. Energetic and exergetic COPs for each single and cascaded heat pump.

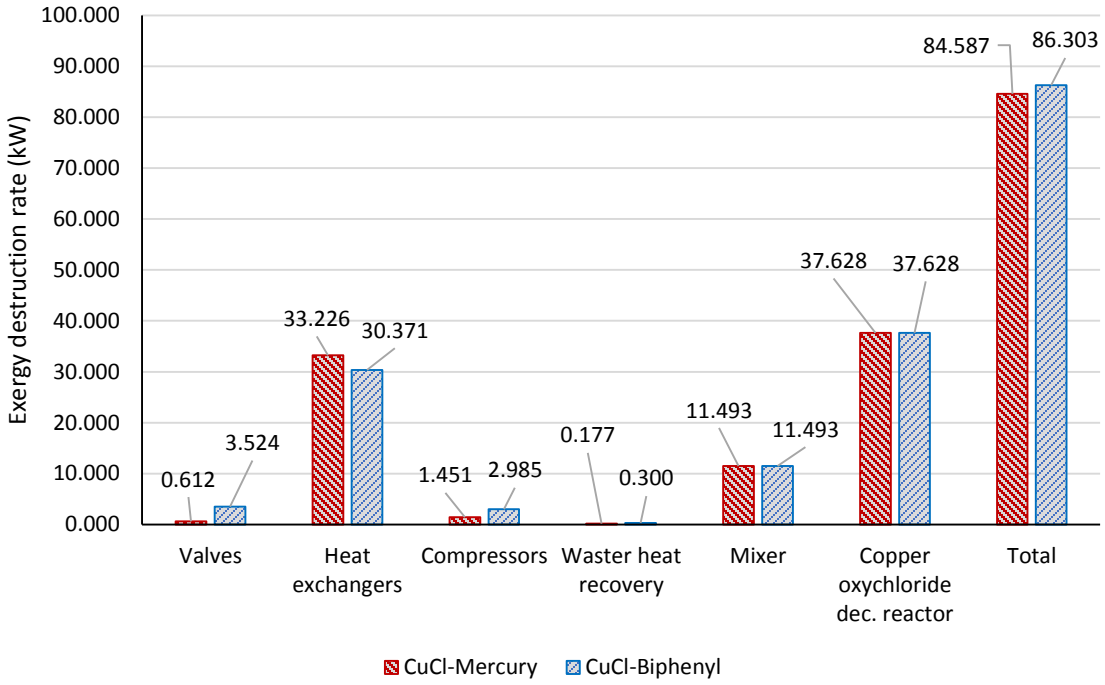

Figure 5.37. Exergy destruction rate for each single and cascaded heat pump.

The exergy destruction variation with respect to ambient temperature for CuCl-mercury and CuCl-biphenyl is shown in Figures 5.38 and 5.39.

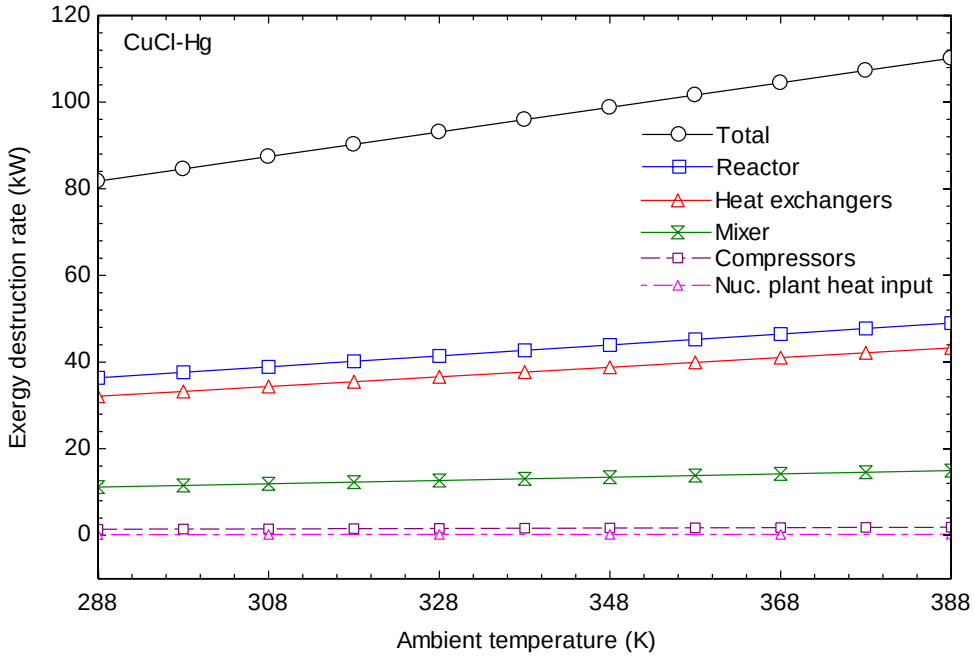

Figure 5.38. The increase in the CuCl-mercury exergy destruction rate with respect to ambient temperature.

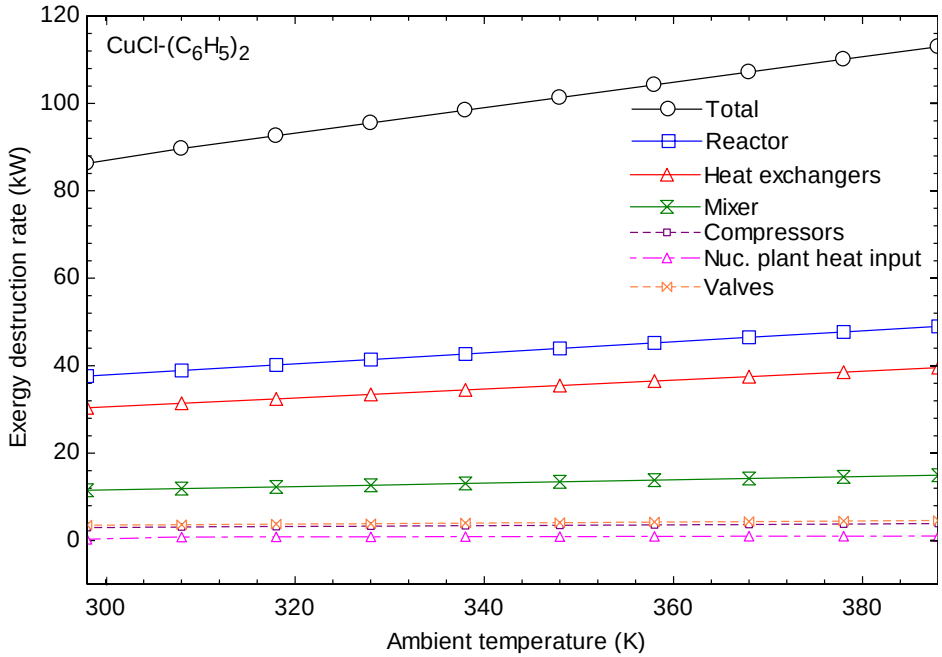

Figure 5.39. The increase in the CuCl-biphenyl exergy destruction rate with respect to ambient temperature.

5.4.5 Exergoeconomic analysis results

The purchase costs of equipment was estimated using equation (3.57) with suitable coefficients shown in table (3.6). Figure 5.40 shows that in both options, most of the costs are going for heat exchangers. The capacity used in the equations (e.g. heat transfer area, power, volume, mass flow rate, etc) are shown in Table 5.2. All of the capacity were obtained from Aspen Plus results, including the heat transfer area required in the heat exchangers. In our exergoeconomic analysis we, the base case interest rate is taken to be 5% and the operation life time is taken to be 15 years.

The purchase cost of the seven heat exchangers in the CuCl-mercury heat pump is considered to be 90% of the heat pump equipment purchase cost. The purchase cost of heat exchangers in the CuCl-biphenyl is also high (83% of total cost). Note that the equipment shared by both systems have the same price (e.g. mixer and reactor). All costs were adjusted for 2015 using proper chemical engineering plant cost index, see Section 3.4.1 for details.

Table 5.2. Parameters used for purchase cost estimation using equations (3.57) and (3.58) based on capacity of equipment.

Equipment	Type, capacity, unit
	Heat Exchangers, capacity (area), (m^2)
HX1	0.339
HX2	0.049
HX3	0.034
HX4	0.019
HX5-Mercury	0.112
HX5-Biphenyl	8.436
HX6-Mercury	0.087
HX6-Biphenyl	2.691
HX7-Mercury	3.336
	Heater , capacity (power), (kW)
Nuclear thermal input -Mercury	47
Nuclear thermal input -Biphenyl	34
	Compressors / pumps, capacity (power), (kW)
C1	11.70
C2	2.59
C3	1.49
C4-Mercury	18.97
C4-Biphenyl	41.10
C5-Mercury	4.97
C6-Mercury	2.86
	Expansion valves, capacity (Mass flow rate), (kg/s)
Valve1	0.039
Valve2	1.694
Valve3-Mercury	0.184
Valve3-Biphenyl	0.365
	Reactor, capacity (Volume), (m^3)
Oxychloride decomposition reactor	0.3
	Mixer, capacity (Volume), (m^3)
Mixer	3

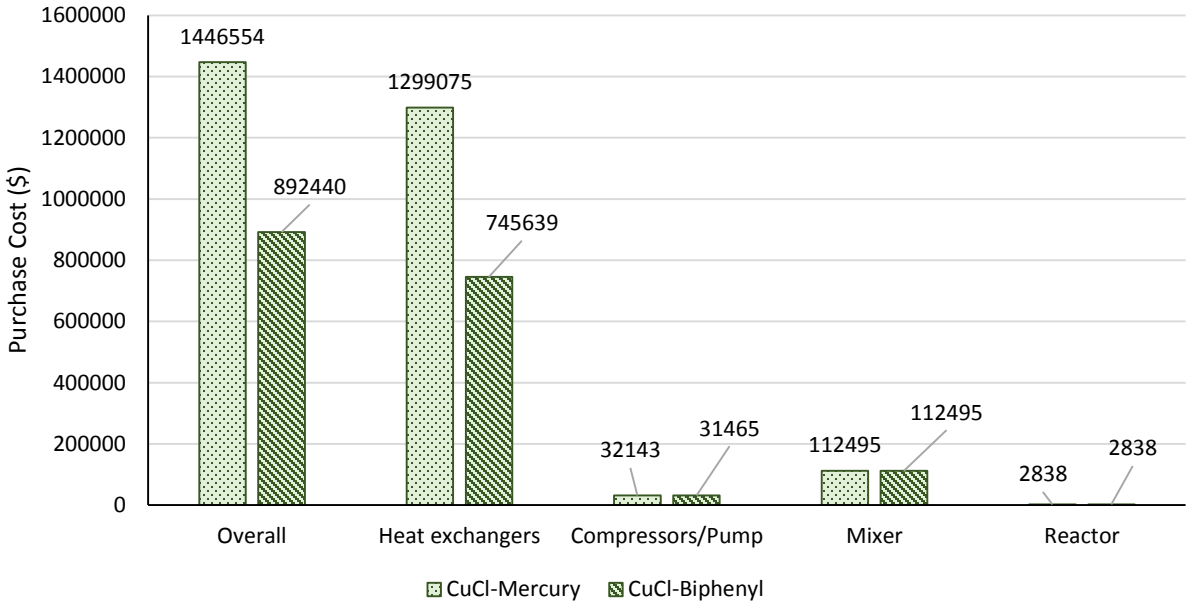

Figure 5.40. Equipment purchase cost according to category in CuCl-mercury and CuCl-biphenyl heat pumps.

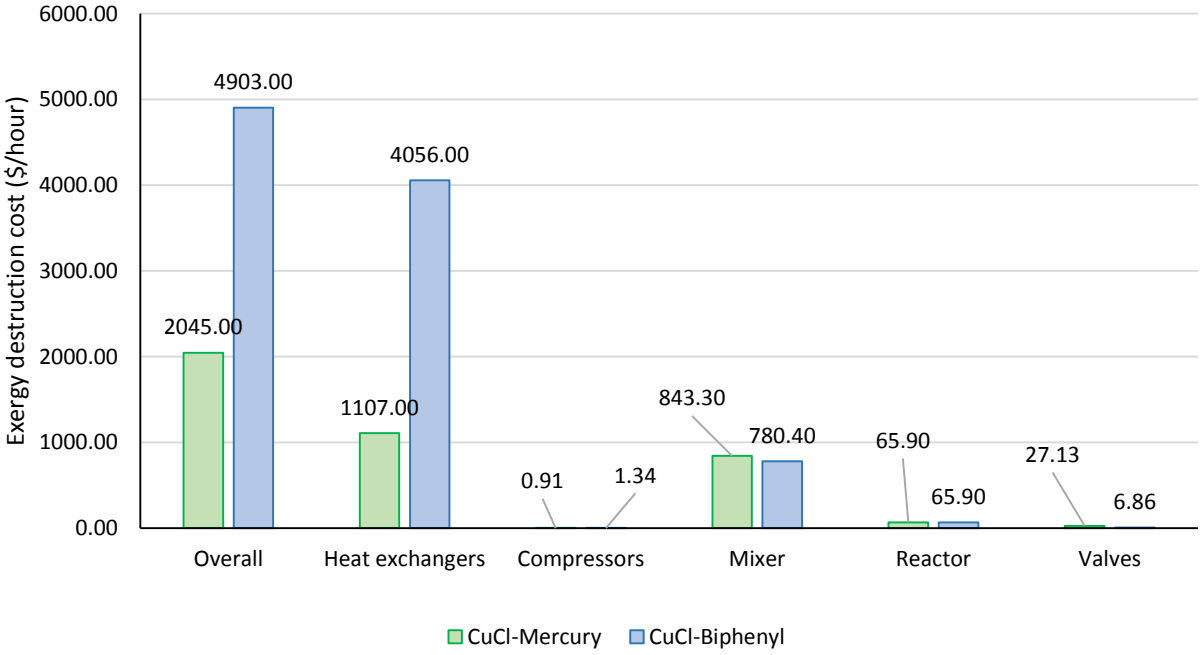

Figure 5.41. Exergy destruction cost flow according to components category presented for the CuCl-mercury and the CuCl-biphenyl heat pumps.

The exergy destruction cost per hour is shown in Figure 5.41. The exergy destruction cost in $/hour is very high in the CuCl-biphenyl configuration (4903 $/hour) compared to the exergy destruction cost in the CuCl-mercury (2045 $/hour) which is even less than 50% of its biphenyl counterpart. The compressors and valves category achieves the least exergy destruction costs.

Table 5.3. The calculated exergoeconomic factor and relative cost difference for each components category.

	CuCl-Mercury		**CuCl-Biphenyl**		
Components category	f	RCD	f	RCD	f typical values (Bejan et al., 1996)
Expansion valve	0.000	0.005	0.002	0.003	-
Compressors + pump	0.994	5.643	0.993	7.918	0.35-0.75
Heat exchangers	0.786	2.751	0.453	0.232	Lower than 0.55
Reactor	0.163	0.159	0.163	0.159	-
Mixer	0.376	0.111	0.115	0.115	-
Total	0.699	0.087	0.454	0.060	-

Besides exergy destruction cost, the exergoeconomic factor f and the relative cost difference RCD are calculated for base case according to components category. The exergoeconomic factor defined in equation (3.81) asses the capital purchase cost and maintenance cost flows with respect the hidden cost flow of exergy destruction (see equation (3.80)). The factor can be taken as an optimization tool for a component performance indicating that exergy destruction cost flow is minimized when the value of the exergoeconomic approaches unity (or 100%). For a low exergoeconomic factor, which is an indication that exergy destruction cost flow is very high, a decision may be studied weather it worth to add an investment cost for the sake of improving the component's performance and reduce its inefficiency. Table 5.3 shows the exergoeconomic factor according to components category. It can be noticed that CuCl-biphenyl heat pump has lower exergoeconomic factors compared to CuCl-mercury heat pump, a result that exactly match the results obtained in exergy destruction cost flow and shown in Figure 5.41. The compressors in both systems have exergoeconomic factors that exceed the typical value recommended by Bejan et al. (1996). Thus, a study may be made to whether or not reduce the capital costs of the compressors at expense of its efficiency. The same statement can be said about the heat exchangers in CuCl-mercury heat pump. The exergoeconomic factor of heat exchangers in the CuCl-biphenyl heat pump are found to be typical (0.453 less than 0.55). The relative cost

difference shows the increase or decrease of product cost with respect to fuel for each component. It is aimed to have it minimized in optimization instead of minimizing the product cost flow.

The exergoeconomic factor and total cost flow (capital cost plus exergy destruction cost) plots versus lifetime in years for CuCl-mercury heat pump are shown in Figure 5.42 and Figure 5.43. Due to the reduction in the value of the asset by time, both the total cost flow and the exergoeconomic factor decrease accordingly. The drop of the capital cost drops rapidly in the earlier years of its life time as it behaves as approaching an asymptote in its greater life time. The effect of interest rate on the exergoeconomic factor is also shown, assuming it being fixed throughout the operation period. Figure 5.44 and Figure 5.45 show the cost flow rate and exergoeconomic factor versus the operation life time in years behave similar to the CuCl-mercury heat pump cost flow rate and exergoeconomic factor. The CuCl-biphenyl systems starts with higher total cost flow rate compared to CuCl-mercury counterpart.

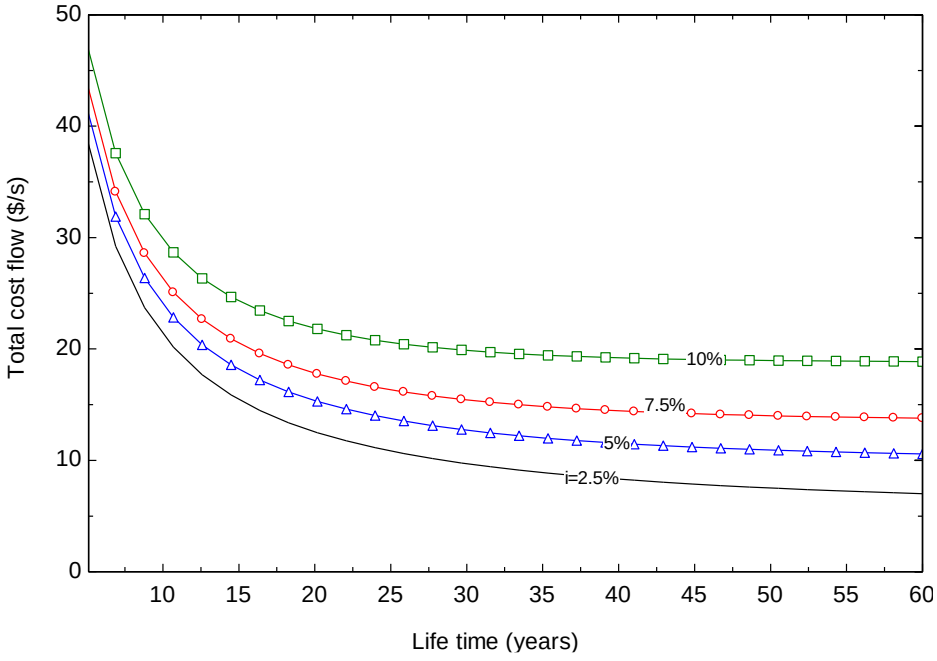

Figure 5.42. Total cost flow of the CuCl-mercury heat pump decrease with operation life time for different interest rate values.

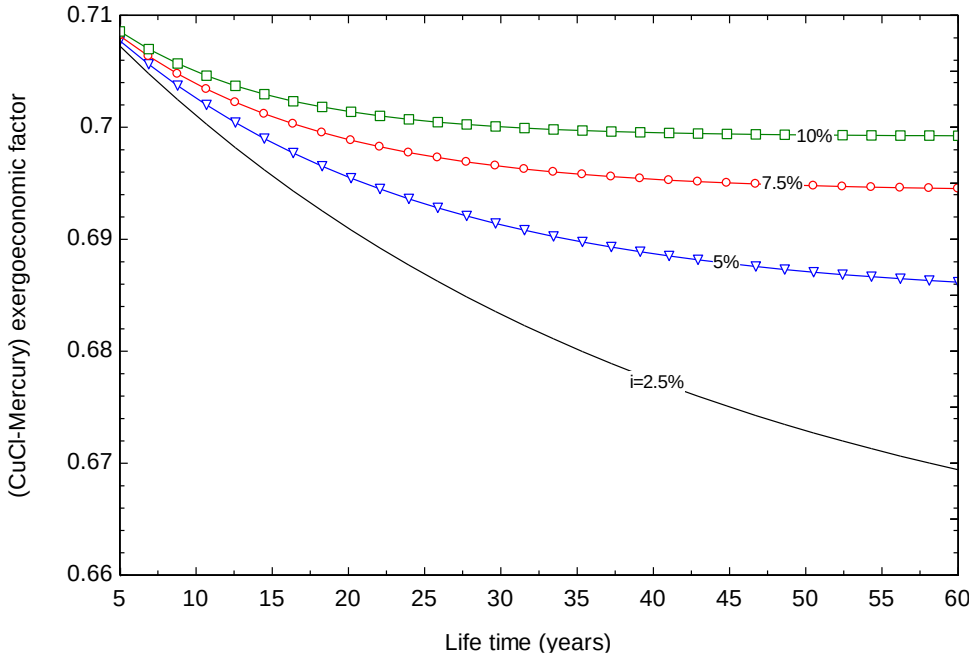

Figure 5.43. The variation of exergoeconomic factor of the CuCl-mercury heat pump with operation life time for different interest rate values.

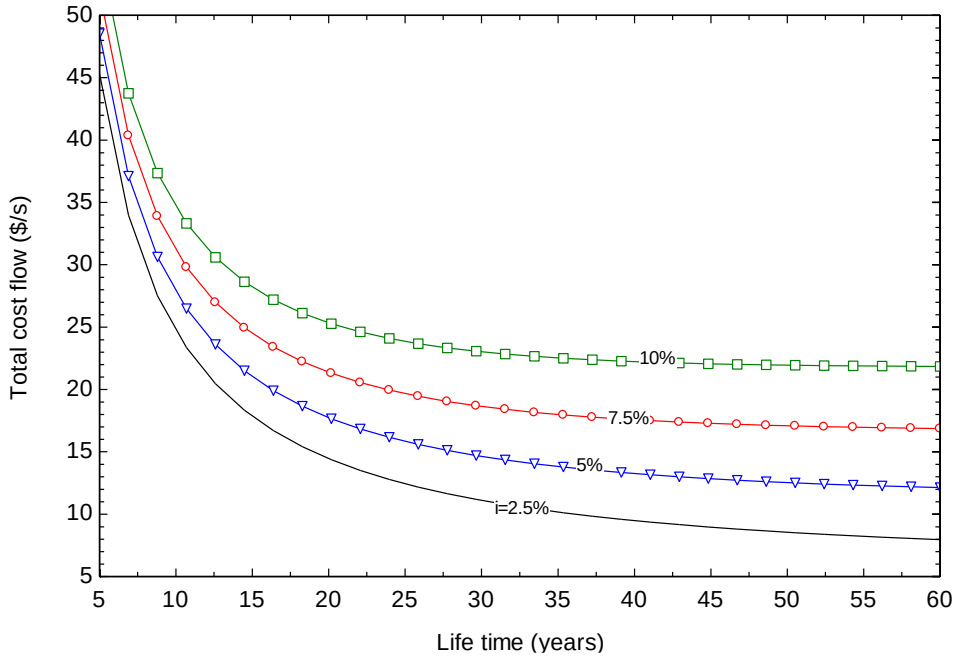

Figure 5.44. Total cost flow of the CuCl-biphenyl heat pump decrease with operation life time for different interest rate values.

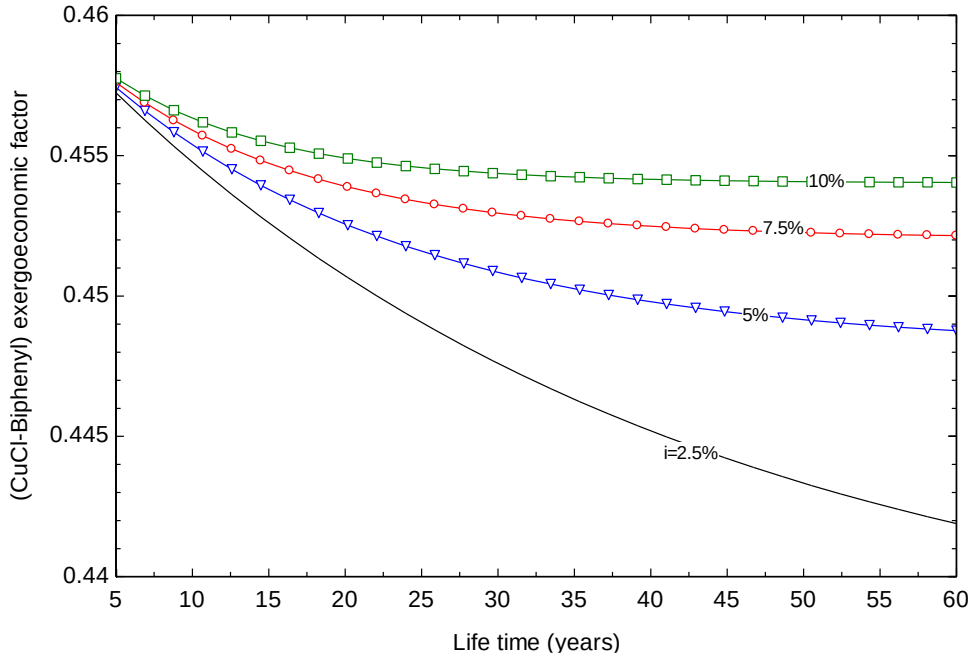

Figure 5.45. The variation of exergoeconomic factor of the CuCl-biphenyl heat pump with operation life time for different interest rate values.

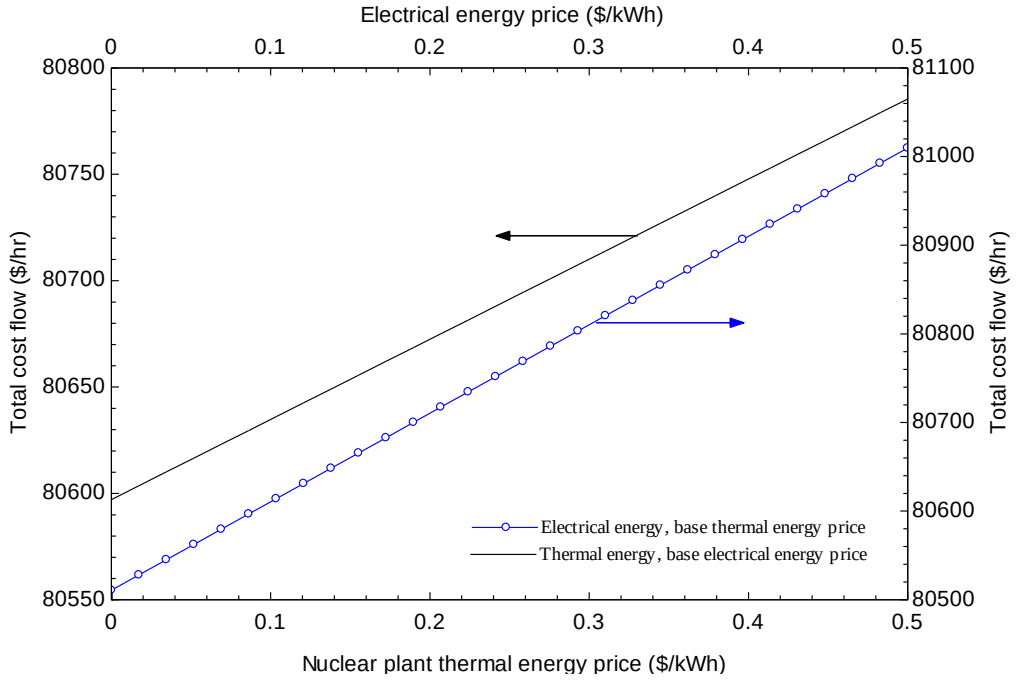

Figure 5.46. The increase of the total cost flow of the CuCl-mercury heat pump with respect to the increase in the electric energy cost or the cost of thermal energy supplied by nuclear power plants.

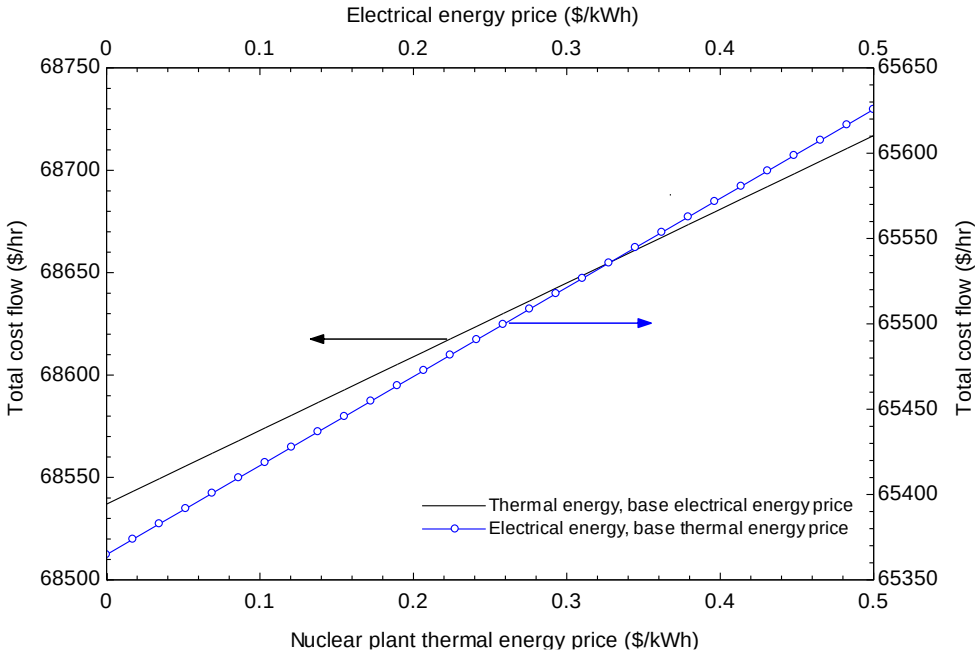

Figure 5.47. The increase of the total cost flow of the CuCl-biphenyl heat pump with respect to the increase in the electric energy cost or the cost of thermal energy supplied by nuclear power plants.

The effect of the cost of electric energy and the cost of the thermal energy obtained from the nuclear power plants on the total cost flow is shown in Figure 5.46 for CuCl-mercury heat pump and Figure 5.47 for CuCl-biphenyl. The total cost flow for the CuCl-mercury cascaded heat pumps increases by 500$/hr in 0-0.5 $/kWh range of electric energy price, while it makes an increase of 175 $/hr in the same nuclear plant thermal energy price. In the same range of $/kWh for the CuCl-biphenyl cascaded configuration, the total cost flow increases by 280 $/h with respect to the electric energy variation and 170 $/hr with respect to the thermal energy variation.

Chapter 6: Conclusions and Recommendations

In this thesis two heat pumps are proposed to upgrade heat from low temperature (as low as 300°C heat supplied from nuclear power plant which is taken as a base case) to the high reaction temperature of the copper oxychloride reactor. The heat is supplied to the endothermic reaction through heating an excess CuCl as a working fluid in a proposed CuCl heat pump and injecting it to the decomposition reactor. The CuCl vapor compression heat pump was studied with two cascading options: the first option is CuCl-mercury cascaded heat pumps, and the second is CuCl-biphenyl heat pump.

6.1 Conclusions

Thermodynamic and exergoeconomic analyses are performed on two proposed heat pump systems and the following conclusions are drawn:

- Both options successfully upgrade heat from the low temperature that can be provided by current nuclear energy plants or industrial waste heat recovery. In the base case, both systems are have energetic and exergetic COPs greater than 1, although the CuCl-mercury option is superior based on coefficient of performance (COP_{en}=1.93, COP_{ex}=1.25) compared to CuCl-biphenyl option (COP_{en}=1.76, COP_{ex}=1.15).
- The COPs of both systems rise if the temperature of the excess CuCl (T_{15}) is increased. A temperature less than 910 K causes the CuCl-biphenyl COP to drop below unity. The CuCl-mercury COP falls below unity when temperature T_{15} falls below 880 K.
- The increase in evaporator pressure (accommodating higher source temperatures) of the bottom heat pumps (i.e. mercury or biphenyl) increases coefficient of performance of the overall cascaded heat pumps. However, the increase in the CuCl heat pump evaporator leads to a decline in the overall performances. The CuCl-mercury heat pump energetic and exergetic COPs remain higher than unity in a 0.05-1 mbar CuCl evaporator pressure range, while the energetic and exergetic COPs of the CuCl-biphenyl heat pump become less than unity in pressures greater than 0.24 mbar and 0.15 mbar, respectively.
- The heat exchanger performance and reduced temperature approach show an increase in the overall COPs of the heat pumps cycles and a better recovery of heat transferred through

them. The CuCl-mercury heat pump COPs increase by 7% as temperature approach in HX5 and HX6 reduces from 250 K to 0 K.

- The increase in the outlet temperature of the biphenyl compressor increases the CuCl-biphenyl energetic and exergetic COPs from 0.54 and 0.36 at 756 K to 1.8 and 1.17 at 830 K, respectively.
- The exergy destruction rate in the CuCl-biphenyl heat pump (86.3 kW) is greater than that in the CuCl-mercury heat pump (84.6 kW), although the difference is very small. The majority of exergy destruction rate in both systems occurs in the reactor in first place (about 45%), and in the heat exchangers in second place (about 39%).
- The equipment purchase cost of the CuCl-mercury heat pump is 62% higher than the CuCl-biphenyl heat pump equipment purchase cost. However, the exergy destruction cost in the CuCl-biphenyl heat pump is two times higher than that in the CuCl-mercury heat pump.

6.2 Recommendations

As a follow up for future research, these recommendations and suggestions are given for any further investigation or progress needed in this sub-topic:

- The performance of the substances mentioned in this thesis, including CuCl, mercury, and biphenyl should experimentally be studied in a lab context as working fluids in high temperature heat pumps. The experiments should be conducted for each individual heat pump, or in cascaded configurations. This should especially be considered for the CuCl as it has very low sub-atmospheric operating pressures.
- The parametric study shows that many parameters are important to the performance of the proposed system and indicates with certainty that there are better base or reference cases than presented. A thermodynamic optimization will certainly show the best parametric setting and higher coefficient of performances.
- To improve the COPs of the systems presented, an investigation of including a third heat pump cascading, or more, will be worthy. This will help the heat pumps operating in a smaller pressure difference between their lowest and highest pressure segments (i.e. evaporator and condenser pressures), leading to a lower mechanical power consumption in compression and an increase in the overall COPs.

- Mercury is an extremely toxic substance and utilizing it in industry or laboratories should be with caution and proper training. Hazard and risk analysis should be conducted for mercury handling to demonstrate the severity, prevention, likelihood of occurrence, and mitigation.
- The mercury heat pump should be accommodated with special high quality sealing due to the toxicity nature of its working fluid. This is especially a concern for the fact that the evaporator operates below atmospheric pressure and it is difficult to detect leaks. Electrically welded joints and air seepage prevention containment are recommended in practices (Gutstein et al., 1975).
- A multi-stage compression analysis on the biphenyl heat pump will be useful as its results are not as efficient as the mercury based heat pumps. A single compressor in the biphenyl can causes a drawback in terms of cost and performance.
- An experimental study and prototype building of the copper oxychloride decomposition reactor heated by high temperature excess CuCl feed would be beneficial.

References

Adewale R. A., Berrouk A. S., Dara S. A process simulation study of hydrogen and sulfur production from hydrogen sulfide using the Fe–Cl hybrid process. Journal of the Taiwan Institute of Chemical Engineers 2015; 54:20-27.

Aghahosseini S., Dincer I., Naterer G. F. Process integration of hydrolysis and electrolysis processes in the Cu–Cl cycle of hydrogen production. International Journal of Hydrogen Energy 2013; 38(23):9633-9643.

Ansari K., Sayyaadi H., Amidpour M. Thermoeconomic optimization of a hybrid pressurized water reactor (PWR) power plant coupled to a multi effect distillation desalination system with thermo-vapor compressor (MED-TVC). Energy 2010; 35(5):1981-1996.

Arjmand M., Liu L., Neretnieks I. Exergetic efficiency of high-temperature-lift chemical heat pump (CHP) based on CaO/CO_2 and CaO/H_2O working pairs. International Journal of Energy Research 2013; 37(9):1122-1131.

Aspen Technology. Aspen Plus. www.aspentech.com [Accessed Feb 2016].

Bakennea A., Nuttalla W., Kazantzisb N. Sankey-Diagram-based insights into the hydrogen economy of today. International Journal of Hydrogen Energy 2016. Available online.

Bejan, A., Tsatsaronis G., Moran M. J. Thermal design and optimization 1996. New York, John Wiley.

Chemical engineering online. Economic indicator. www.chemengonline.com/pci [Accessed Feb 2016].

Dincer I. Green methods for hydrogen production. International Journal of Hydrogen Energy 2012; 37(2):1954-1971.

Dincer I., Rosen M. A. Exergy: Energy, Environment and Sustainable Development. Exergy 2007.UK: Elsevier.

Dincer I., Zamfirescu C. Advanced Power Generation Systems 2014. Boston, Elsevier.

fChart. Engineering Equation Solver. www.fChart.com [Accessed Feb 2016].

Ferrandon M. S., Lewis M. A., Tatterson D. F., Gross A., Doizi D., Croizé L., Dauvois V., Roujou J. L., Zanella Y., Carles P. Hydrogen production by the Cu–Cl thermochemical cycle: Investigation of the key step of hydrolysing $CuCl_2$ to Cu_2OCl_2 and HCl using a spray reactor. International Journal of Hydrogen Energy 2010; 35(3):992-1000.

Gutstein M., Furman E. R., Kaplan G. M. Liquid-metal binary cycles for stationary power. NASA Technical Note 1975; TN D-7955.

Hamut H. S. Exergy and exergoeconomic analyses and optimization of thermal management systems in electric and hybrid electric vehicles. PhD Dissertation 2012. University of Ontario Institute of Technology.

Joshi A. S, Dincer I., Reddy B. V. Solar hydrogen production: A comparative performance assessment. International Journal of Hydrogen Energy 2011; 36:11246-11257.

Kawashima K., Okabe H., Suzuki K., Kuroiwa S., Akimitsu J., Sato K. H., Koda A., Kadono R. Antiferromagnetic ordering in Cu_2OCl_2 studied by the muon spin rotation/relaxation technique. Journal of Physics: Condensed Matter 2007; 19(14):145-275.

Kerskes H., Bertsch F., Mette B., Wörner A., Schaube F. Thermochemische Energiespeicher Thermochemical Energy Storage. Chemie Ingenieur Technik 2011; 83(11):2014-2026.

Khalid F., Dincer I., Rosen M. A. Comparative assessment of CANDU 6 and Sodium-cooled Fast Reactors for nuclear desalination. Desalination 2016; 379:182-192.

Koretsky M. D., Engineering and chemical thermodynamics. 2004. Wiley Hoboken, NJ.

Lattin W. C., Utgikar V. P. Global warming potential of the sulfur–iodine process using life cycle assessment methodology. International Journal of Hydrogen Energy 2009; 34(2):737-744.

Lazzaretto A., Tsatsaronis G. SPECO: A systematic and general methodology for calculating efficiencies and costs in thermal systems. Energy 2006; 31(8–9):1257-1289.

Lewis M. A., Masin J. G., O'Hare P. A. Evaluation of alternative thermochemical cycles, Part I: The methodology. International Journal of Hydrogen Energy 2009; 34(9):4115-4124.

Muradov N. Z., Veziroğlu T. N. From hydrocarbon to hydrogen–carbon to hydrogen economy. International Journal of Hydrogen Energy 2005; 30(3):225-237.

Naterer G., Suppiah S., Lewis M., Gabriel K., Dincer I., Rosen M. A., Fowler M., Rizvi G., Easton E. B., Ikeda B. M., Kaye M. H., Lu L., Pioro I., Spekkens P., Tremaine P., Mostaghimi J., Avsec J., Jiang J. Recent Canadian advances in nuclear-based hydrogen production and the thermochemical Cu–Cl cycle. International Journal of Hydrogen Energy 2009; 34(7):2901-2917.

Naterer G. F., Suppiah S., Stolberg L., Lewis M., Wang Z., Dincer I., Rosen M. A., Gabriel K., Secnik E., Easton E. B., Pioro I., Lvov S., Jiang J., Mostaghimi J., Ikeda B. M., Rizvi G., Lu L., Odukoya A., Spekkens P., Fowler M., Avsec J. Progress of international hydrogen production network for the thermochemical Cu–Cl cycle. International Journal of Hydrogen Energy 2013; 38(2):740-759.

Norwegian University of Science and Technology. Chemical Engineering Plant Cost Index (averaged over year). 2011. http://www.nt.ntnu.no/users/magnehi/cepci_2011_py.pdf [Accessed Feb 2016].

Odukoya A., Naterer G. F. Upgrading waste heat from a cement plant for thermochemical hydrogen production. International Journal of Hydrogen Energy 2014; 39(36):20898-20906.

Odukoya A., Naterer G. F. Calcium oxide/steam chemical heat pump for upgrading waste heat in thermochemical hydrogen production. International Journal of Hydrogen Energy 2015; 40(35):11392-11398.

Ogura H., Yasuda S., Otsubo Y., Mujumdar A. S. Continuous operation of a chemical heat pump. Asia-Pacific Journal of Chemical Engineering 2007; 2(2):118-123.

Orhan M. F., Dincer I., Rosen M. A. Efficiency comparison of various design schemes for copper-chlorine (Cu-Cl) hydrogen production processes using Aspen Plus software. Engergy Conversion and Management 2012; 63:70-86.

Ozbilen A., Dincer I., Rosen M. A. A comparative life cycle analysis of hydrogen production via thermochemical water splitting using a Cu–Cl cycle. International Journal of Hydrogen Energy 2011; 36(17):11321-11327.

Ozbilen A., Dincer I., Rosen M. A. Life cycle assessment of hydrogen production via thermochemical water splitting using multi-step Cu–Cl cycles. Journal of Cleaner Production 2012; 33:202-216.

Ozbilen A., Dincer I., Rosen M. A. Development of a four-step Cu–Cl cycle for hydrogen production – Part I: Exergoeconomic and exergoenvironmental analyses. International Journal of Hydrogen Energy 2016; xxx.

Parry T. Thermodynamics and Magnetisim of Cu_2OCl_2. MSc Thesis 2008. Brigham Young University.

Peng D., Robinson D. B. A New Two-Constant Equation of State. Industrial & Engineering Chemistry Fundamentals 1976; 15(1):59-64.

Pope K., Wang Z., Naterer G. F. Process integration of material flows of copper chlorides in the thermochemical Cu-Cl cycle. Chemical Engineering Research and Design 2016; 109:273-281.

Powles J. G., Is molten cuprous chloride a molecular liquid? Journal of Physics C: Solid State Physics 1975; 8(7):895.

Ratlamwala T. A. H., Dincer I. Energy and exergy analyses of a Cu–Cl cycle based integrated system for hydrogen production. Chemical Engineering Science 2012; 84:564-573.

Ratlamwala T. A. H., Dincer I. Performance assessment of solar-based integrated Cu–Cl systems for hydrogen production. Solar Energy 2013; 95:345-356.

Ratlamwala T. A. H., Dincer I. Experimental study of a hybrid photocatalytic hydrogen production reactor for Cu–Cl cycle. International Journal of Hydrogen Energy 2014; 39(35): 20744-20753.

Rosen M. A. Towards energy sustainability: a quest of global proportions. Forum on Public Policy: A Journal of the Oxford Round Table 2008.

Rowley R. L., Wilding W. V., Oscarson J. L., Yang Y., Zundeland N. A., Daubert T. P., Danner R. P., DIPPR Data Compilation of Pure Chemical Properties 2004. New York, Taylor & Francis Publishing Company.

Sigfusson T. I. Pathways to Hydrogen as an Energy Carrier. Philosophical Transactions: Mathematical, Physical and Engineering Sciences 2007; 365(1853):1025-1042.

Spoelstra S., Haije W. G., Dijkstra J. W. Techno-economic feasibility of high-temperature high-lift chemical heat pumps for upgrading industrial waste heat. Applied Thermal Engineering 2002; 22(14):1619-1630.

Srinivas T., Gupta A. V. S. S. K. S., Reddy B. V. Parametric simulation of steam injected gas turbine combined cycle. Proceedings of the Institution of Mechanical Engineers, Part A: Journal of Power and Energy 2007; 221(7):873-883.

Sugawara S., Sato T., Minamiyama T. On the Equation of State of Mercury Vapour. Bulletin of JSME 1962; 5(20):711-718.

Toronto Hydro. Electricity Rates & Charges. http://www.torontohydro.com/ [Acessed 2016].

Tsatsaronis G., Moran M. J. Exergy-aided cost minimization. Energy Conversion and Management 1997; 38(15–17):1535-1542.

Turton R. Analysis, synthesis, and design of chemical processes. Upper Saddle River, N.J., Prentice Hall 2009.

Zamfirescu C., Dincer I. Performance investigation of high-temperature heat pumps with various BZT working fluids. Thermochimica Acta 2009; 488(1–2):66-77.

Zamfirescu C., Dincer I., Naterer G., Performance evaluation of organic and titanium based working fluids for high-temperature heat pumps. Thermochimica Acta 2009; 496(1–2):18-25.

Zamfirescu C., Dincer I., Naterer G. F. Thermophysical properties of copper compounds in copper–chlorine thermochemical water splitting cycles. International Journal of Hydrogen Energy 2010; 35(10):4839-4852.

Zamfirescu C., Naterer G. F., Dincer I. Vapor compression CuCl heat pump integrated with a thermochemical water splitting cycle. Thermochimica Acta 2011; 512(1–2):40-48.